

Robust Fly-by-Wire under Horizontal Tail Damage

by

Zinhle Dlamini

*Thesis presented in partial fulfilment of the requirements for
the degree of Doctor of Philosophy in Electronic Engineering
in the Faculty of Engineering at Stellenbosch University*

The crest of Stellenbosch University is centered behind the text. It features a shield with various symbols, topped with a crown and a banner. The motto 'Pacta sunt servanda' is visible at the bottom of the crest.

Department of Electrical and Electronic Engineering,
University of Stellenbosch,
Private Bag X1, Matieland 7602, South Africa.

Supervisor: Prof T Jones

December 2016

Declaration

By submitting this thesis electronically, I declare that the entirety of the work contained therein is my own, original work, that I am the sole author thereof (save to the extent explicitly otherwise stated), that reproduction and publication thereof by Stellenbosch University will not infringe any third party rights and that I have not previously in its entirety or in part submitted it for obtaining any qualification.

Date:

Copyright © 2016 Stellenbosch University

All rights reserved.

Abstract

Aircraft damage modelling was conducted on a Boeing 747 to examine the effects of asymmetric horizontal stabiliser loss on the flight dynamics of a commercial fly-by-Wire (FBW) aircraft. Change in static stability was investigated by analysing how the static margin is reduced as a function of percentage tail loss. It is proven that contrary to intuition, the aircraft is longitudinally stable with 40% horizontal tail removed. The short period mode is significantly changed and to a lesser extent the Dutch roll mode is affected through lateral coupling. Longitudinal and lateral trimmability of the damaged aircraft are analysed by comparing the tail-loss-induced roll, pitch, and yaw moments to available actuator force from control surfaces. It is presented that the aircraft is completely trimmable with 50% tail loss.

Robustness of a generic C* FBW control system is investigated by analysing how characteristic eigenvalues move as a result of damage, and comparison to the non-FBW aircraft is made. Furthermore, the extent of stabiliser loss that the system can successfully handle, without loss of acceptable performance, is identified. A handling qualities evaluation is presented to provide an understanding of how the pilot would perceive the damaged aircraft. The results of the study show that a generic FBW system improves robustness such that the aircraft is stable with 50% horizontal stabiliser loss. With 50% damage, the aircraft is controllable but unsafe to fly and may be unable to effectively complete its mission task.

The damaged FBW aircraft is formulated into an H_2 control problem. Convex optimisation techniques are employed to represent the problem as a linear matrix inequality and a solution is synthesised through the interior point method. An analysis of the state feedback gains is carried out to ascertain a suitable control strategy to minimise the in-

fluence of disturbance on longitudinal dynamics. It is proven that pitch angle feedback provides good disturbance rejection in the low frequency range, however, it attenuates the control signal at higher frequencies thus resulting in loss of robustness. By comparison with a different class of aircraft it is shown that pitch angle feedback is only advantageous for aircraft with slow closed-loop longitudinal poles. The generic C^* fly-by-wire system is augmented to include pitch angle feedback and thus creates a novel system, the $C^*\theta$ FBW. This system is compared to the original C^* and its advantages and disadvantages presented. For the case of 50% damage, the phugoid poles of the system are stable whilst the short period poles are within level 2 handling qualities. A small loss in robustness is, however, observed for the short period poles. It is shown through an alternative control strategy that improvement of short period robustness can be achieved by increasing the system gain, however, this destabilises the marginally stable phugoid poles of the aircraft.

The original contributions presented in this thesis are in the field of flight dynamics and robust control. An analysis of change in dynamics due to horizontal tail damage is carried out in a method that provides visibility to changes in trim and manoeuvrability of the aircraft after damage. An evaluation of FBW robustness against this kind of damage is presented as well as change in handling qualities. A novel approach of analysing disturbance rejection capabilities of an aircraft with available actuators through a more robust combination of feedback states is discussed. From this analysis a new FBW control law is developed and its robustness evaluated. Through a comparison with an ideal system the limiting factors to improving the robustness of the B747 class of aircraft are identified.

Opsomming

Vliegtuigskade op 'n Boeing 747 is gemodelleer om die effek van asimmetriese verlies van die horisontale stabiliseerder op die vlugdinamika van 'n kommersiële vliegtuig met 'n elektroniese beheerstelsel (*fly-by-wire*) te toets. Die verandering in statiese stabiliteit is ondersoek deur te analiseer hoe die statiese marge verminder as 'n funksie van die persentasie stertverlies. Dit word bewys dat die vliegtuig longitudinaal stabiel is met 40% van die horisontale stert verwyder. Die kort-periode fase word beduidend deur die skade verander. Die Nederlandse kanteling wyse (*Dutch roll mode*) word tot 'n mindere mate geaffekteer deur laterale koppeling. Die longitudinale en laterale ewewig-instelbaarheid (*trimmability*) van die beskadigde vliegtuig is geanaliseer deur die kanteling, helling en verdraaiing (*roll, pitch, and yaw*) weens stertverlies te vergelyk met die beskikbare aktueerder krag vanaf beheeroppervlaktes. Dit word bevind dat die vliegtuig ten volle ewewig-instelbaar is met 50% stertverlies.

Die robuustheid van 'n generiese C* elektroniese beheerstelsel is ondersoek deur te analiseer hoe die eiewaardes verander weens skade; 'n vergelyk word getref met die vliegtuig sonder 'n elektroniese beheerstelsel. Die vlak van stabiliseerderverlies wat die stelsel suksesvol kan hanteer, sonder om aanvaarbare verrigting te verminder, word bepaal. 'n Hanteringskwaliteit evaluasie word voorgestel om te help verduidelik hoe die vlieënier die skade sal ervaar. Die resultate van hierdie studie dui daarop dat 'n generiese elektroniese beheerstelsel robuustheid verbeter, wat tot gevolg het dat die vliegtuig stabiel sal bly selfs met 50% horisontale stabiliseerder verlies. Met 50% skade is die vliegtuig steeds beheerbaar maar onveilig om te vlieg.

Die beskadigde vliegtuig, met elektroniese beheerstelsel, word as 'n H₂ beheerprobleem geformuleer. Konvekse optimaliseringstegnieke word gebruik om die probleem as 'n lineêre

matriks ongelykheid voor te stel. 'n Oplossing word bewerkstellig met behulp van die interne punt metode. 'n Analise van die toename in toestand terugvoer word gedoen om 'n toepaslike beheerstrategie vas te stel wat die invloed van versteuring op die longitudinale dinamika tot 'n minimum sal beperk. In die studie word bewys dat die hellingshoek-terugvoer goeie versteuringsverwerping verskaf onder lae frekwensies. Dit verswak wel die beheersein onder hoë frekwensies wat dus lei tot 'n verlies aan robuustheid. In vergelyking tot 'n ander vliegtuigklas word dit bewys dat hellingshoek-terugvoer slegs voordelig is vir vliegtuie met stadige geslotelus longitudinale pole. Die generiese C^* elektroniese beheerstelsel is aangepas om hellingshoek-terugvoer in te sluit en skep dus 'n nuwe stelsel—die $C^*\theta$ elektroniese beheerstelsel. Hierdie stelsel word vergelyk met die oorspronklike C^* stelsel en die voor- en nadele word bespreek. Met 50% skade is die langperiode (*phugoid*) pole van die stelsel stabiel, terwyl die kort-periode pole binne vlak-2 hanteringskwaliteit is. 'n Klein verlies aan robuustheid word wel waargeneem vir die kort-periode pole. Deur 'n alternatiewe beheerstrategie word gewys dat 'n verbetering in kort-periode robuustheid bereik kan word deur die stelsel toename te verhoog. Dit destabiliseer hoewel die marginaal stabiele lang-periode pole van die vliegtuig.

Die oorspronklike bydraes van hierdie studie is in die veld van vlugdinamika en robuuste beheer. 'n Analise van die verandering in dinamika weens horisontale stertskade is uitgevoer met 'n metode wat sigbaarheid verleen aan die veranderings in ewewiginstelbaarheid en beweeglikheid na skade aan die vliegtuig. 'n Evaluasie van elektroniese beheerstelselrobuustheid en veranderings in die hanteringseienskappe, na hierdie tipe skade, is voorgelê. 'n Nuwe benadering is bespreek oor die analisering van 'n vliegtuig, met beskikbare aktueerders, se vermoë om versteurings te verwerp by wyse van 'n meer robuuste kombinasie van terugvoer toestande. Vanuit hierdie analise is 'n nuwe elektroniese beheerstelselwet ontwikkel. Die robuustheid van hierdie nuwe wet is ook geëvalueer. Die beperkende faktore om die robuustheid van die Boeing 747 vliegtuigklas te verbeter word identifiseer deur middel van vergelyking met 'n ideale stelsel.

Acknowledgements

I would like to express my sincere gratitude to the following people and organisations for their contributions towards this thesis,

- Prof Thomas Jones for your guidance, constant motivation and support. This would have taken much longer without your guidance.
- My parents and sisters, your support makes all the difference.
- Dr C Kwisanga, thank you for your guidance and support.
- Dr Njabu Gule and Dr Nathie Gule for the support network.
- The ESL team for providing a friendly and professional environment. Aaron Buysse, Andrew de Bruin, Gideon Hugo, Ryan Maggott, Piero Ioppo, Evert Trollip, and Dr Willem Jordaan for constructive feedback.
- The financial assistance of the National Research Foundation (NRF) towards this research is hereby acknowledged. Opinions expressed and conclusions arrived at are those of the authors and are not necessarily to be attributed to the NRF.

Contents

Declaration	i
Abstract	ii
Opsomming	iv
Acknowledgements	vi
Contents	vii
List of Figures	x
List of Tables	xiii
Nomenclature	xiv
1 Introduction	1
1.1 Background	1
1.2 Literature study	5
1.3 Original Contributions	9
1.4 Thesis Overview	10
2 Flight Dynamics Change under Horizontal Tail Damage	11
2.1 Problem overview	11
2.2 Experiment Setup	13
2.3 Results and Discussion	27
2.4 Conclusion	34
3 Fly-by-Wire Robustness	37

3.1	General Architecture	37
3.2	Control Law	39
3.3	Experimental Setup	44
3.4	Handling Qualities	47
3.5	Results and Discussion	48
3.6	Steady State and Transient Response Loop	51
3.7	Conclusion	54
4	Theoretical Development of an Optimal Solution	56
4.1	Modelling uncertainty	56
4.2	Linear Fractional Transformation	59
4.3	Formulation of the control problem	67
4.4	Solution of the optimal control problem: Calculus of variations approach	70
4.5	Conclusion	72
5	Solution of FBW Control Problem through Convex Optimisation	73
5.1	Convex optimisation overview	73
5.2	Linear Matrix Inequalities	76
5.3	Solution of LMIs: Interior point method	78
5.4	Conclusion	89
6	Development of a Robust System	90
6.1	H_2 optimal control solution	90
6.2	H_2 optimal controller analysis	92
6.3	Frequency Domain Analysis: q and θ	95
6.4	Robust Fly-by-Wire	100
6.5	Conclusion	109
7	Conclusion	111
7.1	Summary	111
7.2	Contributions to the field	113
7.3	Further Research	114
	Appendices	115

A Aircraft Equations of Motion	116
A.1 Euler Angles	116
A.2 Time derivative of a vector	118
A.3 Moments and Products of Inertia	118
A.4 Induced Incidence Angles	119
B Longitudinal Fly-by-Wire Control System	121
B.1 FBW transfer function derivation from block diagram	121
B.2 Steady state error	124
C H2 Optimal Control	126
C.1 MIMO Systems - transfer function to state-space [1]: An example for B747 short period dynamics	126
C.2 Parseval's Theorem	128
D Convex Optimisation	129
D.1 Positive and Negative Definite Matrix	129
D.2 Lyapunov Functions	130
E Robust Fly-By-Wire System	132
E.1 Weighting functions and corresponding gain for B747 optimal controller .	132
E.2 B747 Aircraft Data for trim configurations 158m/s at an altitude of 6096m	132
E.3 Phoenix Aircraft Data for trim configurations 20m/s at an altitude of 30m	133
Bibliography	135

List of Figures

2.1	Horizontal stabiliser damage from 10% to 50%	14
2.2	Velocity components illustrating orientation of α and β in the body frame	17
2.3	Angular momentum	18
2.4	Wingtip vortex development	25
2.5	Wingspan illustrating modelling of panels as horseshoe vortices	26
2.6	B747 AVL plot	27
2.7	Poles of decoupled and coupled aircraft model	28
2.8	Roll mode poles of decoupled and coupled aircraft model	29
2.9	Spiral and phugoid mode poles of decoupled and coupled aircraft model	29
2.10	Damaged aircraft in level flight illustrating change in moments and neutral point position	30
2.11	Change in static margin with reduction in stabiliser span	31
2.12	Pitching moment due to damage vs. available elevator moment to trim the aircraft	33
2.13	Damaged open-loop aircraft longitudinal poles (degree of horizontal stabiliser loss as per the legend)	33
3.1	General architecture of a fly-by-wire system	38
3.2	Structure of C* algorithm	41
3.3	Structure of C*U algorithm	42
3.4	Longitudinal control system in C* alternate law	43
3.5	Longitudinal control system in direct law	44
3.6	Pitch rate root locus plot	45
3.7	Normal load root locus plot	46

3.8	Requirements for short period response to pitch controller (ω vs ζ) of a class III aircraft in cruise configuration	48
3.9	Damaged open-loop (OL) vs. closed-loop (CL) aircraft longitudinal poles illustrating change in handling quality levels	49
3.10	Damaged closed-loop aircraft longitudinal poles for 50% and 60% stabiliser loss	50
3.11	Simplified block diagram of Airbus C* FBW	52
3.12	Root locus plot for outer loop with integrator for the case of vertical acceleration measured at CG	53
3.13	Root locus plot for outer loop with integrator for the case of vertical acceleration measured at the pilot seat	53
3.14	Open-loop vs. closed-loop poles at the pilot seat	55
4.1	Additive uncertainty system	58
4.2	Multiplicative uncertainty behaviour	59
4.3	Input multiplicative uncertainty system	59
4.4	Longitudinal control system with pitch input disturbance	60
4.5	LFT of the longitudinal control system	60
4.6	Feedback control system	64
4.7	Typical sensitivity function	65
4.8	Sensitivity function normalisation	66
4.9	Weight function W_u	67
4.10	Optimal trajectory search	71
5.1	Example of convex and non-convex sets	74
5.2	Convex function	75
5.3	Concave function	75
5.4	Contours of objective function against constraint function illustrating tangential point	80
5.5	Indicator function $\frac{1}{t} \log(-u)$ for different values of t	84
5.6	Central path illustrating contours of log barrier function as t varies	85
6.1	Longitudinal control system with pitch input disturbance	90
6.2	H_2 full state feedback optimal control system	91
6.3	B747 pitch rate feedback root locus	93

6.4	B747 pitch angle feedback root locus	94
6.5	Phoenix θ -feedback root locus	95
6.6	Phoenix q-feedback root locus	96
6.7	B747 q and θ bode plot	97
6.8	Phoenix q and θ bode plot	98
6.9	B747 Sensitivity Function $S = \frac{1}{1+G}$	99
6.10	Integration illustrating difference between q and θ feedback	99
6.11	C* with θ feedback	101
6.12	Pole placement for C* with θ feedback system	102
6.13	Closed-loop poles and zeros for C* with θ feedback system	103
6.14	C* with θ feedback vs C* with large q feedback	104
6.15	Damaged short period open-loop poles vs c* with θ feedback	105
6.16	Damaged short period open-loop poles vs C* with large q feedback	106
6.17	The pole plot of the closed-loop C* system with θ feedback, illustrating change in poles after 50% tail damage	107
6.18	SISO loop for a robust system	108
6.19	C* with outer loop	108
6.20	C* vs. C* augmented for robustness	109
6.21	Poles of robust system illustrating unstable phugoid poles	110
A.1	Euler Angles	117
A.2	Moment of Inertia ($I_{yy} = \int_v \rho (x^2 + z^2) \partial v$)	119
A.3	Airfoil illustrating induced angle of incident	119
B.1	Longitudinal control system in C* alternate law	121
B.2	q-feedback inner loop	122
B.3	nz-feedback loop	122
B.4	Outer loop	123
B.5	Step 1: outer loop simplification showing "a" in Eq. B.5	123
B.6	Step 2: outer loop simplification showing "a" in Eq. B.6 and r(s) in Eq. B.7	124
B.7	C* FBW illustrating steady state error without an integral controller	124
E.1	Boeing 747 Aircraft	133
E.2	Phoenix UAV	134

List of Tables

2.1	Aerodynamic coefficients of damaged (40% horizontal stabiliser loss) and undamaged aircraft	35
2.2	Moments resulting from damage, 10^3N.m	36
6.1	Most affected aerodynamic coefficients	100
6.2	Comparison of % change in ω of short period poles after 40% damage, for $C^*\theta$ and open-loop aircraft	104
6.3	Comparison of % change in ω of short period poles after 40% damage, for C^* with large q feedback and open-loop aircraft	105

Nomenclature

Variables

α, β	Angle of attack and sideslip	[rad]
δ_{-}	Actuator deflection as per subscript	[rad]
ρ	Density	[kg/m ³]
ϕ, θ, ψ	Roll, pitch, and yaw angle	[rad]
ω	Angular velocity	[rad]
ω_{-}	Natural frequency as per subscript	[rad/s]
τ	Time lag	[s]
b	Wingspan	[m]
A	Aspect ratio	[n/a]
\bar{c}	Mean aerodynamic chord	[m]
C_{-}	Aerodynamic coefficient as per subscript	[n/a]
E	Error as per subscript	[n/a]
F, M	Force and moment vector	[N, N·m]
H	Angular momentum	[kgm ² /s]

K	Gain as per subscript	[n/a]
L, M, N	Rolling, pitching, and yawing moment	[N·m]
L, D	Lift and drag	[N]
I	Inertia as per subscript	[kgm ²]
m	Mass	[kg]
mg	Gravity constant	[m/s ²]
n	Load factor	[n/a]
p, q, r	Roll, pitch, and yaw rate	[rad/s]
q	Dynamic pressure	[kg/m ²]
r	Distance vector	[m ²]
S	Wing area	[m]
T	Thrust	[N]
u, v, w	Longitudinal, lateral, and directional velocity	[m/s]
V	Velocity	[m/s]
x, y, z	Longitudinal, lateral, and directional position	[m]

Subscripts

a	Aerodynamic force
c	Command input
err	Error

ss	Steady State
g	Gravitational force
I	Inertial reference frame
B	Aircraft body frame
E, A, R	Elevator, aileron, and rudder
ref	Reference input
sp, p	Short period and phugoid
T	Trim
x, y, z	Orthogonal axis notation

Chapter 1

Introduction

This chapter details a discussion of the development of commercial fly-by-wire (FBW) aircraft and fault tolerant control research to improve FBW robustness. The advantages of FBW, over conventional non-FBW and implementation schemes adopted by major manufacturers, are presented. The motivation for the investigation of robustness to air-frame damage of the control system is provided as well as the rationale for fault tolerant control for FBW aircraft. A literature survey of modelling and fault tolerant control for damaged aircraft is detailed. The novel approach to the analysis of the robustness problem for commercial aircraft is also stated in the list of contributions. The last section of the chapter consists of the thesis overview.

1.1 Background

1.1.1 Fly-By-Wire for Commercial Aircraft

The term fly-by-wire (FBW) is commonly used to refer to a flight control system whereby the direct mechanical control linkages between the pilot and the control surfaces of an aircraft are replaced by electrical wires. The Air Force Flight Dynamics Laboratory [2], however, provides the following explicit definitions:

Electrical primary flight control system (EPFCS) is a system where pilot commands are transmitted to the actuator system via electrical wires.

Fly-by-wire is a feedback EPFCS whereby the aircraft motion is the controlled variable.

Pseudo fly-by-wire is a FBW system with a passive mechanical backup.

The first EPFCS implemented on civil aircraft was the Concorde flight control system designed by Aerospatiale [3]. It was an analogue full authority system for all control surfaces with mechanical backup for pitch, roll and yaw motion. The first digital EPFCS for commercial aircraft was implemented by Airbus on the A310 in the early 1980s. This system only controls the slats, flaps and spoilers. The A320 and A340 (certified in 1988 and 1992 respectively) have all control surfaces fully controlled by a digital FBW system and a mechanical backup for the trimmable horizontal stabiliser and rudder. The B777 (first flight in 1995) was the first commercial aircraft manufactured by Boeing to implement FBW technology. All actuators were electrically controlled except the trimmable stabiliser pitch trim system and some spoiler panels (used as speed brakes) which were mechanically controlled [4]. Whilst Airbus and Boeing are the largest manufacturers of commercial FBW aircraft other manufactures include Embraer, Iljuschin, Tupolev, Suchoi, and Antonov.

At the centre of an FBW system is an arrangement of electronic flight computers. Pilot control commands are converted to electrical signals by position transducers. These analogue signals are processed by the actuator control electronics (ACE) interface into a digital form and transmitted to the primary flight computer (PFC). The flight control system in the flight computer produces an output based on the control laws and the input. The output is transmitted to the actuators via the ACE. Surface actuator position feedback is also transmitted to the PFC via the ACE. In the Airbus FBW architecture the flight computers implement both control law and actuator control functionality to avoid a separate ACE subsystem. Typically multiple computers are used for redundancy to create an overall fail-safe system.

The control laws consist of pitch control and stability augmentation, turn compensation, thrust asymmetry compensation, envelop protection (angle of attack, bank angle, pitch angle etc.), stall and over-speed protection, and gust alleviation systems. The main disadvantage of these additional control functions is the requirement for monitoring systems and further control strategies for various failure conditions thus resulting in a higher demand on flight crew proficiency. FBW, however, provides many advantages in terms of safety and handling and aims to provide a largely invariant control response over the

entire flight envelope of an aircraft by employing techniques such as gain scheduling. Similar control stick inputs are thus typically reduced to similar longitudinal load factors (acceleration) and roll rates, independent of the altitude, speed or orientation of the aircraft.

Stability augmentation of the various dynamic modes improves the aircraft's disturbance rejection capabilities resulting in reduced pilot workload. The envelope protection function ensures the avoidance of possible dangerous outside the envelope manoeuvres, as such the pilot can react rapidly in confidence that the aircraft motion will not result into an uncontrollable situation. Further significant advantages include weight reduction, ease of maintenance, flexibility for including new functionality, and the compact integration of multiple subsystems into a new single subsystem. Advanced control requirements such as improved robustness can also be achieved more efficiently.

1.1.2 Motivation for improving robustness against damage

A control system is considered to be robust if it is capable of maintaining its designed response in the presence of uncertain plant models. Under normal conditions, aircraft dynamics are carefully characterised and mathematically modelled in order to ensure minimum plant uncertainty. Uncertainty does however result because of relatively small and unknown variations in, for example, mass, centre-of-mass, aerodynamic behaviour, etc. Fly-by-wire control systems are therefore designed to be robust against such uncertainties. Large model uncertainties are not considered, therefore, FBW systems are not designed to handle altered dynamics because of large CG shifts, or large changes in aerodynamic behaviour due to battle damage, mid-air collision, structural failure, etc. The purpose of this study is to first investigate the robustness of a typical FBW system for a large transport aircraft against horizontal tail damage; then design and analyse a more robust FBW system.

Modern civil aircraft utilise a relaxed static stabilities (RSS) design. The wings and tailplane are reduced in size to optimise for fuel consumption by minimising drag. This results in reduced natural stability [5]. Intuitively, reduced stability poses a threat to the robustness of the aircraft, i.e. for natural poles that are close to the imaginary axis the possibility of them moving to the instability region from a slight change in

aircraft parameters is greater. Since the aircraft is designed to have marginal longitudinal stability, tail damage is presumably difficult to handle. Small changes in tail volume result in significant changes in aircraft dynamics and trim conditions. Tail loss has proven to be beyond the control capacity of the nominal system. Depending on the extent and type of damage the aircraft may become completely uncontrollable. Japan Airlines flight 123 [6] and American Airlines flight 587 [7] (both having lost their vertical stabilisers in-flight) are examples of how structural damage to tail surfaces may lead to catastrophic loss of control. In the Gol Transportes Aéreos Flight 1907 [8] accident, however, after partial damage to the left horizontal stabiliser and left winglet, the aircraft continued flying and landed safely by application of excessive control inputs. In a more recent accident Grob Aerospace's light twinjet aircraft crashed during a demonstration flight after the elevators and the left stabiliser separated from the fuselage [9].

1.1.3 Fault tolerant flight control research at Stellenbosch University

A fault tolerant control (FTC) system is one that is capable of maintaining the plant's performance within acceptable boundaries in the presence of faults. FTC design concepts can be classified as active or passive systems. An active control strategy consists of real-time fault detection, isolation and reconfiguration of the flight control system. In the passive approach a fixed system utilises actuator control to provide satisfactory performance in the presence of faults without reconfiguration of the system [10]. Passive techniques include phase margin design, adaptive control, H_2/H_∞ optimal control etc. Fault tolerant flight control (FTFC) research at Stellenbosch University (SU) is focused on both active and passive methods. This section provides a review of past work that has been done by the FTFC group at SU, the study entailed in this thesis is part of this ongoing research.

In 2010 a study on system identification (SID) was carried out for a modular unmanned aerial vehicle (UAV) with a redundant design that enables reconfiguration in the presence of faults [11]. This research was based on the use of regression methods to continuously provide estimated control and stability derivatives of the aircraft. An advancement of this study was done by Appel in 2013, he investigated the implementation of an SID

algorithm in real time [12]. The study focused on parameter identifiability, i.e. methods to determine accuracy of the estimates and increase probability of getting good estimates. Various methods of obtaining angle of attack and angular acceleration were investigated and implemented on the modular UAV.

In 2011 Basson investigated the use of control reallocation techniques to compensate for actuator failures to minimise the possibility that a fault results in reconfiguration of the system [13]. The problem of allocating available actuators to attain a given number of control objectives was formulated into a multi-objective sequential quadratic programming optimisation problem. The effectiveness of the control allocation system was tested for various fault conditions at different aircraft configurations. Fault detection and isolation was studied by Odendaal on the modular UAV in 2012 [14]. He implemented two different methods, multiple model adaptive estimation and a parity space approach, and used flight-test data to compare and analyse them.

The use of passive control techniques was investigated by Basson [15] and Beeton [16] in 2011 and 2013 respectively. The study of Basson focused on adaptive control for damage induced longitudinal CG shifts on a fixed-wing UAV. Beeton used an acceleration-based control architecture system to obtain robust stability and performance for the problem of asymmetric partial wing loss. Current projects include a study of vertical and horizontal tail damage on a fixed-wing UAV, and combination of partial wing and tail loss on a UAV.

1.2 Literature study

1.2.1 Modelling of damaged aircraft

The increase in threats to the safety of civil and military aircraft has resulted in a renewed interest in the design of more robust control systems for aircraft with structural damage. This kind of damage changes the aircraft's aerodynamic behaviour and thus its dynamics. To facilitate the design of an efficient control system it is essential to formulate a mathematical model of the problem with an acceptable degree of accuracy.

Modelling of damaged aircraft consists of analysing how the conventional aircraft equa-

tions of motion are changed due to damage. These changes may include centre of gravity and centre of pressure shift, change in aerodynamic forces, inertial properties etc. In [17], a commercial transport aircraft model was subjected to wind tunnel testing at the NASA Langley Research Centre. In this study, change in aerodynamic behaviour under wing, vertical tail, and horizontal tail damage was analysed. In the case of asymmetric horizontal stabiliser damage it was proven that longitudinal dynamics are primarily affected and a rolling moment is induced by the loss of symmetry. The aircraft is marginally stable with complete left stabiliser loss and the static margin reduction is proportional to tail surface area loss. Whilst the study of Shah [17] was based on a conventional aircraft without a control system, the research work carried out in this thesis consists of a similar experiment (based on a more cost efficient method) carried out on FBW aircraft. The results of the FBW aircraft are compared to the conventional aircraft to quantify the difference in static and dynamic changes and thus analyse the robustness of the FBW control system.

Zhao [18] used sliding mode control to maintain stability under different degrees of damage of the vertical tail. Paton [19] presented the use of an LMI approach to obtain robust stability after wing damage and Liu [20] discussed a passive controller for vertical tail damage. The studies of these authors are control oriented and the damage problem is modelled as an augmentation of the conventional linearised aircraft state equation. In such an approach a parameter variation matrix which is representative of the damage is added and pre-multiplied by a scalar which is representative of the extent of damage. An example is shown on Eq. 1.1 where μ is a parameter uncertainty diagonal matrix presenting the degree of damage [18].

$$\dot{x}(t) = (A - \mu\bar{A})x(t) + (B - \mu\bar{B})u(t) + Du(t) \quad (1.1)$$

The modelling strategy is a mathematical presentation of the problem, but it does not show a clear association of the damage effect on the nominal model. An efficient alternative to this approach of modelling is a dynamics oriented study. This provides an understanding of the change in flight mechanics of the damaged aircraft. Visibility of how the dynamic modes are changing as a result of the specific damage allows an evaluation of preferable control schemes to be made. One of the objectives of this study is to in-

investigate the change in aircraft dynamics resulting from horizontal tail damage, thereby providing a knowledge base for the efficient design of a robust control system.

As argued by Bramesfeld [21], chances of successfully controlling and landing an aircraft when exposed to damage conditions is greatly increased if the flight crew is trained in unconventional control strategies to mitigate the change in aircraft response. An understanding of how flight dynamics are changed by damage provides a basis from which to develop alternative control strategies. This study seeks to provide an understanding of the dynamic and static effects of tail damage. Particular attention is paid to the aircraft response presented to the pilot after damage has occurred by analysing the change in handling qualities as defined by MIL-STD-1797-A [22]. A significant change in handling qualities may make it difficult, or impossible, for the pilot to either keep the aircraft under control or to execute mission tasks.

1.2.2 Fly-by-wire fault tolerant control

The main objective of an FBW system is to improve the natural flying qualities of the aircraft, i.e. stability and performance over a large flight envelope. In commercial passenger aircraft, design for performance consists of attaining ideal qualities for both the pilot and passengers. Control laws may be employed to satisfy these objectives—there are, however, constraints limiting the degree to which they can be achieved. These are discussed in detail in [23]. The physical limitation of the control surfaces must be considered in the design of the control law, e.g. the elevator of the B747 can only be deflected 17° up and 23° down at $37^\circ/\text{s}$. It is also required that the aircraft's closed-loop behaviour be consistent with the pilot's past training and experience. This implies that, for any control system architecture that is employed, the pilot must not be presented with an aircraft that is significantly different from a conventionally controlled mechanical system. These constraints therefore limit the choice of control techniques that may be implemented on this class of aircraft.

The current FBW control laws for both Airbus and Boeing (inner-loop controllers) are based on the classical PID structure [4],[23]. Robustness of the control laws is ensured by allowing a sufficient stability margin in the design [24]. It is known from control theory that the larger the phase margin is, the better the system's ability to retain stability

in the presence of disturbances and structural changes. The objective of this study is to investigate and evaluate robustness of the PID structure against tail damage. The resulting analysis provides a baseline for comparison with alternative design techniques that focus primarily on robustness. Robust control methods popularly used on aircraft systems include adaptive control, dynamic inversion, and optimisation techniques.

In Ref [25] model reference adaptive control (MRAC) is compared to LQR optimisation for robustness against actuator faults on a B747. The adaptive controller provides good performance, whilst the aircraft with an optimal LQR controller oscillates as a fault occurs and tends towards instability as the fault size increases. In the direct MRAC approach a comparison is made between the ideal model and the actual plant, the error is then feedback as an input to the adaptive law [26]. This law modifies the controller to drive the actual plant to give an output equal to the reference model output. Indirect adaptive laws consists of online parameter estimation, and based on this perceived plant, controller parameters are modified to compute an input to the actual plant that will give the desired output. This approach is used in the studies [27], [28] for robustness against actuator failures in flight control. In Ref [29] a hybrid direct-indirect adaptive control method is used to achieve robustness for wing and tail damage on the NASA generic transport aircraft. From the design constraints stated in this section the aircraft's closed-loop behaviour presented to the pilot must be consistent with his experience. Since the adaptive control law varies in-flight in relation to damage, it is clear that this cannot be guaranteed.

The implementation of dynamic inversion in flight control systems is explored in [30], [31], [32]. This method is based on the cancellation of undesirable dynamics, e.g. nonlinearities. The main disadvantage of dynamic inversion is that due to its open-loop nature, its effectiveness is highly dependent on the accuracy of the model.

The robustness of optimisation control strategies is investigated in [10],[20],[33]. In Ref [33], the author compares an H_2 and H_∞ controller against severe wind gust on a flexible aircraft. The techniques are implemented on a vertical acceleration controller to reduce transient peak loads resulting from the gust. H_∞ control was proven to meet the design performance objectives whilst requiring reasonably small actuator deflection. H_2 and H_∞ techniques implement optimisation strategies to find a control input to drive the

objective function to a minimum which satisfies the norm specification. Intuitively, the greater the number of inputs and feedback states provided to the controller, the greater the efficiency in meeting design objectives. The FBW system forms the inner loop of the aircraft's control system and, therefore, full state feedback is not suitable since some states are required for outer loop systems.

Although these techniques are not directly usable as FBW inner loop controllers, the method may be used to investigate a control strategy to achieve similar objectives. An example of this approach is seen in [21]. Optimal control theory is used to find possible control strategies for an aircraft with vertical tail damage and loss of primary control system. Manoeuvres such as landing and heading change are simulated and an observation made on the control and state variables. The author concludes that in the absence of a vertical tail the controller uses differential thrust to control heading. A similar approach is employed in this study; an H_2 optimal full state feedback controller is synthesised for the large transport aircraft. An analysis of the controller's parameters is made to ascertain the main states and control inputs that minimise the H_2 norm of the system.

1.3 Original Contributions

1. The change in aircraft dynamics due to horizontal tail damage is analysed in a method that provides visibility to the trim and manoeuvre capabilities of the damaged aircraft.
2. An evaluation of the robustness of a generic FBW system against tail damage on a large transport aircraft. Results of the robustness analysis are published in the *Aeronautical Journal* article [34].
3. A concise presentation of degradation in the aircraft's handling qualities due to tail damage.
4. An optimisation approach to analysing disturbance rejection capabilities of an aircraft with available actuators through a more robust combination of feedback states.
5. Framing the complexities of multi-mode FBW design as a robust control optimisation problem under horizontal stabiliser damage.

6. A novel fly-by-wire control law that ensures stability of longitudinal poles and acceptable handling qualities after 50% stabiliser loss.
7. Insight to limiting factors to the improvement of robustness for the class of large transport aircraft.

1.4 Thesis Overview

This thesis is divided into 2 sections. The first section is focused on an investigation of the effects of tail damage on flight dynamics and robustness of the current commercial aircraft FBW system against the resulting change in behaviour. The second section consists of the study of a control scheme to improve the FBW's robustness whilst adequately satisfying the stringent design constraints. In chapter 2 an analysis is carried out to identify the changes on aircraft dynamics after damage. A discussion on the modelling of damaged aircraft is presented and an outline of the experiment that was carried out. The change in static and dynamic stability that was observed and its implications on the controllability of the aircraft are discussed.

Chapter 3 is focused on the FBW aircraft. First a detailed design of a typical FBW system is discussed. The closed-loop aircraft is then analysed under damage conditions and a comparison made with the open-loop aircraft of chapter 2. A conclusion on the robustness of the system is presented and an evaluation of change in handling qualities is made. In chapter 4, fundamentals of modern robust control techniques for MIMO systems are presented. The H_2 control problem is defined and a calculus of variations approach as a solution for optimisation problems is discussed. Chapter 5 discusses the solution of the optimisation problem as a linear matrix inequality (LMI). An introduction to convex optimisation and the use of the interior point method to solve LMIs are presented.

In chapter 6 an analysis of the optimal controller parameters is provided and based on the results, a suitable control strategy for robustness is presented. Chapter 7 entails the conclusion and a summary of results obtained from the study. Finally, further research advancing from this study is presented.

Chapter 2

Flight Dynamics Change under Horizontal Tail Damage

This chapter details an analysis of how aircraft behaviour is changed by in-flight damage to the horizontal stabiliser. Firstly, an overview of the problem and expected change to aircraft behaviour is presented, followed by details of the study that was carried out to investigate these changes. A discussion of equations of motion for damaged aircraft and aerodynamic modelling is provided. The results obtained in the test, as well as an analysis of changes in static stability, dynamic stability, and coupling of lateral and longitudinal modes, are presented. Also detailed is an investigation of the trimmability of the damaged aircraft with remaining control surfaces.

2.1 Problem overview

Whilst an aircraft's wings are the primary lifting surfaces and govern lateral motion, the vertical tail determines directional behaviour and the horizontal tail sets its longitudinal characteristics. Generally, aircraft with relatively large horizontal tail volume have a greater degree of longitudinal stability than aircraft with smaller tail volume. It is, therefore, inevitable that tail loss will reduce the stability. In the derivation of aircraft equations of motion, due to its symmetric design it is often assumed that if angular motion is restricted to small angles then the lateral, directional and longitudinal modes can be separated. In the case that the stabiliser damage is asymmetric it may be expected that these modes will couple into each other.

The static margin is the distance between the aircraft's CG and aerodynamic centre (also referred to as the neutral point). As discussed in the literature review in chapter 1, the static margin is reduced proportionally to tail surface area loss. Under trim conditions the reduction in static margin induces a pitching moment; thus, elevator control is required to counter the resultant motion. In the case of spanwise damage, part of the elevator will be assumed to be lost and, hence, there will be a reduction in available control moment. Depending on the aircraft's nominal proportion of elevator/stabiliser ratio, it is possible for the aircraft to have an acceptable static margin after damage, yet insufficient elevator for controllability of the aircraft. Due to the loss of symmetry a rolling and yawing moment is expected to result from the damage. Similarly the induced moments may be larger than what the control moment from the ailerons and rudder can counter.

The short period mode oscillation is a transient motion after a disturbance in pitch angle. It manifests itself as an up/down oscillation about the CG that reduces in amplitude and eventually settles if the aircraft is longitudinally stable. Stability of the short period mode is largely dependent on the horizontal tail. A similar analogy to the effects of the tail to the aircraft is that of a mass spring and damper system. The spring stiffness effect is analogous to the tail's tendency to align with the airflow. A logical observation is that a reduction in tail span would therefore reduce the equivalent spring stiffness (restoration) effect, resulting in reduced dynamic stability.

If symmetry is lost as a result of damage, the aircraft's lateral dynamic mode may be expected to change. The Dutch roll is a yaw transient motion that couples into roll. Yaw restoration occurs in an aerodynamic spring-like effect determined primarily by the relative vertical fin size. Differential lift and drag over the forward moving and aft moving wings result in a roll restoring moment which lags the yawing moment by 90° . The delayed roll response results in the forward moving wing to induce more lift than the aft moving wing. If this mode is stable, it eventually settles to a steady state. Due to the additional lateral moment induced by tail damage, this mode may take longer to settle, i.e. its damping may be increased and frequency decreased.

Manoeuvring is deemed as changing from one trim position to another by accelerating in a desired direction. This is achieved by modification of the wing lift vector, e.g. when carrying out a left turn the aircraft lift vector would change from being vertical

to having a horizontal component in the direction of the turn. To maintain the same forward speed, the additional lift has to be compensated for with an increased angle of attack. Manoeuvrability analysis consists of an evaluation of how much additional pitch is required to sufficiently increase the angle of attack for the aircraft to be "pulled up" or "pushed over" [35]. Since the horizontal stabiliser is required to pitch the aircraft, it is possible that after damage the aircraft has stable static and dynamic modes and sufficient controllability to trim, but is not manoeuvrable. The test detailed in the following sections was carried out to investigate the change in flight dynamics (trim, dynamic stability, controllability, and manoeuvrability) of the aircraft after tail damage.

2.2 Experiment Setup

From studies presented in [36] [16], structural damage may change an aircraft's centre of mass, aerodynamic characteristics, and inertial properties. The main focus of damage modelling is, therefore, an investigation into the changes of these parameters. The derivation of the six degrees of motion for a conventional aircraft is discussed in [35] [37]. The CG is assumed to be fixed, although in practice it varies as the aircraft's weight is reduced as it sheds fuel in-flight. Since this change is gradual and limited to a relatively small weight difference in comparison to the aircraft's total weight, this assumption is acceptable. It is also assumed that the aircraft is symmetric about the xz plane and that the mass is uniformly distributed; hence the products of inertia $I_{xy} = I_{yz} = 0$. After an aircraft suffers tail damage, it loses part of its mass and the CG is shifted. When the CG position is changed the inertial composition may change as well since it is a function of mass distribution about the CG. The preceding assumptions produce a less accurate mathematical model of the aircraft after tail damage. A more accurate model is presented in [36]. It is based on selecting an alternative point as a reference point, such as the aerodynamic centre instead of the CG, then track the motion of the CG with reference to the fixed reference point. The mass and inertia in the asymmetric aircraft force and moment equations are correctly calculated by subtracting the mass and inertia of the separated piece.

Boeing 747 aircraft data are widely used in dynamics and control studies of large transport aircraft. It is therefore used in this study to enable comparison with similar research. If

it is assumed that aerodynamic tail surfaces are to be partially removed, then the effect of change in moment of inertia and mass on the dynamic behaviour of a huge B747 is relatively small [18], [20]. The primary effects are aerodynamic in nature. A reduction in rear weight due to tail loss, results in a forward centre of gravity shift which in turn increases the stability margin. By assuming a fixed CG position an underestimation is made on the actual static stability. This error is considered small and insignificant. The stabiliser loss is modelled as smooth and straight break lines as shown in Fig.2.1. In practice irregular edges would be formed, resulting in effects such as increased drag and lateral motion. These non-linear effects are considered to be outside the scope of this study. The stabiliser size is reduced in chordwise cuts along the span at intervals of 10% from 0% to 50% as illustrated in Fig. 2.1.

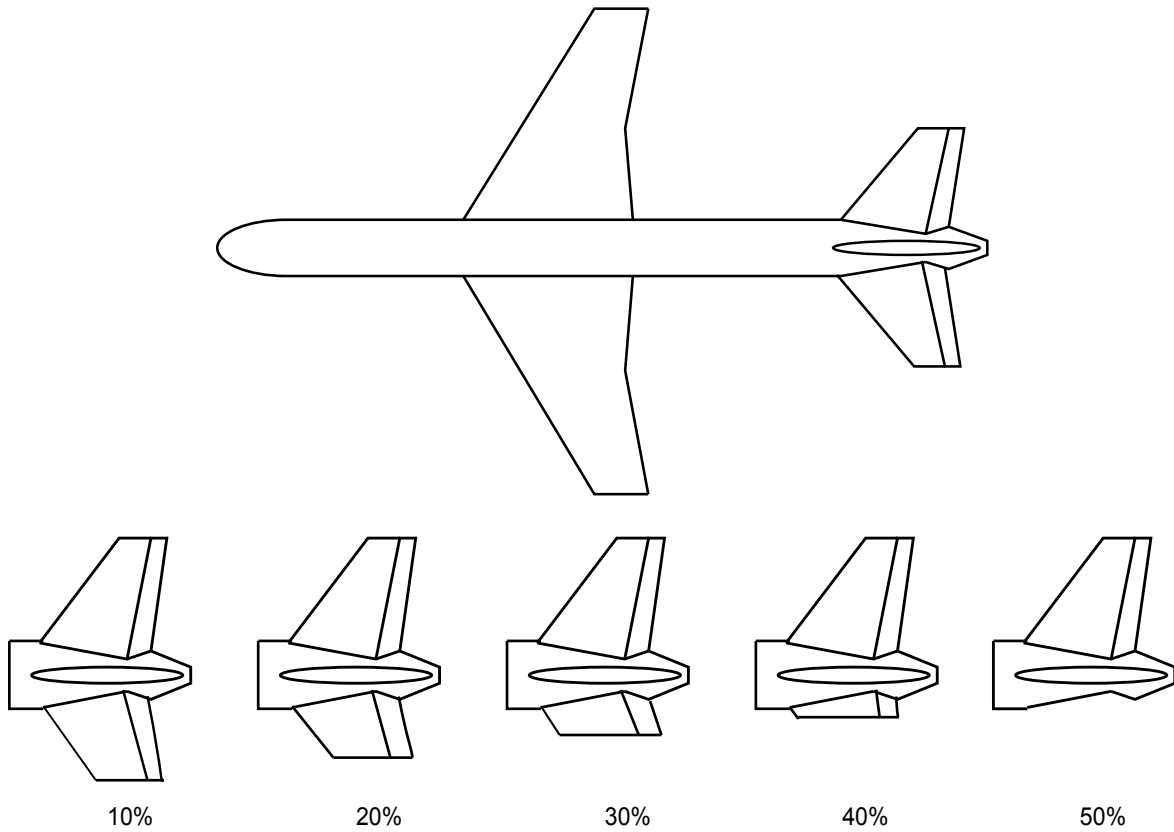


Figure 2.1: Horizontal stabiliser damage from 10% to 50%

2.2.1 Equations of motion for damaged aircraft

An aircraft can be mathematically modelled by representing it as a point mass centred around the CG as well as considering the motion of the airframe around the CG. The

six-degrees-of-freedom aircraft model consists of 3 translational and 3 rotational equations relating the aircraft's motion resulting from thrust, gravitational, and aerodynamic disturbances. The effect of atmospheric disturbance will not be considered in this study. A rigid aircraft is assumed, i.e. each mass component is fixed in relation to the body axis. Three axes systems are used in the derivation of equations of motion. These are defined as follows:

- Inertial axis system: Newton's law is valid only in this frame, the equations are therefore determined in inertial plane. The earth's axis system is typically used as the inertial frame for aircraft. A reference point on the earth's surface is considered the origin of a right-handed orthogonal axes system xyz , x points to the north, y to the east and z points down along the gravity vector.
- Body axis system: The origin of this frame lies on the CG of the airframe, x is towards the nose, y points towards the starboard wing and z completes the right-handed orthogonal axes system.
- Wind axis system: This reference frame has its origin at the aircraft's centre of mass. The wind vector lies on the x axis, the z axis is orthogonal to x and lies in the aircraft's plane of symmetry. For an aircraft at level flight where α and β is zero the wind axis lies on the body axis.

2.2.1.1 Translational Equations

The translational equations are derived by realising Newton's second law of motion for longitudinal, lateral, and directional forces acting on the aircraft [38]. This relationship is shown by Eq 2.1 where V_T is the velocity vector $[u \ v \ w]$ corresponding to the aircraft's motion along xyz in body reference frame.

$$F = \frac{\partial(mV_T)}{\partial t}|_I \quad (2.1)$$

Equation 2.2 relates the derivative of the velocity vector in inertial frame to its derivative in body frame as presented in Appendix A. By substituting 2.2 in Eq 2.1 and considering the assumption that mass is constant the Newton equation in inertial space can be written as shown by Eq 2.3.

$$\frac{\partial V_T}{\partial t}|_I = \frac{\partial V_T}{\partial t}|_B + \omega \times V_T \quad (2.2)$$

$$\mathbf{F} = m \left(\frac{\partial \mathbf{V}_T}{\partial t} \Big|_B + \boldsymbol{\omega} \times \mathbf{V}_T \right) \quad (2.3)$$

The translational and angular velocity vectors for the xyz axes can be written as seen in Eq 2.4 and Eq 2.5 respectively. If these are substituted into Eq 2.3 as shown by Eq 2.6 and Eq 2.7 the 3 translational equations of motion for the aircraft obtained are depicted by Eq 2.8.

$$\mathbf{V}_T = ui + vj + wk \quad (2.4)$$

$$\boldsymbol{\omega} = pi + qj + rk \quad (2.5)$$

$$\mathbf{F} = m \left(\dot{u}i + \dot{v}j + \dot{w}k + \begin{vmatrix} i & j & k \\ p & q & r \\ u & v & w \end{vmatrix} \right) \quad (2.6)$$

$$\mathbf{F} = m [(\dot{u} + qw - rv)i + (\dot{v} + ru - pw)j + (\dot{w} + pv - qu)k] \quad (2.7)$$

$$F_x = m(\dot{u} + qw - rv)$$

$$F_y = m(\dot{v} + ru - pw) \quad (2.8)$$

$$F_z = m(\dot{w} + pv - qu)$$

It is common practice to conveniently express the terms $[u \ v \ w]$ as $[V \ \alpha \ \beta]$ in the translational equations. The association of these two vectors is illustrated in Fig 2.2. Equations 2.10 and 2.11 show the trigonometric relationship between the velocity vectors w, v and the angle α, β respectively. Small angle approximation is used to linearise the equation, such that they can be conveniently substituted into Eq 2.8.

$$V_T = \sqrt{u^2 + v^2 + w^2} \quad (2.9)$$

$$\begin{aligned} \sin \alpha &= \frac{w}{V_T \cos \beta} \\ \alpha &\approx \frac{w}{V_T} \end{aligned} \quad (2.10)$$

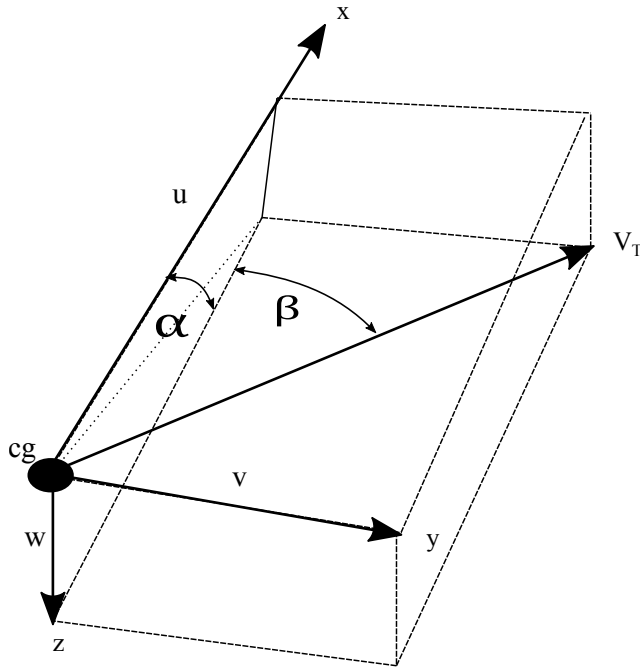


Figure 2.2: Velocity components illustrating orientation of α and β in the body frame

$$\begin{aligned}\sin \beta &= \frac{v}{V_T} \\ \beta &\approx \frac{v}{V_T}\end{aligned}\tag{2.11}$$

2.2.1.2 Rotational Equations

Equations describing the rotational motions of an aircraft are derived from Newton's moment equation, 2.12. It is, however, only applicable if both angular momentum H and moment M are in inertial reference frame. The equation for angular momentum is shown by Eq 2.13, r is the distance from the centre of rotation, m is the rotating mass, and V_m is the velocity as illustrated in Fig 2.3.

$$M = \left. \frac{\partial H}{\partial t} \right|_I \tag{2.12}$$

$$H = rmV_m \tag{2.13}$$

Since H must be expressed in inertial frame, the rate of change of r (i.e V_m) is expanded using the relationship of Eq 2.2. By assuming that r is not changing with time ($\dot{r} = 0$)

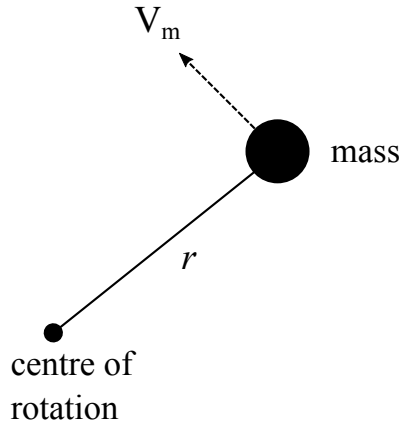


Figure 2.3: Angular momentum

and making a substitution of Eq 2.14 into Eq 2.13, the angular momentum can be expressed as shown by Eq 2.15

$$\begin{aligned} V_m &= \frac{\partial r}{\partial t} \Big|_I \\ V_m &= \frac{\partial r}{\partial t} \Big|_B + \omega \times r \end{aligned} \quad (2.14)$$

$$H = m(r \times \omega \times r) \quad (2.15)$$

Figure 2.3 depicts the angular momentum of a point mass, since this representation is not a realistic model of an aircraft a more accurate model can be obtained by integrating the mass density over the entire aircraft volume as shown by Eq 2.16.

$$H = \int_v \rho [r \times \omega \times r] \partial v \quad (2.16)$$

By substituting for the vectors r and ω (Eq 2.17 and Eq 2.5 respectively) in Eq 2.16 the angular momentum can be computed as shown by Eq 2.18 - Eq 2.21

$$r = xi + yj + zk \quad (2.17)$$

$$\omega \times r = \begin{vmatrix} i & j & k \\ p & q & r \\ x & y & z \end{vmatrix} \quad (2.18)$$

$$\omega \times r = (qz-ry) i + (rx-pz) j + (py-qx) k \quad (2.19)$$

$$H = \int_v \rho \begin{vmatrix} i & j & k \\ x & y & z \\ (qz-ry) & (rx-pz) & (py-qx) \end{vmatrix} \partial v \quad (2.20)$$

$$\begin{aligned} H_x &= p \int_v \rho (y^2 + z^2) \partial v - q \int_v \rho xy \partial v - r \int_v \rho xz \partial v \\ H_y &= q \int_v \rho (z^2 + x^2) \partial v - r \int_v \rho yz \partial v - p \int_v \rho xy \partial v \\ H_z &= r \int_v \rho (x^2 + y^2) \partial v - p \int_v \rho xz \partial v - q \int_v \rho yz \partial v \end{aligned} \quad (2.21)$$

Considering the definitions of inertia presented in Appendix A, the angular momentum equations for rotation around each of the 3 axes can be written as shown by Eq 2.22

$$\begin{aligned} H_x &= pI_{xx} - qI_{xy} - rI_{xz} \\ H_y &= qI_{yy} - rI_{yz} - pI_{xy} \\ H_z &= rI_{zz} - pI_{xz} - qI_{yz} \end{aligned} \quad (2.22)$$

The aircraft is symmetric on the xz plane, $I_{xy} = I_{zy} = 0$. Hence,

$$H = (pI_{xx} - rI_{xz})i + qI_{yy}j + (rI_{zz} - pI_{xz})k \quad (2.23)$$

If the momentum equations are substituted into Eq 2.12 and considering the expansion on Eq 2.2, the moment equations can be calculated as shown by Eq 2.24 - Eq 2.26.

$$M = \dot{H}_x i + \dot{H}_y j + \dot{H}_z k + \begin{vmatrix} i & j & k \\ p & q & r \\ H_x & H_y & H_z \end{vmatrix} \quad (2.24)$$

$$M = (\dot{p}I_{xx} - \dot{r}I_{xz})i + (\dot{q}I_{yy})j + (\dot{r}I_{zz} - \dot{p}I_{xz})k + \begin{vmatrix} i & j & k \\ p & q & r \\ \dot{p}I_{xx} - \dot{r}I_{xz} & \dot{q}I_{yy} & \dot{r}I_{zz} - \dot{p}I_{xz} \end{vmatrix} \quad (2.25)$$

$$\begin{aligned} M_x &= \dot{p}I_{xx} + qr(I_{zz} - I_{yy}) - (\dot{r} + pq)I_{xz} \\ M_y &= \dot{q}I_{yy} - pr(I_{zz} - I_{xx}) - (p^2 - r^2)I_{xz} \\ M_z &= \dot{r}I_{zz} + pq(I_{yy} - I_{xx}) - (qr - \dot{p})I_{xz} \end{aligned} \quad (2.26)$$

The cross product of inertia I_{xz} is typically small and negligible for conventional aircraft, if this assumption is applied to Eqs 2.26, the moment equations can be presented as shown by Eqs 2.27 where $[L M N]$ are the moments in xyz .

$$\begin{aligned}\frac{L}{I_{xx}} &= \dot{p} + \frac{I_{zz} - I_{yy}}{I_{xx}}qr \\ \frac{M}{I_{yy}} &= \dot{q} + \frac{I_{xx} - I_{zz}}{I_{yy}}pr \\ \frac{N}{I_{zz}} &= \dot{r} + \frac{I_{yy} - I_{xx}}{I_{zz}}pq\end{aligned}\quad (2.27)$$

2.2.1.3 Forces and Moments

The equations discussed in the previous subsections are a mathematical description of the aircraft's response to disturbance forces and moments. This section entails a discussion on the factors that contribute to these forces and how they are suitably modelled to be substituted into the rotational and translational equations. Aerodynamics, gravitation, and propulsion are the forces that affect the aircraft's motion.

Gravitation - Gravity is an inertial force that acts along the normal axis of the aircraft. Its model is derived by rotating the gravitational vector (mg) into the body axis airframe using the DCM matrix discussed in Appendix A. Equation 2.28 is the gravitational force vector representation used in the motion equations. Since the CG coincides with the CM the moment produced by gravitational force is zero.

$$\mathbf{F}_g = \begin{bmatrix} -\sin \theta \\ \cos \theta \sin \phi \\ \cos \theta \cos \phi \end{bmatrix} mg \quad (2.28)$$

Aerodynamics - When a trimmed aircraft experiences a disturbance its aerodynamic balance is distorted and as a result the motion variables in the equations change. To attain a comprehensive model of this change it is assumed that only the variables and their derivatives contribute to the total aerodynamic forces and moments. This is mathematically presented as a sum of the Taylor series of each variable. Since the variables are small, considering only the first derivative provides a reasonable estimation. Equations Eq 2.30 - Eq 2.35 are the mathematical representation of the normalised aerodynamic force and moment equations (for better readability the notation C_{ab} is used instead of

$\frac{\partial C_a}{\partial b}$). Drag is considered to be the only aerodynamic force acting along the x-axis. The total drag is a sum of parasitic and induced drag.

$$C_D = C_{D0} + C_L^2/\pi Ae \quad (2.29)$$

$$C_x = -C_D \quad (2.30)$$

$$C_y = C_{y\alpha}\alpha + C_{y\beta}\beta + \frac{b}{2V}C_{yp}p + \frac{\bar{c}}{2V}C_{yq}q + \frac{b}{2V}C_{yr}r + C_{y\delta E}\delta E + C_{y\delta R}\delta R + C_{y\delta A}\delta A \quad (2.31)$$

$$C_z = C_{L0} + C_{L\alpha}\alpha + C_{L\beta}\beta + \frac{b}{2V}C_{Lp}p + \frac{\bar{c}}{2V}C_{Lq}q + \frac{b}{2V}C_{Lr}r + C_{L\delta E}\delta E + C_{L\delta R}\delta R + C_{L\delta A}\delta A \quad (2.32)$$

$$C_l = C_{l\alpha}\alpha + C_{l\beta}\beta + \frac{b}{2V}C_{lp}p + \frac{\bar{c}}{2V}C_{lq}q + \frac{b}{2V}C_{lr}r + C_{l\delta E}\delta E + C_{l\delta R}\delta R + C_{l\delta A}\delta A \quad (2.33)$$

$$C_m = C_{m\alpha}\alpha + C_{m\beta}\beta + \frac{b}{2V}C_{mp}p + \frac{\bar{c}}{2V}C_{mq}q + \frac{b}{2V}C_{mr}r + C_{m\delta E}\delta E + C_{m\delta R}\delta R + C_{m\delta A}\delta A \quad (2.34)$$

$$C_n = C_{n\alpha}\alpha + C_{n\beta}\beta + \frac{b}{2V}C_{np}p + \frac{\bar{c}}{2V}C_{nq}q + \frac{b}{2V}C_{nr}r + C_{n\delta E}\delta E + C_{n\delta R}\delta R + C_{n\delta A}\delta A \quad (2.35)$$

Since the centre of rotation is not collocated with the centre of lift on the wings, an angle of incident is induced. The aerodynamic angular rates p, q, r are thus more accurately written as $\frac{b}{2V}p$, $\frac{\bar{c}}{2V}q$ and $\frac{b}{2V}r$. The subject of induced angles of incidence is discussed in details in appendix A.

Various aerodynamic modelling techniques are used to compute the stability and control derivatives in equations Eq 2.30 to Eq 2.35. The derivatives are commonly presented as normalised non-dimensional coefficients independent of the aircraft's geometry and flight conditions. The specific forces and moments can be calculated from the generalised coefficients by considering geometry and atmospheric conditions as shown by Eq 2.36 – 2.41, q is dynamic pressure, S, b, \bar{c} are the wing area, wing span, and mean aerodynamic chord respectively.

$$X_a = qSC_x \quad (2.36)$$

$$Y_a = qSC_y \quad (2.37)$$

$$Z_a = qSC_z \quad (2.38)$$

$$L_a = qSbC_l \quad (2.39)$$

$$M_a = qS\bar{c}C_m \quad (2.40)$$

$$N_a = qSbC_n \quad (2.41)$$

Since aerodynamic coefficients are measured/calculated in the wind reference frame, they must be rotated into the body axis frame to be used in the equations of motion. Eq 2.36 – 2.41 are multiplied by the inverse DCM in Appendix A to rotate them into the body axis through α and β .

Propulsion - The B747 propulsion system consists of 4 jet engines; 2 on each wing. Under normal operation these produce a thrust force along the aircraft's x-axis. For the purpose of this study the simple first order lag model of Eq 2.42 is considered an acceptable representation of the thrust force. T_c is the commanded thrust and τ is the time lag.

$$\dot{T} = \frac{1}{\tau}T + \frac{1}{\tau}T_c \quad (2.42)$$

Attitude rates - Also included in the state space representation of the aircraft's motion are the attitude rates in the inertial reference frame. These are computed by rotating the body angular velocities $[p \ q \ r]$ as seen in equation 2.28.

$$\begin{bmatrix} \dot{\phi} \\ \dot{\theta} \\ \dot{\psi} \end{bmatrix} = \begin{bmatrix} 1 & \sin \phi \tan \theta & \sin \phi \cos \theta \\ 0 & \cos \phi & -\sin \phi \\ 0 & \sin \phi \sec \theta & \cos \phi \sec \theta \end{bmatrix} \begin{bmatrix} p \\ q \\ r \end{bmatrix} \quad (2.43)$$

The forces and moments are substituted into the equation of motion Eq 2.8 and Eq 2.27 and written in the state space representation:

$$\begin{aligned} \dot{x} &= Ax + Bu \\ y &= Cx \end{aligned} \quad (2.44)$$

The 8 x 8 state equation is shown by Eq 2.45 where $V_T = V$.

$$\begin{bmatrix} \dot{V} \\ \dot{\alpha} \\ \dot{q} \\ \dot{\theta} \\ \dot{\beta} \\ \dot{p} \\ \dot{r} \\ \dot{\phi} \end{bmatrix} = \begin{bmatrix} \frac{\partial \dot{V}}{\partial V} & \frac{\partial \dot{V}}{\partial \alpha} & \frac{\partial \dot{V}}{\partial q} & \frac{\partial \dot{V}}{\partial \theta} & \frac{\partial \dot{V}}{\partial \beta} & \frac{\partial \dot{V}}{\partial p} & \frac{\partial \dot{V}}{\partial r} & \frac{\partial \dot{V}}{\partial \phi} \\ \frac{\partial \dot{\alpha}}{\partial V} & \frac{\partial \dot{\alpha}}{\partial \alpha} & \frac{\partial \dot{\alpha}}{\partial q} & \frac{\partial \dot{\alpha}}{\partial \theta} & \frac{\partial \dot{\alpha}}{\partial \beta} & \frac{\partial \dot{\alpha}}{\partial p} & \frac{\partial \dot{\alpha}}{\partial r} & \frac{\partial \dot{\alpha}}{\partial \phi} \\ \frac{\partial \dot{q}}{\partial V} & \frac{\partial \dot{q}}{\partial \alpha} & \frac{\partial \dot{q}}{\partial q} & \frac{\partial \dot{q}}{\partial \theta} & \frac{\partial \dot{q}}{\partial \beta} & \frac{\partial \dot{q}}{\partial p} & \frac{\partial \dot{q}}{\partial r} & \frac{\partial \dot{q}}{\partial \phi} \\ \frac{\partial \dot{\theta}}{\partial V} & \frac{\partial \dot{\theta}}{\partial \alpha} & \frac{\partial \dot{\theta}}{\partial q} & \frac{\partial \dot{\theta}}{\partial \theta} & \frac{\partial \dot{\theta}}{\partial \beta} & \frac{\partial \dot{\theta}}{\partial p} & \frac{\partial \dot{\theta}}{\partial r} & \frac{\partial \dot{\theta}}{\partial \phi} \\ \frac{\partial \dot{\beta}}{\partial V} & \frac{\partial \dot{\beta}}{\partial \alpha} & \frac{\partial \dot{\beta}}{\partial q} & \frac{\partial \dot{\beta}}{\partial \theta} & \frac{\partial \dot{\beta}}{\partial \beta} & \frac{\partial \dot{\beta}}{\partial p} & \frac{\partial \dot{\beta}}{\partial r} & \frac{\partial \dot{\beta}}{\partial \phi} \\ \frac{\partial \dot{p}}{\partial V} & \frac{\partial \dot{p}}{\partial \alpha} & \frac{\partial \dot{p}}{\partial q} & \frac{\partial \dot{p}}{\partial \theta} & \frac{\partial \dot{p}}{\partial \beta} & \frac{\partial \dot{p}}{\partial p} & \frac{\partial \dot{p}}{\partial r} & \frac{\partial \dot{p}}{\partial \phi} \\ \frac{\partial \dot{r}}{\partial V} & \frac{\partial \dot{r}}{\partial \alpha} & \frac{\partial \dot{r}}{\partial q} & \frac{\partial \dot{r}}{\partial \theta} & \frac{\partial \dot{r}}{\partial \beta} & \frac{\partial \dot{r}}{\partial p} & \frac{\partial \dot{r}}{\partial r} & \frac{\partial \dot{r}}{\partial \phi} \\ \frac{\partial \dot{\phi}}{\partial V} & \frac{\partial \dot{\phi}}{\partial \alpha} & \frac{\partial \dot{\phi}}{\partial q} & \frac{\partial \dot{\phi}}{\partial \theta} & \frac{\partial \dot{\phi}}{\partial \beta} & \frac{\partial \dot{\phi}}{\partial p} & \frac{\partial \dot{\phi}}{\partial r} & \frac{\partial \dot{\phi}}{\partial \phi} \end{bmatrix} \begin{bmatrix} V \\ \alpha \\ q \\ \theta \\ \beta \\ p \\ r \\ \phi \end{bmatrix} + \begin{bmatrix} \frac{\partial \dot{V}}{\partial \delta e} & \frac{\partial \dot{V}}{\partial T} & \frac{\partial \dot{V}}{\partial \delta a} & \frac{\partial \dot{V}}{\partial \delta r} \\ \frac{\partial \dot{\alpha}}{\partial \delta e} & \frac{\partial \dot{\alpha}}{\partial T} & \frac{\partial \dot{\alpha}}{\partial \delta a} & \frac{\partial \dot{\alpha}}{\partial \delta r} \\ \frac{\partial \dot{q}}{\partial \delta e} & \frac{\partial \dot{q}}{\partial T} & \frac{\partial \dot{q}}{\partial \delta a} & \frac{\partial \dot{q}}{\partial \delta r} \\ \frac{\partial \dot{\theta}}{\partial \delta e} & \frac{\partial \dot{\theta}}{\partial T} & \frac{\partial \dot{\theta}}{\partial \delta a} & \frac{\partial \dot{\theta}}{\partial \delta r} \\ \frac{\partial \dot{\beta}}{\partial \delta e} & \frac{\partial \dot{\beta}}{\partial T} & \frac{\partial \dot{\beta}}{\partial \delta a} & \frac{\partial \dot{\beta}}{\partial \delta r} \\ \frac{\partial \dot{p}}{\partial \delta e} & \frac{\partial \dot{p}}{\partial T} & \frac{\partial \dot{p}}{\partial \delta a} & \frac{\partial \dot{p}}{\partial \delta r} \\ \frac{\partial \dot{r}}{\partial \delta e} & \frac{\partial \dot{r}}{\partial T} & \frac{\partial \dot{r}}{\partial \delta a} & \frac{\partial \dot{r}}{\partial \delta r} \\ \frac{\partial \dot{\phi}}{\partial \delta e} & \frac{\partial \dot{\phi}}{\partial T} & \frac{\partial \dot{\phi}}{\partial \delta a} & \frac{\partial \dot{\phi}}{\partial \delta r} \end{bmatrix} \begin{bmatrix} \delta e \\ T \\ \delta a \\ \delta r \end{bmatrix} \quad (2.45)$$

2.2.2 Aerodynamic modelling for partial tail loss

As air flows over a moving aircraft, pressure and friction effects on the airframe surfaces generate forces and moments that act on it. Aerodynamic modelling pertains obtaining a mathematical model of these aerodynamic forces and moments—ideally in a suitable form that can be used in the equations of motion. Such a representation of the aerodynamic properties of the airframe is formulated from control and stability derivatives. There are several methods used to acquire a usable model for stability derivatives, these are discussed extensively in [35]. One method may give certain derivatives better estimation accuracy than another method, the choice of method to use depends on the application for which the overall equations are to be used. In the analytical method, forces and moments are calculated from first principle. Whilst this is the most convenient method in terms of cost and availability, it is not well suited for modelling non-linear behaviour because the derivatives are acquired through linearisation by assuming small disturbance angles about a trim point.

A preferable method when dealing with non-linearity is wind tunnel testing. A reduced scaled model of the aircraft is suspended in an air stream at various test velocities at different inclination angles and control surface configurations. A drawback of this technique is that it suffers from scaling errors since a model aircraft is used in the measurements and it is relatively expensive. An alternative approach that eliminates the issue of scaling

errors is flight test measurement. The actual aircraft is flown and the different dynamic modes are excited whilst measuring the parameters of interest. Based on the input–output response an estimate of the mathematical model of the aircraft is made. The control and stability derivatives are then obtained from this model. Although this is an established and well developed method it is not a suitable method for modelling aircraft damage in terms of cost, safety, and availability.

The semi-empirical method is an advancement of the analytical approach and provides improved accuracy. The theoretical calculations are modified with experimental data accumulated over many years and stored as a collection of volumes of documents. Interactive computer programmes based on this approach have been made available through which simple data on the aircraft's geometry and aerodynamics are required to calculate relatively accurate derivatives. These programmes are designed for conventional aircraft and accuracy may be questionable for non-conventional configurations. From the preceding discussion of the different methods of aerodynamic modelling it is evident that the most suitable method for resolving the modelling problem of this study is the analytical method. There is a wide range of software programmes that implement this approach, one such is the vortex lattice code.

2.2.2.1 Vortex lattice method

Linear aerodynamics pertains the study of motion of a profile (such as an airframe) when it flies through an airstream at low Mach numbers and small angles of attack. In this region pressure force is dominant and friction force may be considered less significant. When air flows through a cambered and or inclined wing the flow velocity increases at the upper surface and reduces at the lower surface. This results in a pressure difference between the two regions. The low pressure at the upper region and high pressure in the lower region results in upwards lift. At the wing tips, air from the high pressure region moves up to the low pressure region. This air combines with oncoming free stream air to form vortices at the wing tips [39]. An illustration is shown in Fig. 2.4.

Helmholtz's vortex theorems state [40]:

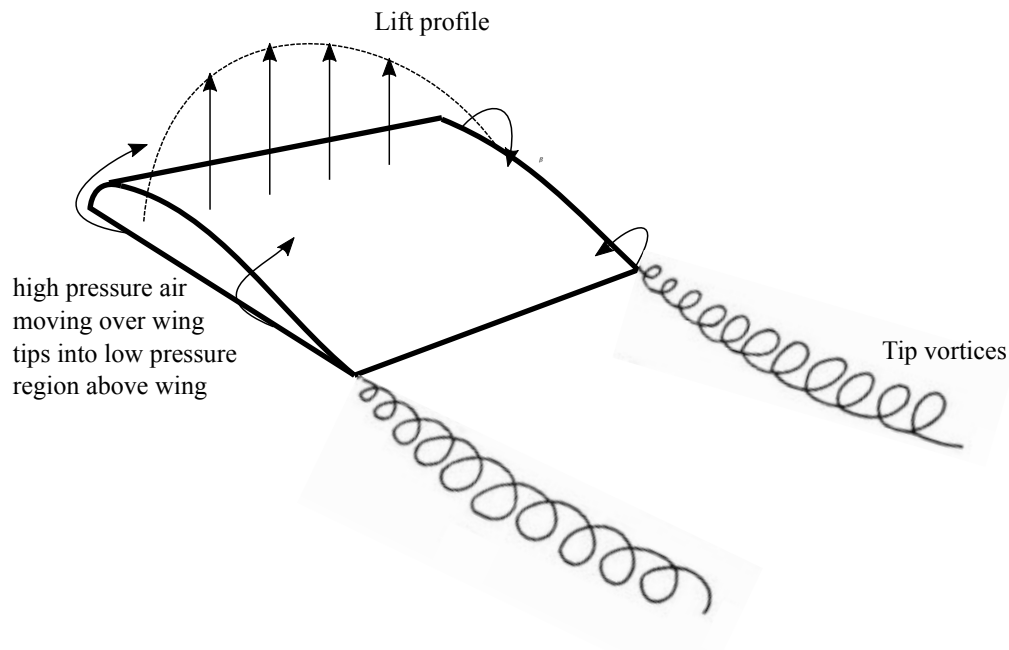


Figure 2.4: Wingtip vortex development

- The strength of the vortex τ is constant all along its length.
- The vortex cannot end inside the fluid. It must either extend to infinity, or end at a solid boundary, or form a closed loop.
- An initially irrotational, inviscid flow will remain irrotational.

In the vortex lattice method the flow field around a lifting surface is modelled as a horse shoe vortex in a free stream. The flow dynamics around the lifting surface are consistent with Helmholtz's theorem, i.e. the strength of the circulation is constant along the vortex line and the line extends downstream to infinity. Since the local lift/span across the entire span of the wing is not constant (it reduces towards the edges) a more accurate model is obtained by subdividing the wing into smaller panels and computing the elementary flow of each panel as illustrated in Fig. 2.5. This method is often used in the early stages of aircraft design to estimate the forces acting on lifting surfaces. It is a comparatively simple method to carry out an aerodynamic analysis of trim and dynamic stability properties for a given aircraft configuration. The classic vortex lattice method is concerned with the estimation of an aerodynamic model due to pressure forces, whilst the extended vortex lattice code is modified to consider compressibility in higher Mach regions. AVL is an extended vortex lattice code used in this study. It was first developed in 1988 at MIT

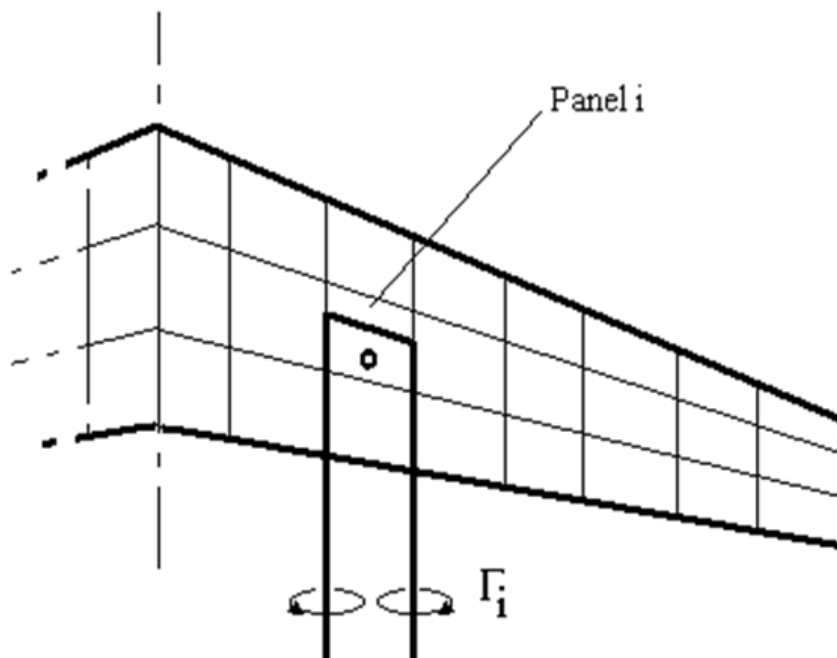


Figure 2.5: Wingspan illustrating modelling of panels as horseshoe vortices

and has since been modified over time to include a wider range of applications such as wing sweep, dihedral, fuselages etc.

Large commercial transport aircraft operate at both subsonic and transonic airspeeds. For compressibility effects, AVL uses the Pradtl–Glauert method to transform the model such that it is solvable by incompressible methods. The expected validity of the PG transformation is from Mach 0 to 0.6. Due to available data for trim configurations Mach 0.5 at 20 000ft was selected as the flight condition for this test. The trim angle of attack is 6.8° and the horizontal stabiliser is inclined at -0.8° . The coefficients from the Boeing report [41] are used directly for the case of 0% damage. An approximation of the change in coefficients is computed in AVL for tail damage from 10% to 50% and the change is deducted from the coefficients of the undamaged aircraft. The resulting damaged coefficients for the case of 40 % are shown in Table 2.1. The aircraft is modelled in AVL as illustrated in Fig. 2.6.

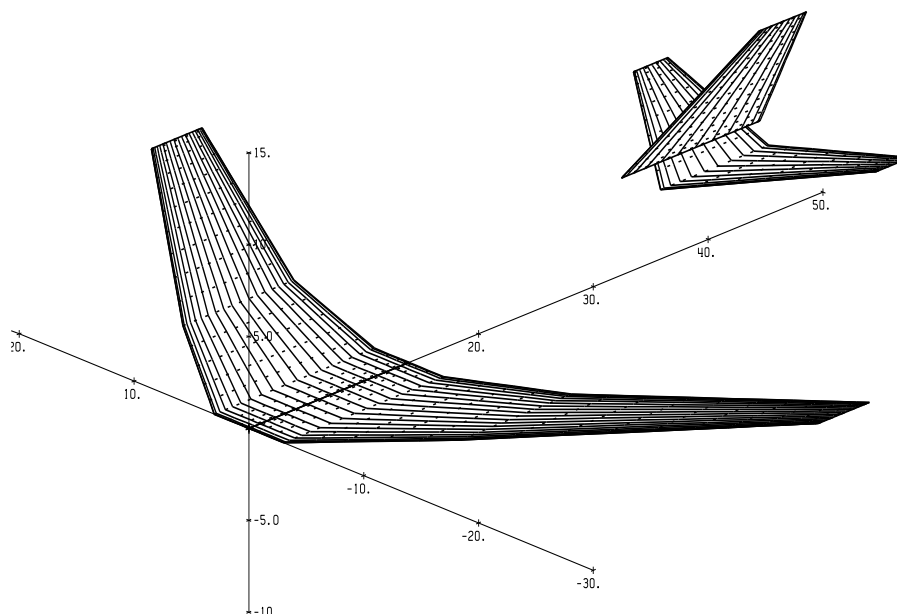


Figure 2.6: B747 AVL plot

2.3 Results and Discussion

2.3.1 Longitudinal and Lateral Coupling

The aerodynamic coefficients of the aircraft with 40% damage were obtained using AVL and compared with the undamaged aircraft coefficients to investigate the effect of tail damage on lateral and longitudinal coupling. These results are shown in Table 2.1. The lateral aerodynamic coefficients that contribute to longitudinal motion ($C_{l\beta}$, C_{Lp} , C_{Lr} , $C_{m\beta}$, C_{mp} , C_{mr}) are negligibly small for the conventional symmetric aircraft. With 40% stabiliser damage they do however become relatively significant. From this observation the longitudinal dynamics of the damaged aircraft will be influenced by lateral motion. Similarly the longitudinal coefficients contributing to lateral motion ($C_{y\alpha}$, C_{yq} , $C_{l\alpha}$, C_{lq} , $C_{n\alpha}$, C_{nq}) become significant after damage.

A comparison of the characteristic poles for the case of decoupled and coupled damaged models show the magnitude by which each dynamic mode is changed, specifically due to coupling of lateral and longitudinal motion. Fig. 2.7 shows the poles of the damaged aircraft with 40% stabiliser loss for the coupled and decoupled equations against the undamaged (0% damage) poles. Above 40% the behaviour of the open-loop aircraft completely changes due to instability, hence 40% was selected to investigate coupling effects.

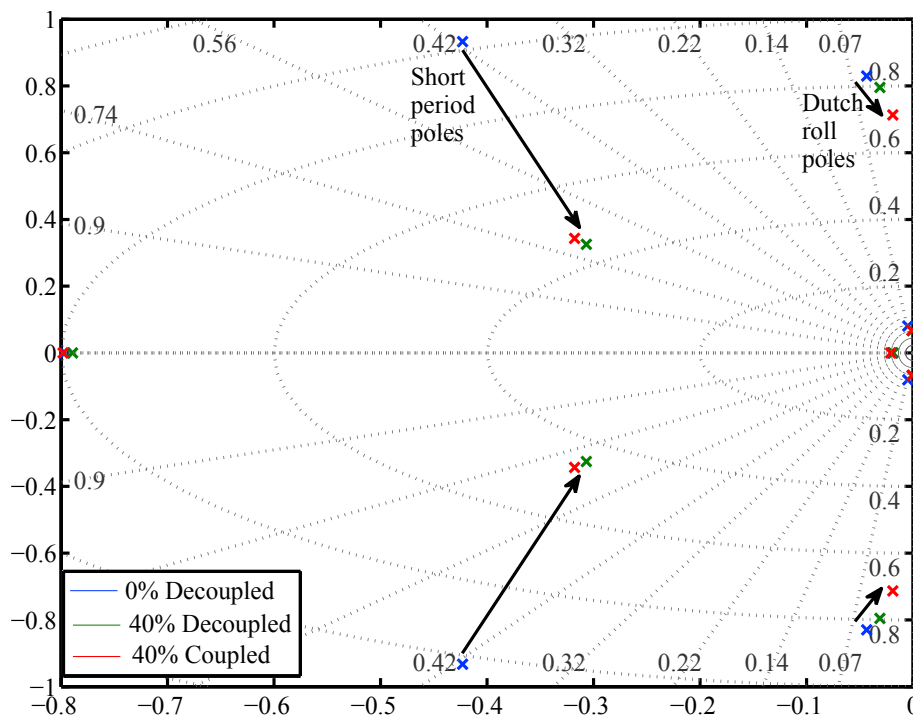


Figure 2.7: Poles of decoupled and coupled aircraft model

Dutch roll poles show a slight change due to damage and a more significant change due to longitudinal mode coupling. The damping ratio and frequency are reduced, resulting in less stability and a more sluggish response to the pilot's lateral inputs. Figures 2.8 and 2.9 are scaled images of Fig. 2.7 (scale 1:10) to show roll and spiral mode poles respectively. From Table 1 it can be observed that C_{lq} is increased by 18.13% with damage, this increases the total aerodynamic rolling moment. The resultant change in dynamics is evident in the roll mode poles moving towards the instability region and the time constant is increased by less than 0.02s. The spiral mode poles show an even smaller change than the roll mode poles. It is assumed that a lateral controller will be in place to limit lateral motion; thus, the coupling effect is considered as lateral disturbance and not included further in this analysis.

Equation 2.46 shows the short period frequency approximation [42]. The mode is greatly influenced by the value of $C_{m\alpha}$ and C_{mq} , from Table 2.1 it can be seen that these have the highest percentage change (85% and 53% respectively). As expected, the short period poles are primarily changed by horizontal stabiliser damage whilst the effect of lateral mode coupling is relatively small. The rest of this study is therefore based on the decou-

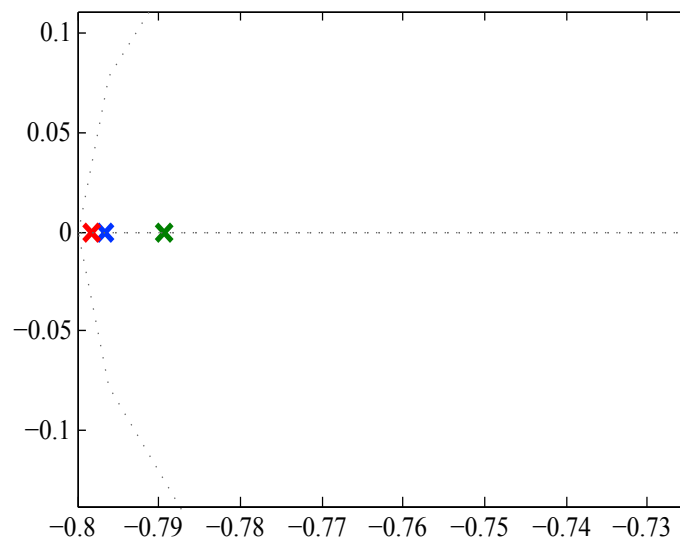


Figure 2.8: Roll mode poles of decoupled and coupled aircraft model

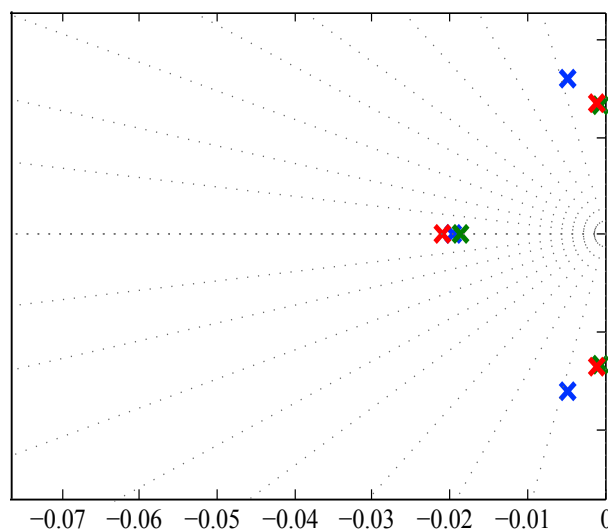


Figure 2.9: Spiral and phugoid mode poles of decoupled and coupled aircraft model

pled aircraft model and is mainly focused on longitudinal dynamics.

$$\omega_{sp}^2 = \frac{\frac{\bar{c}}{2U} C_{mq} C_{L\alpha} - \frac{mU}{qS} C_{m\alpha}}{\frac{I_y}{qS\bar{c}} \frac{mU}{qS}} \quad (2.46)$$

2.3.2 Static Stability

Figure 2.10 shows a conventional aircraft in cruise at a zero lift angle of attack with the neutral point (np) behind the CG. The distance between these two points is the static margin and determines the aircraft's degree of longitudinal static stability. For the CG position at 25% of the mean aerodynamic chord, the static margin of the B747 is 1.78 meters. As the stabiliser surface area is reduced along the span, the neutral point moves

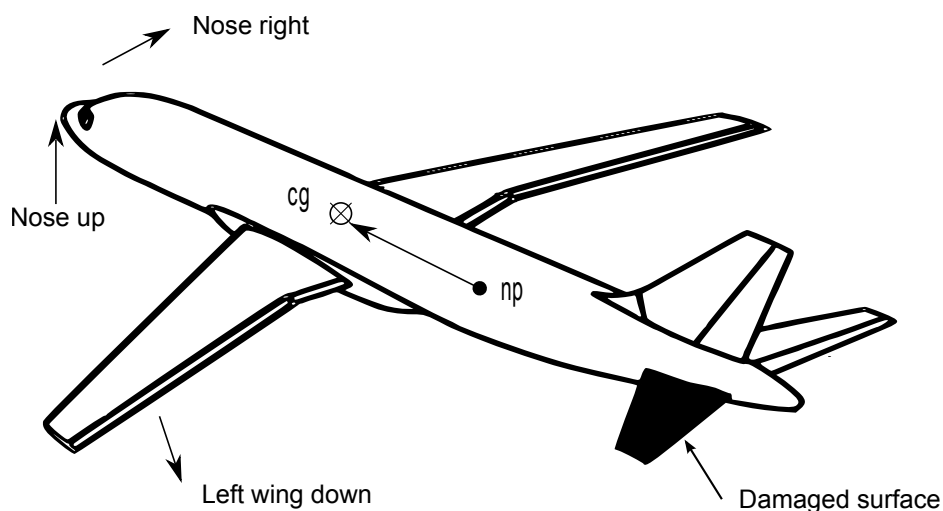


Figure 2.10: Damaged aircraft in level flight illustrating change in moments and neutral point position

forward towards the CG and the static margin is decreased. The longitudinal (aircraft x-axis) position of the neutral point at each damage case was obtained from AVL. There may be a lateral shift of the np due to the non-symmetry of the damage, it is however not considered in this analysis. The primary focus is the effect of change of np position on longitudinal stability.

The percentage reduction of the static margin at each damage instant is plotted in Fig. 2.11. The amount of stabiliser surface area loss along the span is proportional to the reduction in static margin. The reduction ratio for this aircraft is approximately 1:2 (i.e. for 10% stabiliser loss, the static margin is reduced by 20%). The amount of surface area loss increases at each interval due to the 'swept' geometry of the tail, hence the change in static margin ratio shows a slight increase with damage along the span (e.g. at 40% damage the ratio is 1:2.15). With 50% damage the sm is reduced by more than 100%, i.e. the neutral point is in front of the CG and longitudinal stability is lost.

2.3.3 Trim

When the aircraft is cruising at the predefined trim settings the total roll, pitch, and yaw moment is zero. Since the centre of pressure location is designed to be behind the CG, the aircraft has a natural negative (nose down) pitching moment. Hypothetically, if the CG and the cp were colocated no elevator deflection would be required to trim in level flight. When the stabiliser span is reduced, the cp shifts forward towards the CG and

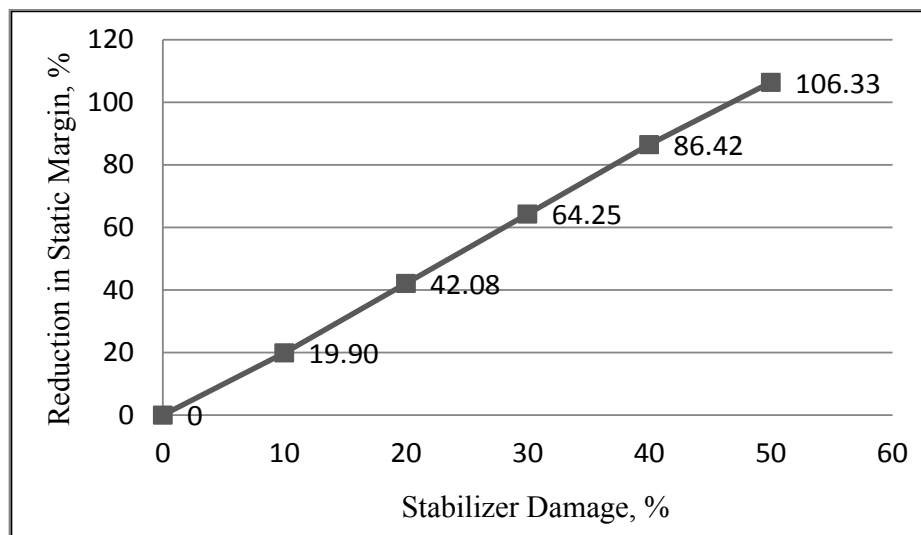


Figure 2.11: Change in static margin with reduction in stabiliser span

hence less elevator is required to trim. Since the aircraft is already trimmed to a nose up position when damage occurs, moving the c_p forward induces a nose up moment. This moment is, however, slightly reduced by the loss of elevator span. This was proven by observing the total moments in AVL (Table 2.2).

If the aircraft is trimmed to the flight conditions of this study with the trimmable horizontal stabiliser and elevator, and the stabiliser span is reduced, the resulting change in moments can be observed. The aircraft nose pitches up and yaws to the right whilst the port wing moves in a downward direction as illustrated in Fig. 2.10. The moments for each damage case were calculated from AVL coefficients as shown by the standard equations Eqs. 4-6.

$$L = qSbC_l \quad (2.47)$$

$$M = qS\bar{c}C_m \quad (2.48)$$

$$N = qSbC_n \quad (2.49)$$

Table 2.2 indicates that the roll and yaw moments steadily increase with damage until the aircraft loses its longitudinal stability at more than 40% stabiliser loss. The roll moment attainable from maximum inboard aileron deflection ($\pm 20^\circ$) was calculated and compared to the roll moment induced by the damage. The highest value of the roll moment induced by damage, as seen in Table 2.2, is for the case of 40% loss. This moment is less than 55% of the available inboard aileron force. Therefore, it can be concluded that for tail

damage up to 50% there is sufficient aileron actuation to retain lateral trim. The yaw moment due to damage remains below 3% of total available rudder force for all cases investigated. The pitch moment shows the greatest change with damage. The amount of elevator force available to control the aircraft is reduced by the elevator surface loss. Since minimal elevator deflection is required to trim as the static margin is reduced, this reduction becomes significant when the centre of pressure is in front of the CG. At 50% damage the aircraft is unstable and positive elevator is required to trim nose down. From Fig. 2.11 it can be seen that the static margin is reduced by more than 100%, The cp is in front of the CG but only slightly. It can therefore be assumed that minimal elevator is required to trim.

To investigate if there is sufficient actuation available to trim the aircraft nose down for the case of damage up to 50% stabiliser loss, it was assumed (worst case) that the aircraft is initially trimmed to the flight conditions of this study with the adjustable horizontal stabiliser only—it remains fixed and only elevator control is accessible. The nose down moment that is attainable by full elevator deflection was calculated for each damage case according to equation 7. The maximum allowable downwards deflection (δe_{Total}) is $+17^\circ$ for the B747. The value of $C_{m\delta e}$ calculated by AVL is the sum of the inner and outer elevator.

$$M_{\delta e} = C_{m\delta e} \times \delta e_{\text{Total}} \times qS\bar{c} \quad (2.50)$$

Figure 2.12 is a plot of the nose up pitching moment resulting from the damage and the available elevator force to pitch the aircraft nose down to maintain the predefined trim conditions. In the possible case that the stabiliser becomes immobile due to damage, there is sufficient elevator to trim the aircraft to the flight conditions of this study for damage up to 40%. If the stabiliser is movable, the aircraft can be trimmed with both elevator and stabiliser for the case of 50% loss. The effect of transient impact forces is not within the scope of this study, however, if these are considered the percentage of stabiliser damage that the actuators can handle may be less.

2.3.4 Dynamic Stability

The value of $C_{m\alpha}$ is dependent on the aircraft's static margin. The change in $C_{m\alpha}$ can be observed on the short period poles in Fig. 2.13. They gradually approach the real

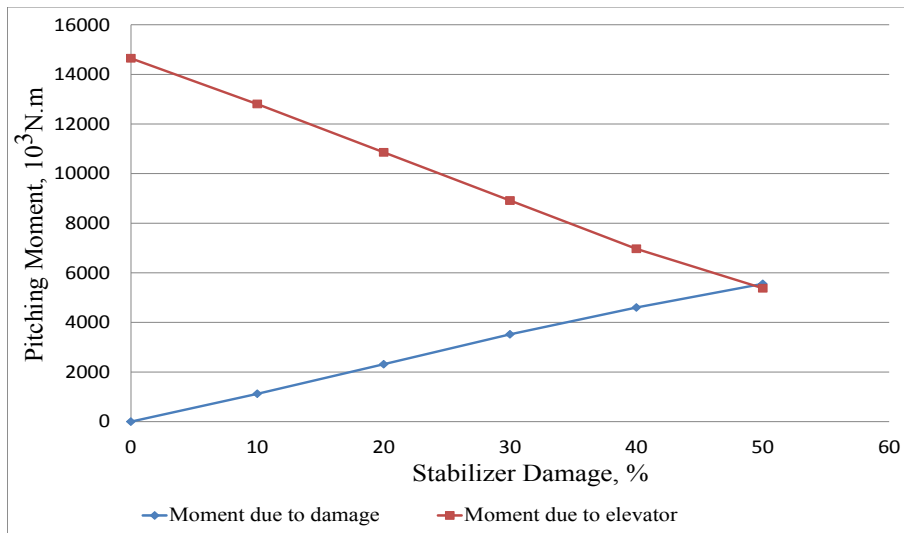


Figure 2.12: Pitching moment due to damage vs. available elevator moment to trim the aircraft

axis as stability reduces, become real and one moves to the right half plane when $C_{m\alpha}$ becomes positive at 50% stabiliser loss. As the poles move towards the real axis the mode frequency is reduced and as a result the pilot will experience a slower response to elevator input.

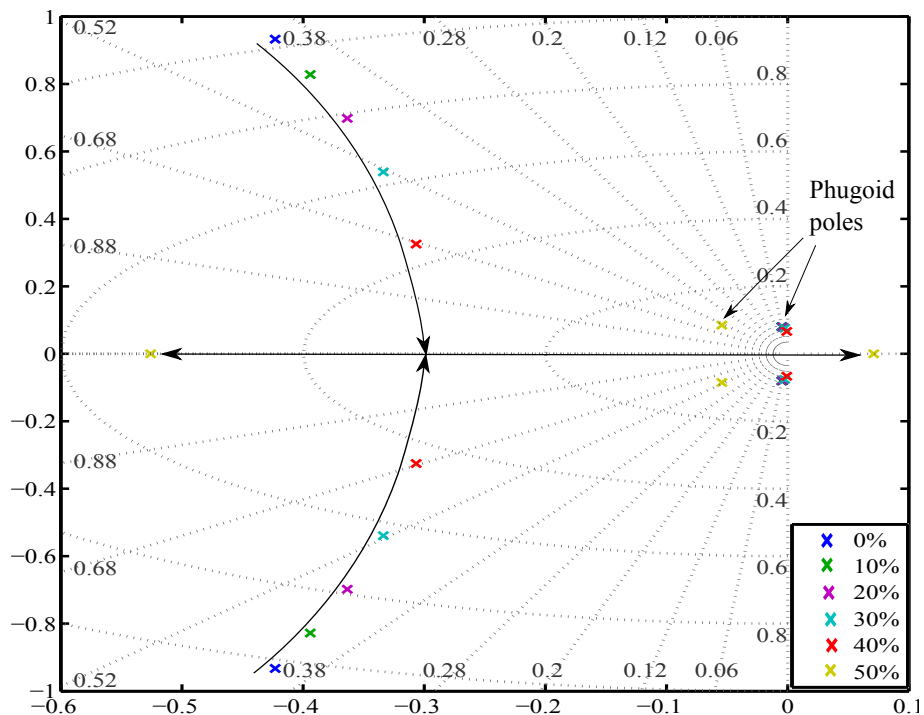


Figure 2.13: Damaged open-loop aircraft longitudinal poles (degree of horizontal stabiliser loss as per the legend)

The phugoid mode is typically a lightly damped airspeed oscillation that manifest as a climb and descend of the aircraft in a sinusoidal flight path. This motion gradually reduces in amplitude due to drag and the aircraft eventually settles to trim, if the mode is stable. Lift and drag are the main contributors to characteristics of the phugoid mode. These are not significantly affected by tail damage, thus the phugoid mode poles in Fig. 2.13 only show considerable change at 50% tail loss where they move to a new equilibrium.

2.4 Conclusion

In this chapter the problem of change in flight dynamics after horizontal tail damage was investigated. A discussion of the experimental setup, including equations of motion and aerodynamics of a damaged aircraft, was presented. From the results obtained in the study it may be concluded that non-symmetric horizontal tail damage greatly changes short period dynamics and to a lesser extent the Dutch roll mode through coupling. The short period frequency is lowered resulting in reduced responsiveness to the pilot elevator input. The asymmetry in the damage induces lateral motion, since this is a secondary effect this problem can be considered as increased lateral disturbance.

With 50% stabiliser loss the aircraft is statically unstable and the neutral point moves to the front of the CG. The aircraft has sufficient actuator movement to trim for stabiliser damage up to 50%. More longitudinal control authority is available through the trimmable horizontal stabiliser, however, if it is jammed in the initial trim conditions, elevator control only is sufficient to maintain trim.

Coefficients	Conventional Aircraft	40% tail Removed	Change(%)
<i>Longitudinal</i>			
$C_{m\alpha}$	-1.15	-0.15	86.95
$C_{m\delta e}$	-1.43	-0.686	51.99
C_{mq}	-20.7	-10.095	51.23
C_{Lq}	5.13	3.167	38.25
C_{mr}	0	0.156	15.68
$C_{m\beta}$	0	-0.084	8.41
C_{mp}	0	-0.081	8.10
$C_{L\alpha}$	4.67	4.360	6.62
C_{Lr}	0	-0.048	4.86
$C_{L\beta}$	0	0.026	2.64
C_{Lp}	0	0.025	2.54
<i>Lateral</i>			
C_{yq}	0	-0.229	22.99
C_{lq}	0	-0.181	18.13
C_{yp}	0	0.139	13.91
C_{nq}	0	0.118	11.81
C_{yr}	0	0.089	8.99
C_{nr}	-0.278	-0.253	8.88
$C_{n\beta}$	0.147	0.135	7.68
$C_{y\beta}$	-0.9	-0.843	6.22
C_{lr}	0.212	0.200	5.50
C_{np}	-0.0687	-0.065	4.26
$C_{l\beta}$	-0.193	-0.186	3.28
$C_{y\alpha}$	0	-0.024	2.40
$C_{n\alpha}$	0	0.014	1.43
$C_{l\alpha}$	0	-0.014	1.43
C_{lp}	-0.323	-0.321	0.50

Table 2.1: Aerodynamic coefficients of damaged (40% horizontal stabiliser loss) and undamaged aircraft

Damage(%)	L	M	N
0	0	0	0
10	-251.008	1120.86	125.504
20	-476.916	2314.14	238.458
30	-602.42	3517.76	301.21
40	-622.501	4600.68	351.412
50	-567.279	5552.55	351.412

Table 2.2: Moments resulting from damage, 10^3N.m

Chapter 3

Fly-by-Wire Robustness

The effects of tail damage on the open-loop aircraft have so far been discussed. This chapter details how a similar study is carried out on a fly by wire (FBW) aircraft. First, a general description of FBW systems as implemented on large transport aircraft is given, followed by details of the control laws used. The longitudinal control law and its implementation on the B747 model is presented. An analysis of the aircraft response after damage is detailed and compared to the open-loop aircraft to evaluate the improvement in robustness provided by the FBW controller. Also entailed is a discussion of handling qualities for augmented aircraft and how the standard is used in this study to quantify performance degradation due to tail damage.

3.1 General Architecture

As previously discussed in chapter 1 there are several commercial FBW aircraft manufacturers, however, the FBW presented in this chapter is based on Airbus and Boeing. The structural diagram of a typical FBW is shown in Fig. 3.1. Pilots' inputs are considered as control objectives and under normal operation do not directly move actuators. The control law consists of an algorithm that computes an output from a combination of the pilot's input and sensor measurements. The pilot inputs may be stick/control column, wheel, rudder, and thrust lever from the cockpit or commands from an autopilot system.

For Airbus FBW aircraft (A320, A321, A330, A340) all control surfaces are electrically

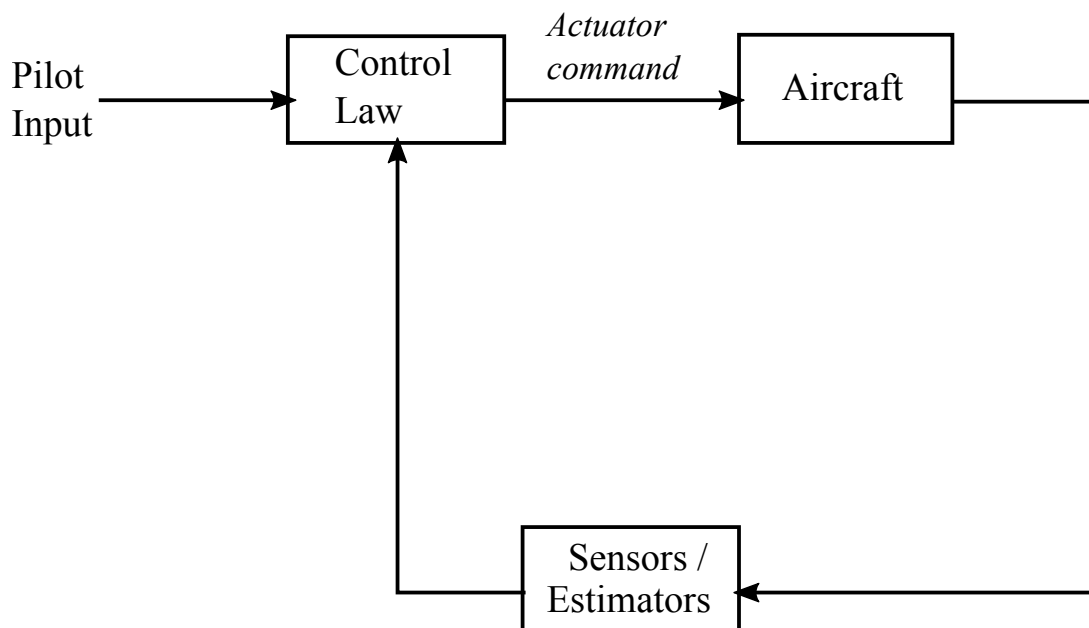


Figure 3.1: General architecture of a fly-by-wire system

controlled, hence availability of the control system is a critical feature[43]. To ensure availability of the system at all times the control law is executed on 5 different computers. Both the hardware and software of the computers are from various different manufacturers to minimise the possibility of common failures associated with one manufacturer. All 5 computers are active simultaneously in normal functionality, the A320/A321 has 2 elevator and aileron computers (ELAC) and 3 spoiler and elevator computers (SEC), whilst the A330/A340 has 2 operating as primary flight computers and the remaining 3 are secondary. Each computer is divided into command and monitor subcomputers. Results from both are compared and if the difference between the two is above a certain threshold, that specific computer is considered faulty and the communication of results to other systems is disconnected.

The FBW system has full authority of the aircraft, thus, it is essential that information provided to the flight control laws be verified as correct. The Airbus system has 3 air data and inertial reference units (ADIRU) which compare and validate data from independent sources before relaying it as input to the control law. An analytical approach is used to verify data; for example, the load factor is estimated from pitch rate information and compared to accelerometer measurements, if the two results are similar the value is then forwarded to the longitudinal control law.

The B777 is Boeing's only commercial FBW aircraft so far. It has 3 flight computers. Each computer has 3 computing channels which can function independently of each other[4]. This is equivalent to 9 simultaneously operating computers. Each channel, on any one computer, calculates an output based on the control law and inputs. This output is compared with the other two channels to verify correctness. The mid value from the 3 channels is considered to be the output from that specific computer. If any output from the 3 channels deviates significantly it is considered faulty. Furthermore, each computer compares its output with the other 2 computers to verify correctness.

3.2 Control Law

The primary objective of the law is to improve the aircraft's flying qualities and ensure all manoeuvres are within its flight envelope. The B777 control laws consist of pitch, yaw, and roll control. The pitch control strategy is based on the C*U law which is discussed in detail in section 3.2.2. Also, included in pitch control is turn compensation which reduces the pilot's workload during a bank turn. The system controls the aircraft's pitch angle such that altitude is maintained whilst turning. Furthermore, the law implements stall and overspeed protection. This feature ensures the aircraft is flown within its airspeed envelope by regulating the control column force required to change airspeed. For speeds above and below the envelope margins the force required to move the control column increases. In this approach the pilot's airspeed control is not limited to within the allowable speed, however, he is aware of his speeding action.

The pitch control law implemented on all Airbus FBW aircraft differs from Boeing's; it is derived from the C* control law. In the case that the pilot commands a speed above the allowable maximum the overspeeding protection function is activated, the algorithm commands the elevator through the C* law to pitch the aircraft nose up thus reducing airspeed. Nose down commands are overridden and in this way it is not possible to fly the aircraft above allowable airspeed. This is one significant difference in the envelope protection features between Airbus and Boeing FBW. Boeing's envelope protection laws make it possible for the pilot to fly the aircraft outside of its flight envelope but with added control effort; whilst Airbus's system inhibits out of envelope commands. At low speed below the minimum allowable airspeed the C* law is deactivated and a switchover

to angle of attack protection law is made. When this law is active, stick input commands an angle of attack instead of pitch rate at low speeds. A full aft deflection of the control stick commands a predefined maximum allowable angle of attack.

The typical lateral control system consists of an inner yaw rate feedback loop to improve the damping of the Dutch roll mode and an outer loop of lateral motion measurement feedback to eliminate lateral acceleration in a coordinated turn. The FBW system is developed from the conventional system, it further includes gust suppression, thrust asymmetry compensation, and bank angle protection. Wind gust measurements obtained from sensors mounted on the fin are used in a rudder control law to counter the gust motion. Similarly a yawing moment resulting from asymmetric thrust (such as in the case of engine failure) is compensated for by rudder actuation. As discussed in chapter 2 horizontal tail damage primarily affects longitudinal dynamics, this chapter is therefore focused on the longitudinal FBW laws only.

3.2.1 C*

Reducing the static stability of an airframe has been shown to be a significant contributing factor in decreasing aerodynamic drag to improve operational efficiency [5]. The disadvantage of this design approach is degradation in natural handling qualities. Stability augmentation by a control system is typically implemented in modern aircraft as a solution. In conventional (non-FBW) aircraft pitch rate feedback is commonly used to modify longitudinal short period response to provide ideal handling. Studies in handling qualities however revealed that at high airspeed, normal acceleration is the predominant longitudinal motion cue for pilots, whilst at low speeds pitch rate is dominant. Thus an efficient longitudinal control system must feedback a blend of pitch rate at low speed and normal acceleration at high speeds. This led to the development of the C-star control law, which has since become the basis for longitudinal control laws for modern commercial FBW aircraft [44].

$$C^* = K_{nz}n_z + K_qq \quad (3.1)$$

The original C* handling qualities criterion, as published by H Tobie, H Elliott, and L Malcolm in the 1960s [45], is shown by Eq. 3.1. Whilst the ratio of K_{nz} to K_q is fixed, the contribution of n_z and q varies with the aircraft's velocity. This can be more clearly

illustrated in the control diagram in Fig. 3.2. When the airspeed (V) is small, the outer loop has no significant effect on the aircraft's pitch dynamics. For a large value of V , the inner loop becomes insignificant. At the crossover velocity, pitch rate contribution is equal to normal load contribution.

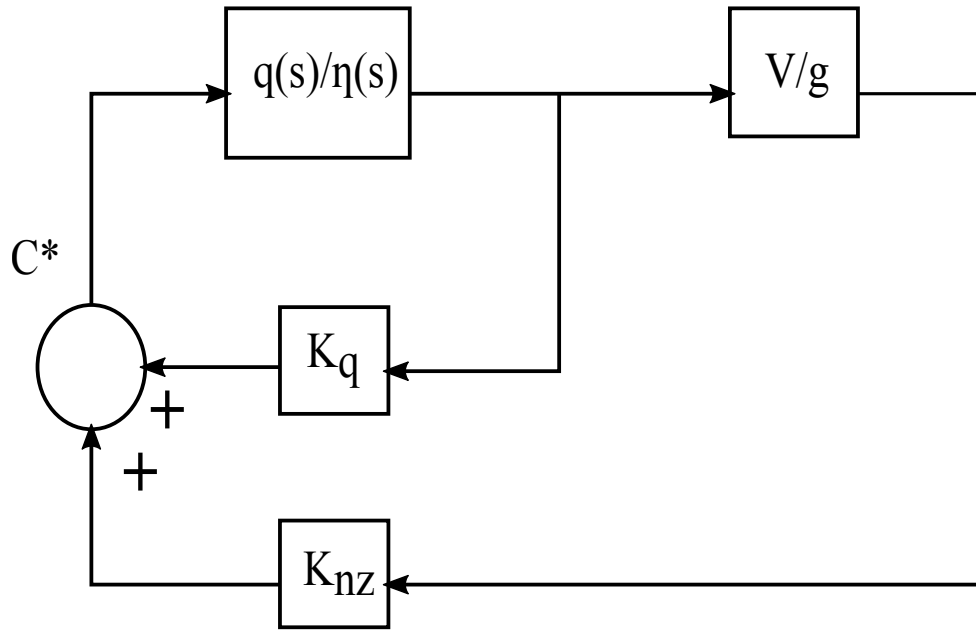


Figure 3.2: Structure of C^* algorithm

Equation 3.2 is the approximation of the load factor as discussed in [35]. If $\dot{\alpha}$ is assumed to be very small n_z can be simplified to Eq. 3.3.

$$n_z = \frac{V}{g}(\dot{\alpha} + q) \quad (3.2)$$

$$n_z = \frac{V}{g}q \quad (3.3)$$

From Eq. 3.4 if K_{nz} is fixed to 1, the value of K_q can be calculated by substituting n_z with Eq. 3.3. For crossover velocity of 400ft/s in accordance with the original criterion[44], the ratio of K_q/K_{nz} is 12.4.

$$K_{nz}n_z = K_qq \quad (3.4)$$

Most aircraft manufacturers, however, do not conform to the original C^* law. Selection of the ratio is arbitrary and varies between companies. The ratio is typically set to achieve ideal handling qualities for the specific aircraft type. As such the term C^* refers to a blend of pitch rate and normal load factor in some proportion.

3.2.2 C*U

The C*U is an extension of the C* control law. It includes an additional airspeed control loop which introduces airspeed stability to the system [3]. Figure 3.3 shows the control diagram of the C*U control law as defined in Eq. 3.5. If the aircraft's airspeed is increased above the reference airspeed, the C*U control law computes an output to deflect the elevator up and pitch the nose up, thereby reducing the speed. In the same way, if the speed is lower than the reference speed, the elevator is deflected downwards to nose down and increases speed. This law is implemented on Boeing's standard FBW system.

$$C^*U = K_{n_z}n_z + K_qq + K_VV_{err} \quad (3.5)$$

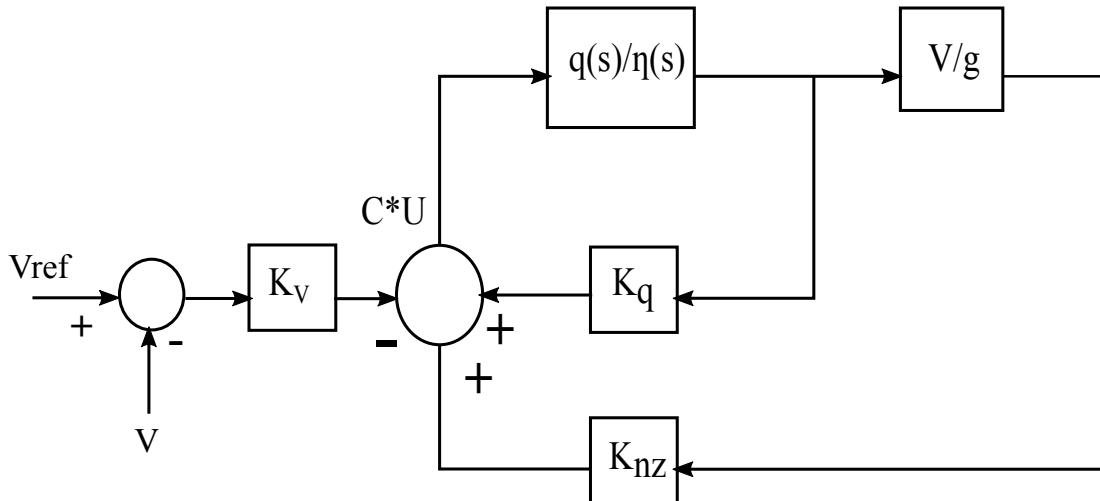


Figure 3.3: Structure of C*U algorithm

3.2.3 Control Law Reconfiguration

The pilot's input is transmitted to an inner loop which computes three possible actuator signals according to so-called "Normal", "Alternate", and "Direct" control laws. The normal law represents a fully operational FBW system. If the system is subjected to multiple failures such that normal mode functionality is compromised, the system automatically reconfigures to alternate mode (also called secondary mode). One example of such an occurrence would be in the case of complete loss of aircraft data from all the ADIRUs. The alternate law implements the C* or C*U law without envelope protection.

The direct law consists of basic functionality similar to the conventional non-FBW aircraft. In the Airbus system direct law implements only a pitch rate feedback loop and operates on a different PFC. In the direct law of the Boeing FBW, system pilot commands are transmitted directly from pilot controller transducers to the ACE, bypassing all flight computers. It is also possible for the pilot to intentionally select the direct mode from the flight deck.

The aircraft's modal behaviour as perceived by the pilot should ideally be the same for all 3 laws and close to the natural aircraft behaviour to ensure that the modes remain invariant so that the pilot is not presented with hugely varying aircraft responses when switching between the various laws [23]. Only the alternate mode is considered in this study since the envelope protection and gust alleviation functions have a negligible effect on the nominal pole positions and these functions are outside the scope of this study. Figure 3.4 shows the longitudinal control law in alternate mode of the Airbus FBW system [23],[46].

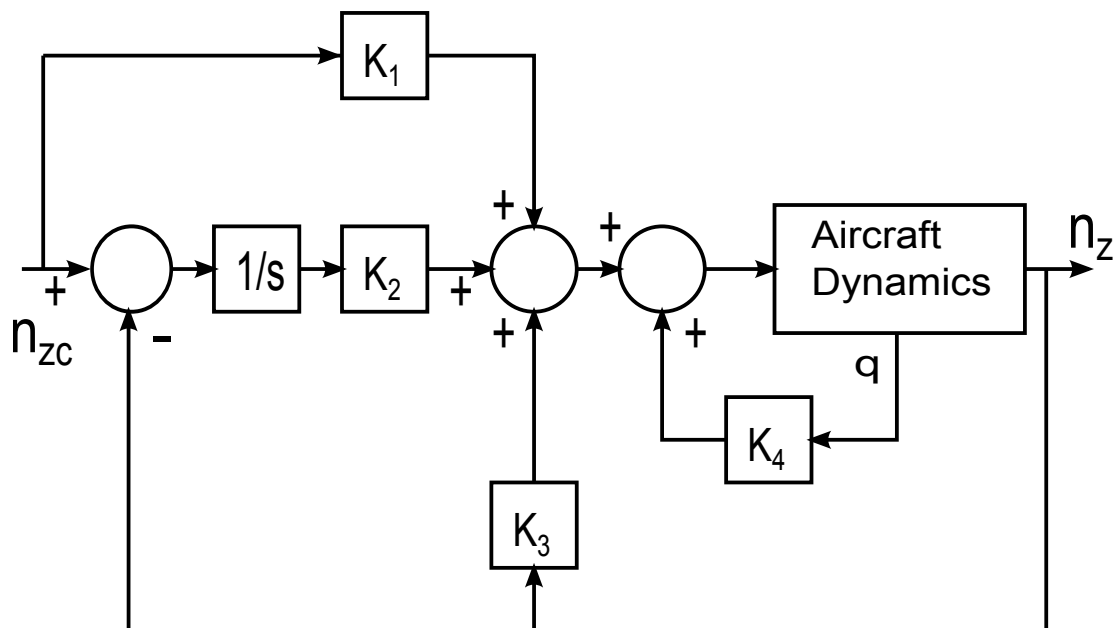


Figure 3.4: Longitudinal control system in C^* alternate law

3.3 Experimental Setup

The mathematical model of the B747 is discussed in chapter 2. This section details the design procedure that was carried out to implement C^* FBW on that aircraft model. The control system of Fig. 3.4 is used in this study. The proportional pitch rate and normal acceleration feedback gains were selected to represent a practical aircraft that meets certification requirements. An integrator in the outer loop is included to improve steady state tracking and reference feed-forward to cancel the resulting closed-loop pole. To simplify the robustness analysis problem, the change in aircraft behaviour is analysed for the pure C^* control system (Fig. 3.2) and effects of the steady state tracking and reference feed-forward loop will be dealt with separately.

In the actual aircraft the gains are scheduled to vary as a function of airspeed, altitude, and CG position. For this study the aircraft is analysed around one state condition (Mach 0.5 at 20 000ft and the CG at 25% \bar{c}), so the gains are assumed to be fixed. The following subsections discuss the design objectives and procedure of each control loop of the system depicted in Fig. 3.4.

3.3.1 Pitch Rate Feedback: Direct Law

Pitch rate feedback is traditionally used in stability augmentation of the short period mode. In FBW aircraft it is the longitudinal control system in direct mode and in normal mode it is the dominant pitch controller at low airspeed. It is thus imperative that the aircraft behaviour, i.e. handling qualities, be perceived by the pilot as acceptable under this law. The subject of handling qualities is discussed in detail in section 3.4.

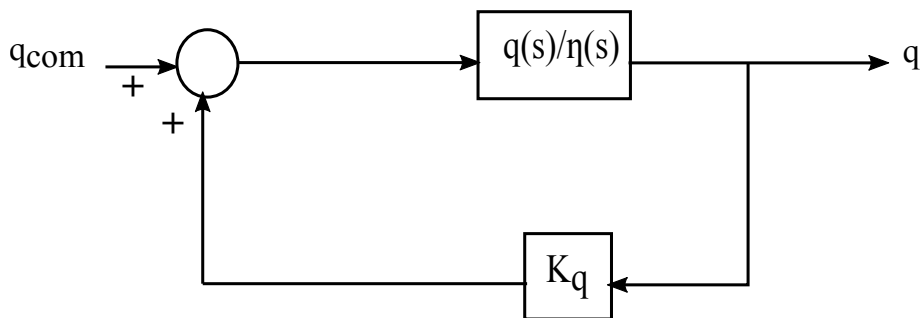


Figure 3.5: Longitudinal control system in direct law

The control diagram of the direct law is shown in Fig. 3.5. Pitch rate output to elevator input is used to model the aircraft's dynamics. Equation 3.6 shows the system's open-loop function. The pair of two complex conjugate poles describes the characteristics of the aircraft's dynamics. The primary objective of this loop is to improve the damping of the short period poles. The effect of pitch rate feedback on the phugoid mode is relatively insignificant for low gain values.

$$\frac{q(s)}{\eta(s)} = \frac{K_q s(s + \frac{1}{T_{\theta 1}})(s + \frac{1}{T_{\theta 2}})}{(s^2 + 2\zeta_p \omega_p s + \omega_p^2)(s^2 + 2\zeta_{sp} \omega_{sp} s + \omega_{sp}^2)} \quad (3.6)$$

From the root locus plot of Fig. 3.6, it is evident that in increasing the short period damping ratio, the natural frequency of the mode is increased. In the discussion of FBW design constraints in [23], the author states that the difference between open-loop poles and closed-loop poles must be small in order to minimise the demand on actuators. It is also a requirement that the closed-loop behaviour does not deviate significantly from open-loop behaviour. If the closed-loop poles are placed as shown in Fig. 3.6, the gain K_q is set at 0.8, the damping ratio is 0.7, and the natural frequency is increased from 1 to 1.2. This change in pole position is considered relatively small and gives ideal behaviour of the short period mode.

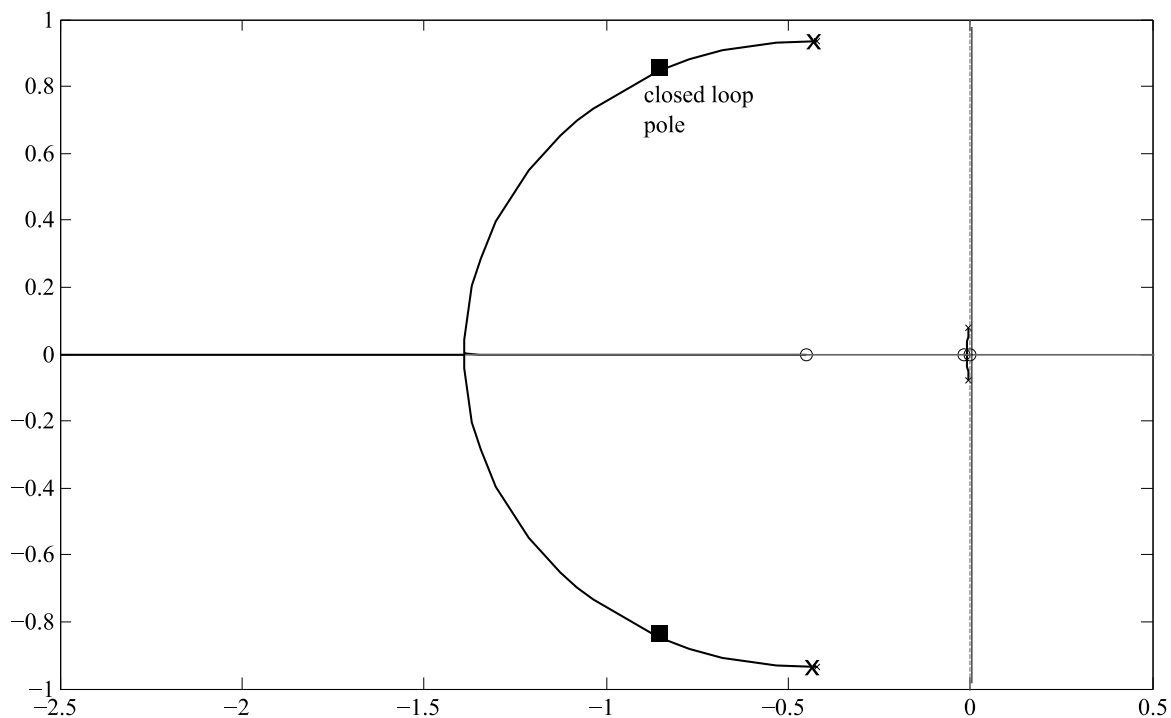


Figure 3.6: Pitch rate root locus plot

3.3.2 Normal Load Feedback: Alternate Law

The aircraft's behaviour in alternate mode is similar to the normal mode for an aircraft operating within its flight envelope. The alternate law is, therefore, required to augment the aircraft to achieve ideal longitudinal behaviour. Since the objective of this study is to evaluate degradation in handling qualities resulting from tail damage, load factor measurement is assumed to be taken at the pilot seat. This ensures consistency with the pilot's perception of longitudinal behaviour [44]. Equation 3.3 is thus modified to Eq. 3.7, where x is the distance between the CG and pilot seat.

$$n_z = \frac{V}{g}q + x\dot{q} \quad (3.7)$$

The control law is implemented as shown by Fig. 3.2, where V/g is substituted with $(V/g + xs)$. The root locus plot of the open-loop system is depicted in Fig. 3.7. The gain must be selected to give the desired crossover velocity whilst providing ideal handling qualities. Increasing the gain reduces the damping ratio and increases the natural frequency. Since

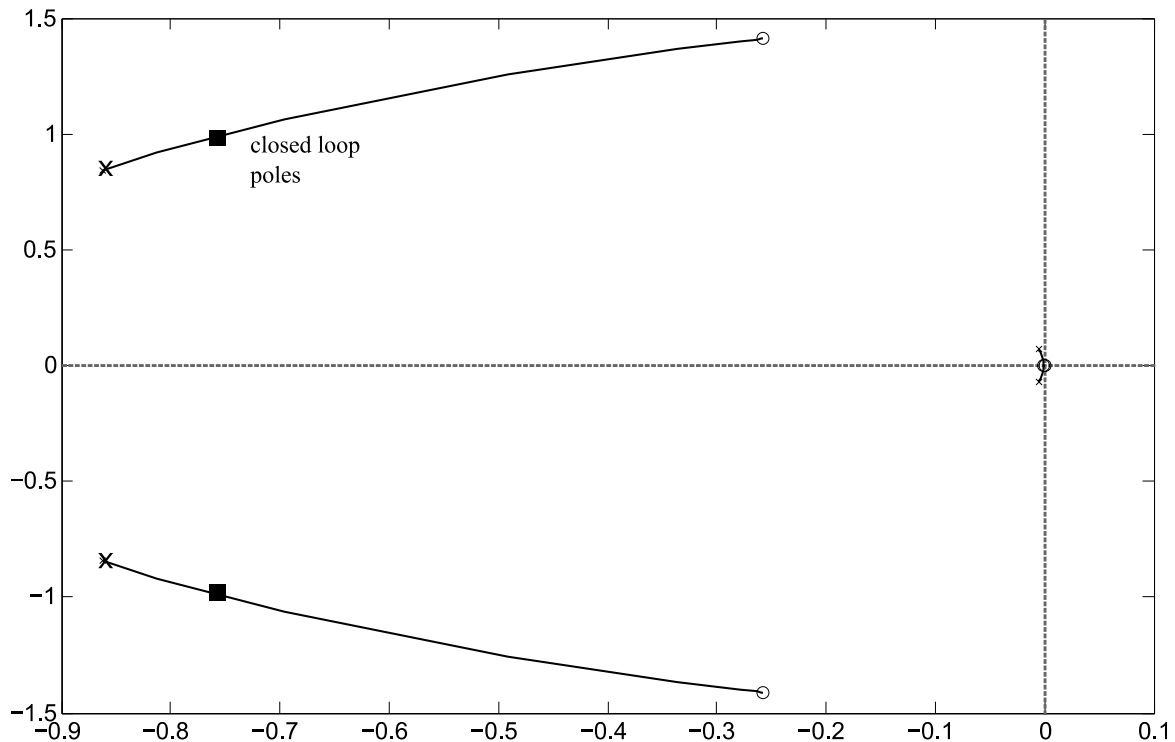


Figure 3.7: Normal load root locus plot

these are both undesirable attributes it is thus necessary to select a minimum possible gain to achieve the two objectives. If the gain is selected in accordance with the original

C* criterion (K_q/K_{nz} ratio of 12.4), the gain is 0.06 and the closed-loop poles are as shown in Fig. 3.7. The damping ratio is reduced to 0.6 and the frequency is increased to 1.25.

3.4 Handling Qualities

Flying and handling qualities reflect the level of ease and precision with which the pilot can accomplish the mission task. Handling qualities standards provide predefined levels of acceptability for ranges of stability and control parameters based on flight test data accumulated over years. MIL-STD-1797A standard contains the requirements for flying and ground handling qualities. It is intended to ensure flying qualities for adequate mission performance and flight safety, regardless of the design implementation or flight control system augmentation [22].

The requirements are formulated for different classes of aircraft at various stages of the flight phase and specify 3 levels of acceptability of an aircraft in terms of its ability to accomplish its mission task. Aircraft classification is according to weight, size, and level of manoeuvrability. Flight phase categories are defined according to the required level of tracking precision, path control, and whether terminal or non-terminal. This study is based on a Class III aircraft (large, heavy, low to medium manoeuvrability) on category B (non-terminal, flight phase requiring gradual manoeuvring, less precise tracking, and accurate flight path control).

The 3 levels of flying qualities are:

- Level 1 (satisfactory): adequate for mission flight phase.
- Level 2 (acceptable): adequate to accomplish mission flight phase but with increased pilot workload and or degradation in effectiveness.
- Level 3 (controllable): aircraft can be controlled in the mission flight phase but with excessive pilot workload and/or inadequate effectiveness. This level is not necessarily defined as safe, it is recommended to improve aircraft flying qualities if safety is a requirement.

Response to pilot inputs is influenced by static and dynamic stability properties of the aircraft. Frequency, damping ratio, and time constant significantly affects handling qualities. Based on an empirical study, certain combinations of these values give acceptable handling qualities. Figure 3.8 shows the requirements for short period response to a pitch controller for a class III aircraft on category B phase.

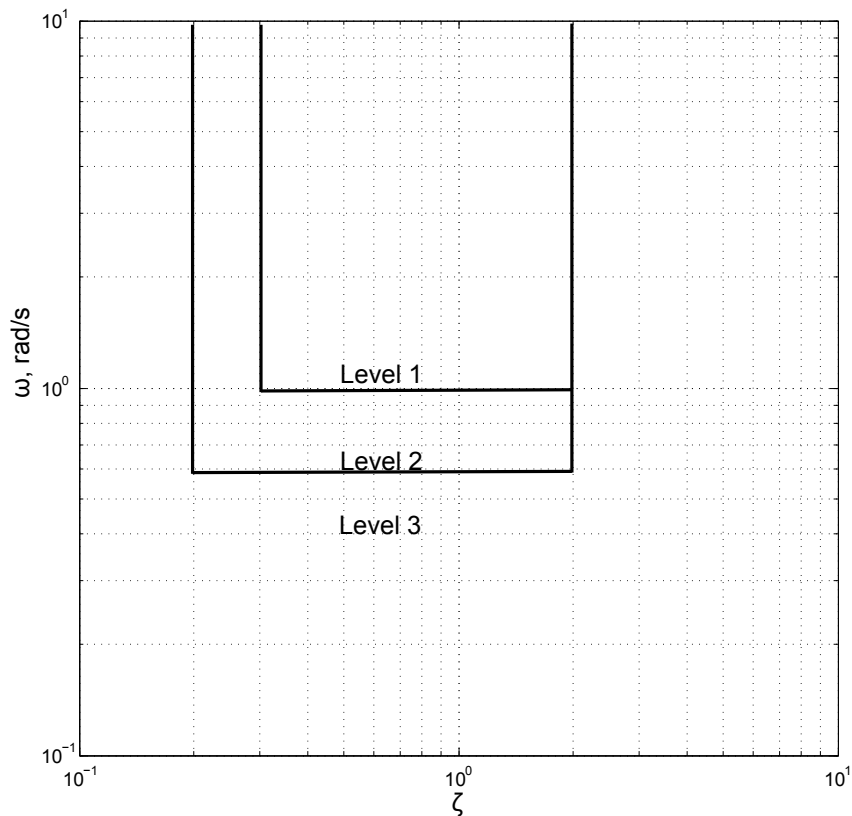


Figure 3.8: Requirements for short period response to pitch controller (ω vs ζ) of a class III aircraft in cruise configuration

3.5 Results and Discussion

Feedback systems should be relatively insensitive to external disturbances and parameter variations. As discussed in the previous chapter, tail damage causes a large variation to the open-loop aircraft short period poles—resulting in complete loss of stability when half the tail is removed. The efficiency of the longitudinal FBW controller in limiting variation of these poles due to the damage is analysed by comparing the pole variation of the FBW (closed-loop) aircraft model to the open-loop model. Figure 3.9 shows that with

40% damage the frequency decreases from 1.25 to 0.72 rad/s, i.e. a reduction of 42%. The open-loop aircraft's short period poles have a natural frequency of 1.02 rad/s which decreases to 0.447 rad/s with 40% damage, a reduction of 56%. From this comparison it can be concluded that the FBW system improves robustness to tail damage. For the FBW aircraft, approximately up to 15% more stabiliser surface area may be lost for an equivalent change in dynamics to the open-loop aircraft.

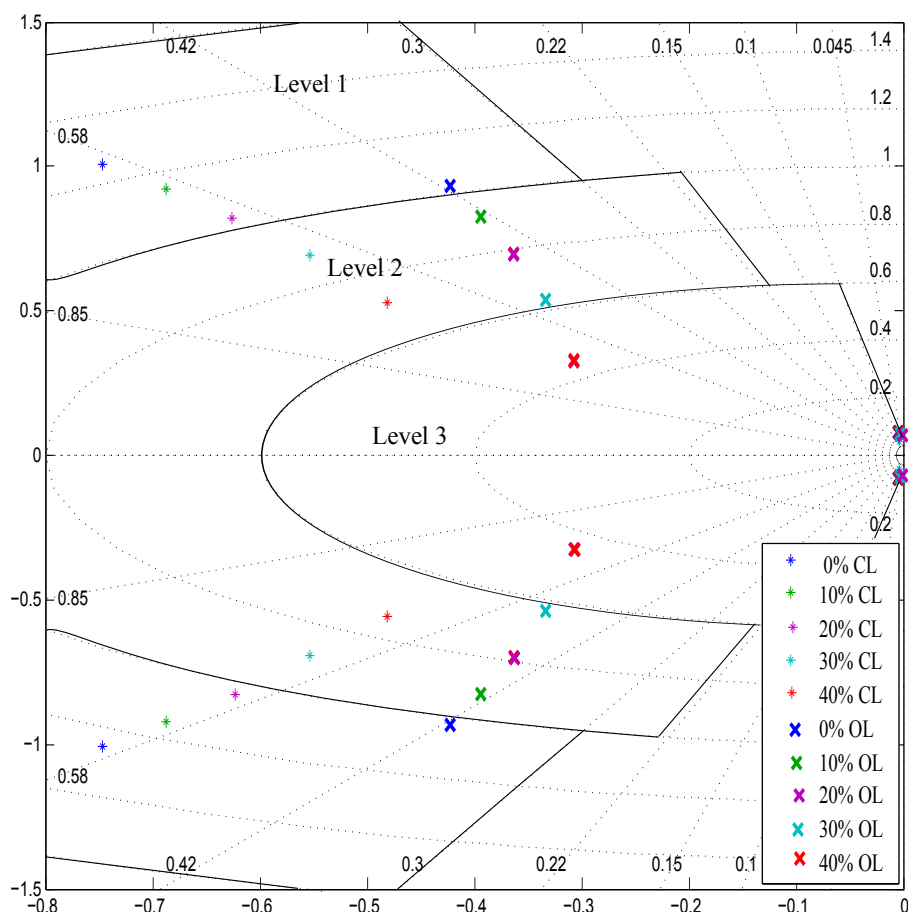


Figure 3.9: Damaged open-loop (OL) vs. closed-loop (CL) aircraft longitudinal poles illustrating change in handling quality levels

At 50% damage, the short period poles of the closed-loop aircraft are stable. Figure 3.10 shows the phugoid poles and short period poles with 50% damage. The control system restrains the short period poles and keeps them within the stable region with half the horizontal tail removed. The previously marginally stable phugoid poles become real and one moves to the unstable region when the aircraft loses its natural stability. The unstable phugoid pole has a low frequency that is within the pilot's control capability.

Stability of the mode can be retained with a basic feedback loop to limit phugoid pole movement.

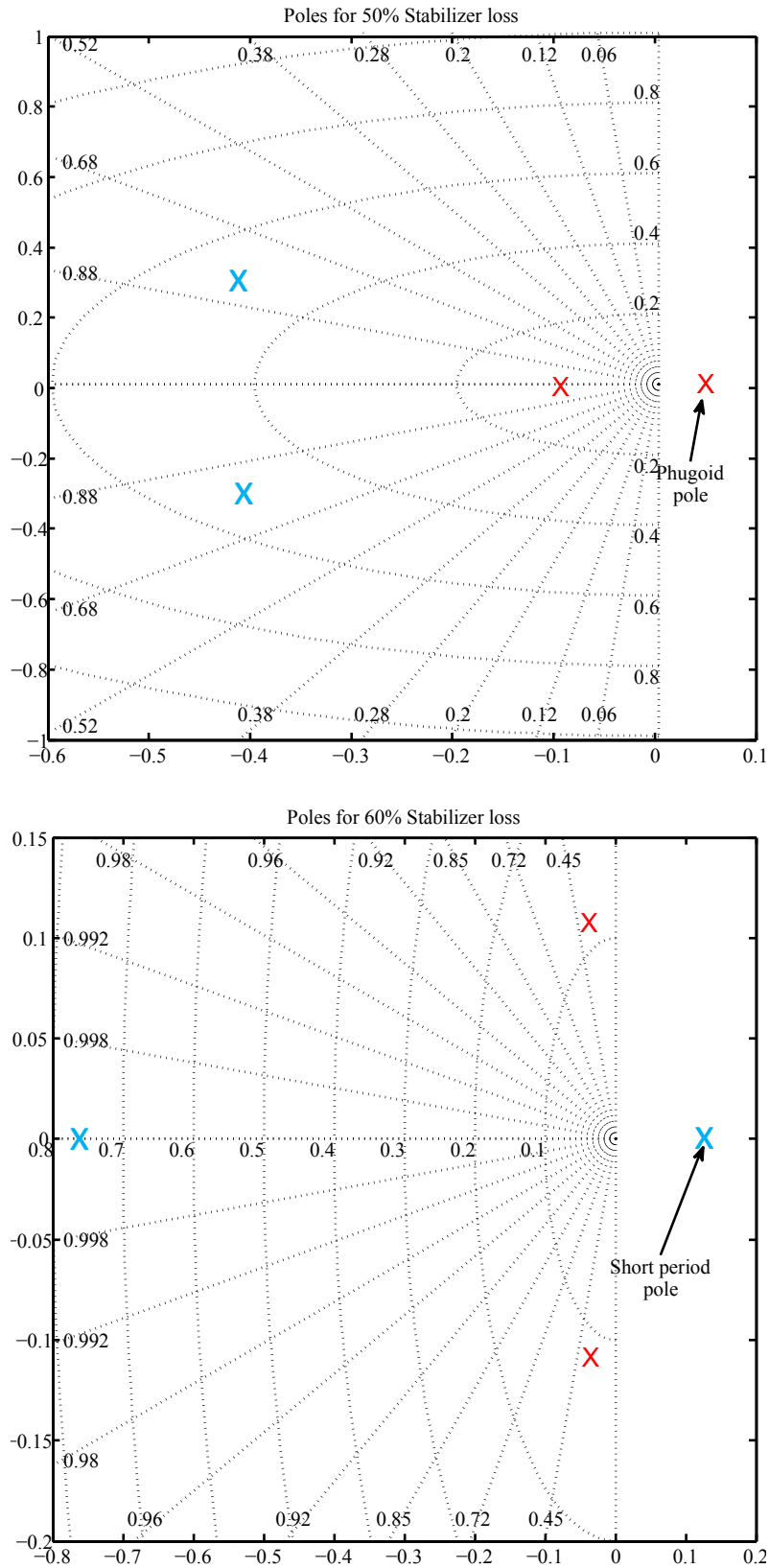


Figure 3.10: Damaged closed-loop aircraft longitudinal poles for 50% and 60% stabiliser loss

The longitudinal poles for the case of 60% loss are shown in Fig. 3.10. The phugoid poles become complex and stable whilst the short period poles move further apart with one being unstable. The closed-loop pole position is approximately equal to the open-loop poles for 50% damage (Fig. 2.13). Whilst the conventional aircraft becomes unstable for damage above 40%, the FBW aircraft remains stable with half the horizontal stabiliser lost (if the phugoid poles are retained within the stability region).

Figure 3.9 shows how the handling qualities of the B747 at cruise are degraded from one level to the other as the extent of damage is increased. For the FBW aircraft with 20% tail loss its response to pilot input is still adequate and satisfactory with behaviour quantified as Level 1. With 30% tail loss the control response is downgraded to Level 2, so increased pilot workload is required to manoeuvre. Although the aircraft has acceptable flying qualities up to 40% damage at cruise, it may be more difficult to handle in landing configurations and can be classified at Level 3. With 50% damage the short period poles are stable, the value of ζ is 0.8 and ω is 0.513 rad/s thus it has Level 3 qualities. Excessive pilot workload is required, the aircraft may be unsafe and ineffective towards completing its mission task.

3.6 Steady State and Transient Response Loop

The foregoing analysis of the closed-loop C* aircraft is focused on its change in behaviour as perceived by the pilot, i.e. accelerometer measurements are assumed to be taken from the cockpit. The control system however receives the aircraft's measured states from the ADIRU which is located at the CG. It is hence necessary to design the outer loop from the CG whilst ensuring that the closed-loop behaviour still meets acceptable requirements at the pilot's position.

Figure 3.11 shows a simplified diagram of the Airbus C* FBW in Fig. 3.4. This representation can be further simplified into two loops, an integration loop and another to add a zero close to the origin to cancel out the undesirable transient effects of the integrator pole. The derivation of the simplified diagram is detailed in Appendix B. If normal load factor is considered to be as defined in Eq. 3.3 and the gain values are fixed to the

previously selected values, then the C^* closed-loop aircraft equation is given by Eq. 3.8.

$$\frac{C^*(s)}{\eta(s)} = \frac{K_c s (s + \frac{1}{T_{\theta 3}}) (s + \frac{1}{T_{\theta 4}})}{(s^2 + 2\zeta_p \omega_p s + \omega_p^2) (s^2 + 2\zeta_{sp} \omega_{sp} s + \omega_{sp}^2)} \quad (3.8)$$

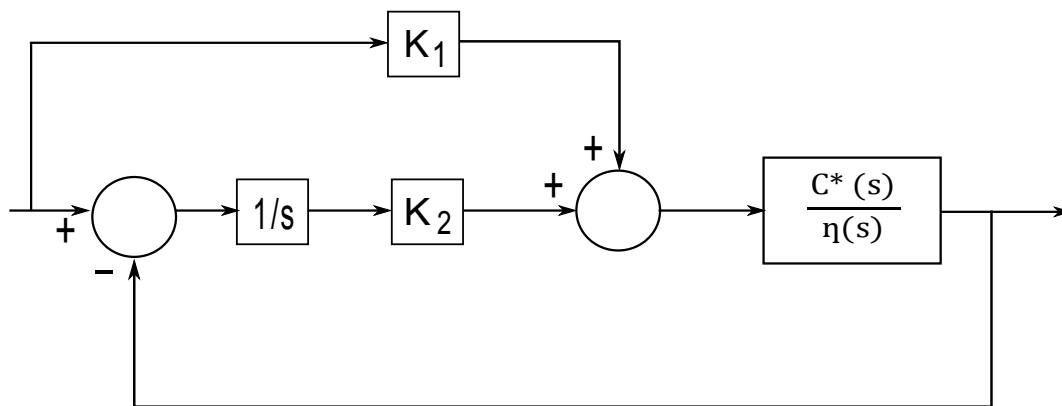


Figure 3.11: Simplified block diagram of Airbus C^* FBW

The open-loop C^* aircraft has a zero at the origin and no free integrator. The steady state error is, therefore, infinite for a step input, i.e. the output cannot track the input. If an integrator is added to the system it becomes type 0 and the steady state error is $1/(1+K)$ whereby K is the position error constant. The root locus for the system with an integrator is shown in Fig. 3.12.

The phugoid locus is pulled into the instability region such that for a small increment in gain the poles become unstable. Marginal stability of the phugoid poles is acceptable since the mode has a low frequency which is within the pilot's control capacity. For the Airbus FBW, the poles have neutral stability whilst in the Boeing system airspeed feedback of the C^*U law pulls the poles back into the stability region. A more significant problem with increasing the gain is its effect on short period dynamics at the pilot's seat (shown in Fig. 3.13). The damping ratio is further decreased and frequency increases. The objective of this loop is to reduce the steady state error, without destabilising the phugoid poles, whilst minimising the change on short period poles. If the gain is 0.01 the short period frequency with reference to handling qualities is increased to 1.27 and the damping ratio remains at 0.6. The steady state error is 0.99, this is considered a very high value, however, it is the best possible value that meets the constraints on both

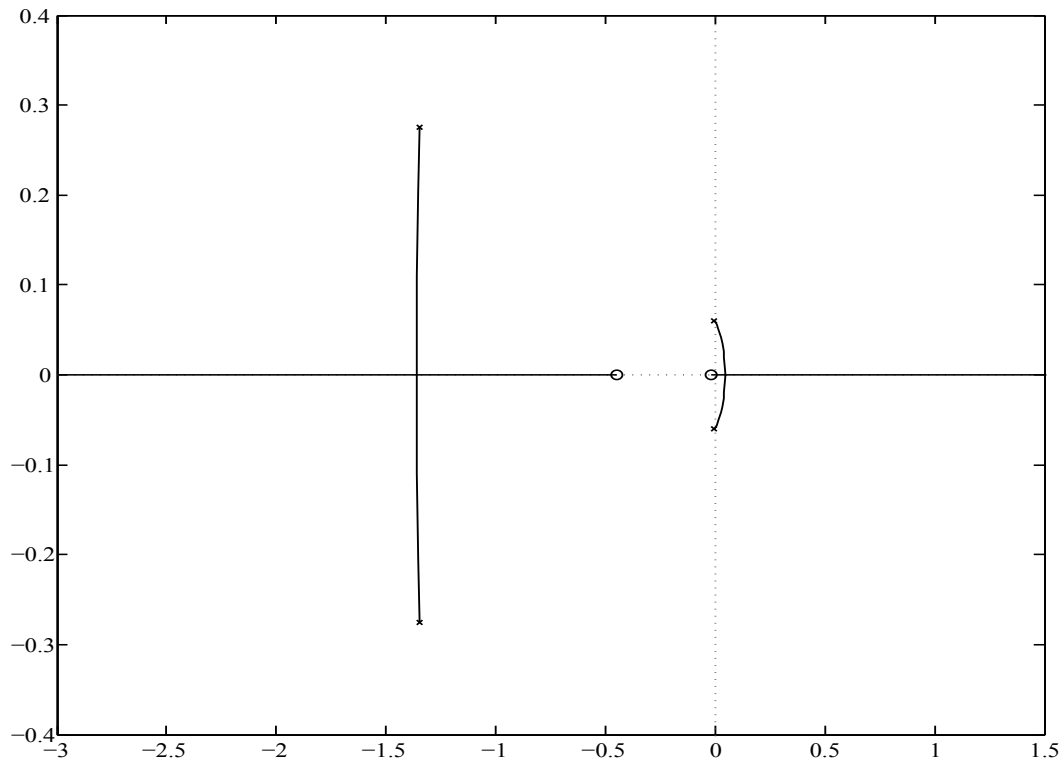


Figure 3.12: Root locus plot for outer loop with integrator for the case of vertical acceleration measured at CG

phugoid and short period mode. The detailed calculation of the steady state error as presented in [47] is found in Appendix B.

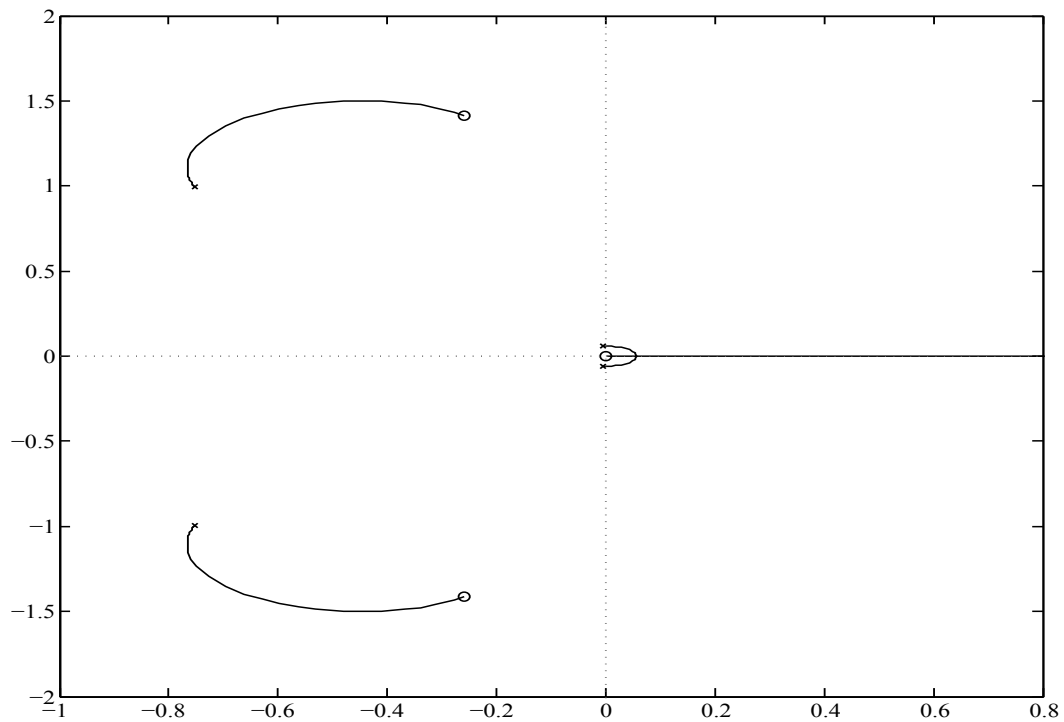


Figure 3.13: Root locus plot for outer loop with integrator for the case of vertical acceleration measured at the pilot seat

The main disadvantage of integration is that it pushes the system towards instability and also decreases the response time. In particular, the slow phugoid mode becomes even slower. The aim of the reference feed-forward path (shown in Fig. 3.11) is to place a zero ideally on top of the integrator pole to recover the phugoid mode's transient response. From the simplified structure in appendix B, the position of the zero is $(s + K_2/K_1)$, hence to place the zero close to the origin, a very large value of K_1 is required. This gain is limited by the design constraint imposed on actuators.

For a zero to have an effect on the transient response of complex poles, the zero must not be far removed from the poles by a factor of more than 3 [48]. This means that for the zero position shown by Eq. 3.9 if σ is the real part of the complex pole then $\alpha \leq 3$, for the zero to have an effect on the phugoid poles. The real part of the marginally stable phugoid poles after closing the integration loop is 0.01. If the zero is placed at 0.01, K_2 is 1 and σ is 0.01. This position of the zero meets the constraint on the actuator and is within acceptable bounds of the phugoid mode.

$$s = -\alpha\sigma \quad (3.9)$$

The short period pole position is not changed by placement of the zero, damping therefore remains at 0.6 and $\omega_{sp} = 1.27$.

Robustness of the complete FBW system against tail damage was tested and the open-loop poles compared with closed-loop poles. From Fig. 3.14 it may be verified that the robustness of the FBW system is not modified by the outer loop. The frequency of undamaged short period poles is 1.27 rad/s, with 40% damage it reduces to 0.753 rad/s, i.e. a reduction of 41%. This is approximately the same percentage as for the pure C* system in section 3.5.

3.7 Conclusion

The detailed design of a typical FBW control system based on the C* law was presented in this chapter. The system was implemented on a B747 model and an analysis of the change in flight dynamics due to tail damage was made. This change was evaluated against the ideal flying qualities as defined by MIL-STD-1797A handling qualities standard. The version of the C-star FBW control system implemented in this study improves robustness

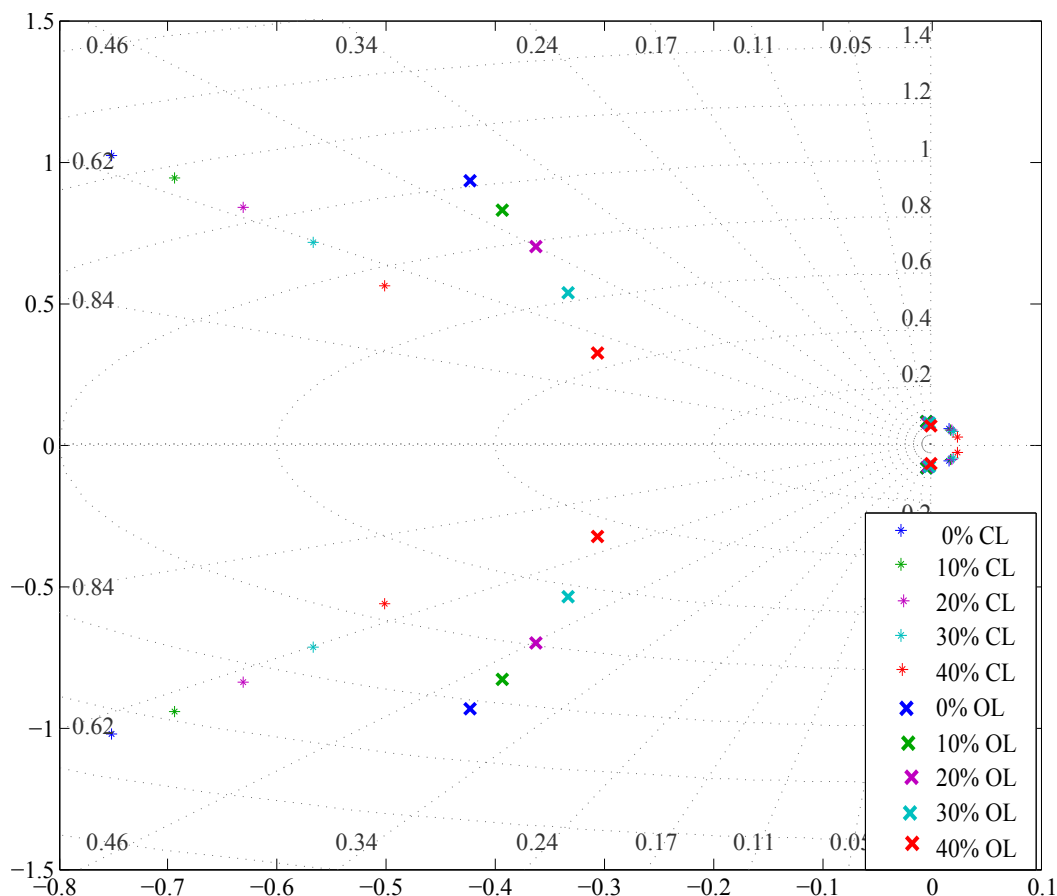


Figure 3.14: Open-loop vs. closed-loop poles at the pilot seat

such that with 50% stabiliser loss the aircraft is stable. Instability occurs when 60% of the stabiliser is damaged.

The FBW aircraft with 50% tail loss has level 3 short term longitudinal handling qualities. It is stable and controllable, although it is not considered safe to fly. The phugoid poles do not change significantly for damage up to 40%. With 50% loss these poles divide and one becomes unstable. The unstable pole has a very low frequency and is within the control capability of the pilot. From the results of this study it may be concluded that is necessary to improve the robustness of FBW to horizontal tail damage by minimising short period pole movement such that they are contained within an acceptable level of handling qualities (Level 2) with half the stabiliser removed.

Chapter 4

Theoretical Development of an Optimal Solution

In the preceding chapter, it was presented that the typical FBW system, based on a classical control structure, is not robust enough to retain the short period poles within level 2 handling qualities under 50% tail damage. H_2 optimal control was used to investigate alternative strategies to improve the system's robustness. This chapter details the theoretical development of the aircraft control problem into an optimisation problem solvable through H_2 control. Fundamentals of robust control, employed in techniques such as H_2 and H_∞ , are presented. These include uncertainty and disturbance modelling, linear fractional transformation, and conversion of MIMO transfer functions into state space representation. Furthermore, an optimal controller synthesis method is presented.

4.1 Modelling uncertainty

The model of a system describes the mathematical relationship between inputs and outputs. Typically the model is acquired through estimations based on fundamental theories and or measurements. Ideally the model should be an exact representation of the system, however, such a model would have a high mathematical complexity and thus be of limited usage. Inherently, modelling inaccuracies result from the simplification techniques used (such as linearisation, model order reduction, omission of high order dynamics, etc.). Efficient control design techniques must therefore take these inaccuracies into account. The difference between the actual system and its model is often referred to as dynamic

perturbation, which is a form of uncertainty [49]. Another type of uncertainty that will be considered in this study is that resulting from input disturbances.

Uncertainty may be represented as structured or unstructured uncertainty. If the physical mechanism that results in dynamic perturbation is known and can be adequately modelled, then the system and its perturbations can be formulated as a structured uncertainty problem. An example is the modelling of parametric uncertainty of an RLC circuit, whereby the expected variation of each component from its normal value is known. A rather more common example of structured uncertainty is the modelling of systems with white noise inputs in LQG optimal control. In both examples the disturbances are considered as additive uncertainty that results in a deviation in the output from its nominal response. Apart from LQG optimal control, singular value synthesis is another method used to design controllers specifically for structured uncertainty problems. This method is discussed in detail in [50].

The structured uncertainty model may be used in formulating the control problem of the damaged aircraft discussed in chapter 2. The difference in aerodynamic coefficient values between the undamaged and damaged aircraft can be presented as the deviation from nominal values and a controller synthesised to minimise the effect of this uncertainty on the output. One disadvantage of this approach is that only horizontal tail damage is considered as the source of uncertainty on the longitudinal aircraft dynamics. From the derivation of dynamic equations in chapter 2, it is evident that the model has approximation errors arising from linearisation and simplification assumptions such as airframe rigidity and symmetric inertia. Since these inaccuracies are ignored in the structured approach, they can thus be a source of additional error.

The damaged aircraft is modelled under a selected trim condition (Mach 0.5 at 20 000ft in a non-turbulent atmosphere with the CG at 25% MAC). Both the flight environment and aircraft configurations, however, vary throughout the flight. The effects of damage on the aircraft's dynamics varies with its configuration, which is in turn dependent on flight phase (cruise/landing/take-off). This variation is not considered in a structured uncertainty problem. In the unstructured model, dynamic perturbations are collectively represented as a single perturbation block, Δ . This block consists of bounded model sets of the deviation or error taken at the various operating points of the system (e.g. at

different flight conditions and aircraft configurations). In a more generalised form, for finite dimension linear time invariant systems, Δ is an unknown stable transfer matrix representing the maximum deviation.

The error Δ may be considered as absolute or relative uncertainty. The absolute model set consists of the range of values in which the true value of the variable lies. A distinctive feature of this model is that the error is constant throughout the considered operating points. This method is typically used in structured uncertainty problems whereby the error is additive, shown in Fig. 4.1. The system output y is the sum of the estimated and error output.

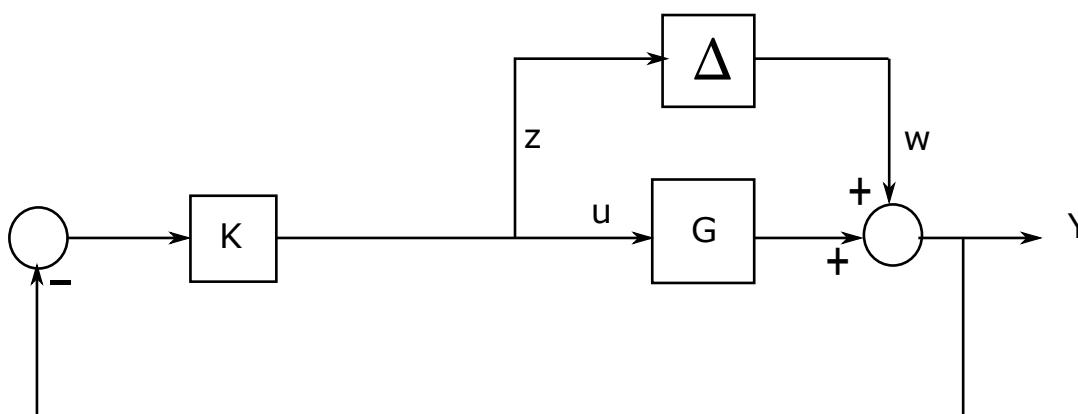


Figure 4.1: Additive uncertainty system

In practice, uncertainty increases with increasing frequency—an illustration of this is shown on the bode plot in Fig. 4.2. In the low frequency region, where system noise is not dominant, a more structured or absolute uncertainty model may be used. If, however, the high frequency region is considered then the relative model is more suitable. In this approach the degree of uncertainty is relative to varying plant characteristics and inputs. The multiplicative model is used to model relative uncertainty. The error may be input or output multiplicative. Input errors include those associated with actuation, whilst output ones typically arise from sensor noise. Figure 4.3 shows the input multiplicative model with output disturbance. Other dynamic perturbation models include coprime factor uncertainty, inverse multiplicative, etc.

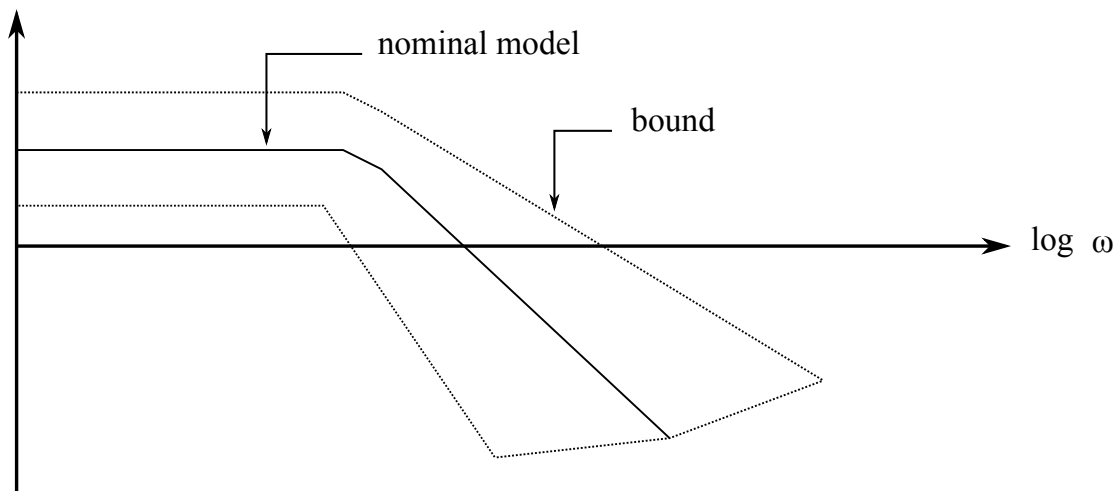


Figure 4.2: Multiplicative uncertainty behaviour

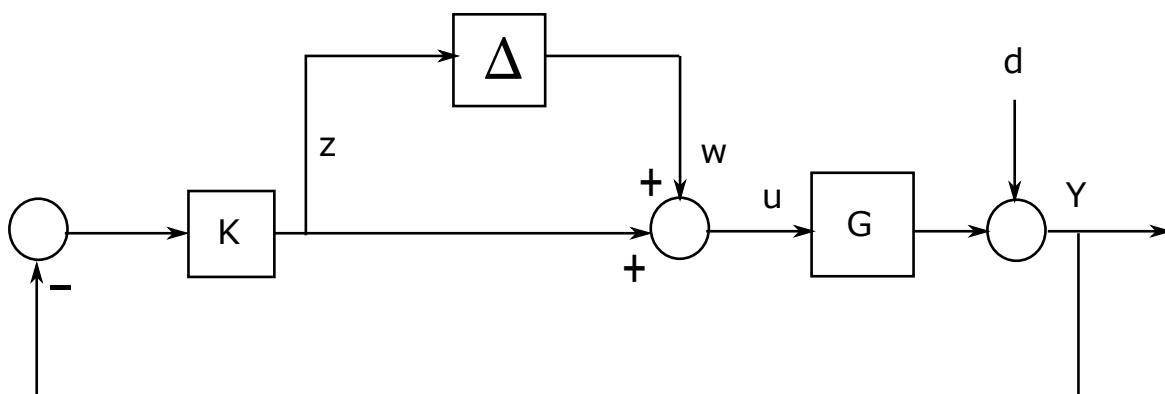


Figure 4.3: Input multiplicative uncertainty system

4.2 Linear Fractional Transformation

From Chapter 2, section 2.3.3, it was presented that the primary effect of horizontal tail damage on trim characteristics is the induction of a large pitching moment that pushes the aircraft's nose up (Table 2.2). If this moment is considered as a disturbance in the longitudinal dynamics, the control problem can be formulated as illustrated in Fig. 4.4. Input to the aircraft is the sum of controlled actuation and disturbance input, as such the control problem is to find a gain K that minimises the effect of disturbance d on the plant G_p . In an ideal system the output of the plant is a product of plant dynamics and actuation. Whilst the effect of disturbance is completely suppressed, this is however not an attainable objective. Various control techniques may be employed to reduce the effect of disturbance to an acceptable level. From classical control theory it is known that this may be achieved by increasing the gain. This, however, increases

the operational bandwidth of the system making it more susceptible to high frequency noise. From the discussion in chapter 3, one of the design objectives of an FBW system is to retain the aircraft's natural poles position so that the pilot is not presented with significantly different handling qualities when changing from normal to alternate or direct mode. Increasing the gain will, however, significantly move the poles and hence the control system will not meet the requirements. A suitable approach for the problem of this study is, therefore, one which improves disturbance rejection without significantly increasing the feedback gain. Optimisation methods can conveniently be used to find the gain for which the transmission of disturbance input d to output z_2 is minimised.

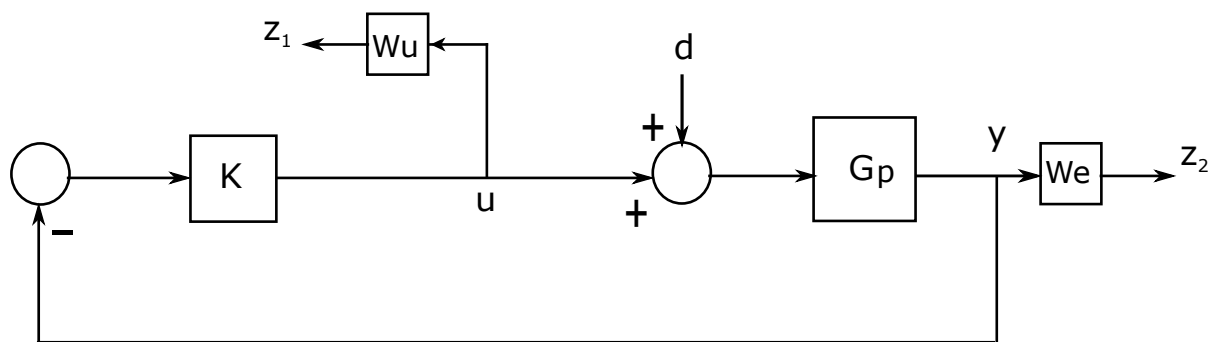


Figure 4.4: Longitudinal control system with pitch input disturbance

In Fig. 4.4, y is the measured output of the system, z_2 is the output due to the disturbance input, and u is the controlled input. Since the control objective is to find a suitable value of K that minimises the effect of d on the output, it is necessary to obtain first the transfer function between the disturbance input and resulting output z_2 . The system can

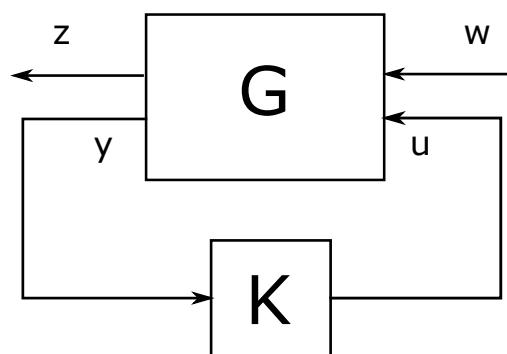


Figure 4.5: LFT of the longitudinal control system

be rearranged into the linear fractional transformation shown by Fig. 4.5. The variable

w represents all exogenous inputs to the systems (input disturbances, sensor noise, etc.), z represents the system outputs that are dependent on w inputs. From Fig. 4.4, the mapping from inputs w (d), u to outputs z, y can be written as shown by Eq. 4.1 and Eq. 4.2; where $W_u = W_e = 1$. The importance of weighting matrices W_u and W_e are discussed in section 4.2.2.

$$z_1 = \frac{K}{1 + G_p K} w + u \quad (4.1)$$

$$y = \frac{1}{1 + G_p K} w + \frac{G_p}{1 + G_p K} u \quad (4.2)$$

These equations are written in matrix notation to formulate the MIMO transfer function of Fig. 4.5; depicted in Eq. 4.3 ($z = z_1$). Since the optimisation methods used in this study are based on state space functions, it is required to convert this transfer function to a suitable representation.

$$\begin{bmatrix} z \\ y \end{bmatrix} = \begin{bmatrix} \frac{K}{1+G_p K} & 1 \\ \frac{1}{1+G_p K} & \frac{G_p}{1+G_p K} \end{bmatrix} \begin{bmatrix} w \\ u \end{bmatrix} \quad (4.3)$$

4.2.1 State space realisation of transfer functions

A simple realisation can be carried out by realising each element of the transfer function matrix using any canonical form (controllable, observable, or Jordan) and cascading them as illustrated by Eq. 4.4 and Eq. 4.5 [51].

$$G(s) = \begin{bmatrix} G_1(s) & G_2(s) \\ G_3(s) & G_4(s) \end{bmatrix} \quad (4.4)$$

$$G = \left[\begin{array}{cccc|cc} A_1 & 0 & 0 & 0 & B_1 & 0 \\ 0 & A_2 & 0 & 0 & 0 & B_2 \\ 0 & 0 & A_3 & 0 & B_3 & 0 \\ 0 & 0 & 0 & A_4 & 0 & B_4 \\ \hline C_1 & C_2 & 0 & 0 & D_1 & D_2 \\ 0 & 0 & C_3 & C_4 & D_3 & D_4 \end{array} \right] \quad (4.5)$$

A disadvantage of this method is that the resulting matrices are much larger than the original system matrix and may become difficult to work with. For example, the state matrix of the aircraft longitudinal model in chapter 2 has 4x4 elements. If this realisation is used, the state matrix of $G(s)$ has 16x16 elements. Moreover, the system $G(s)$ may be uncontrollable or unobservable in such a manner that the optimisation techniques of this study may not be usable. A minimal realisation is one in which the resulting system is controllable and observable. Kalman decomposition and balanced realisation methods are typically used on these large matrices to eliminate the unobservable and uncontrollable modes. A detailed discussion of these techniques are presented in [52].

An alternative approach to these tedious methods is direct minimal realisation techniques such as Gilbert's realisation [53]. This method uses partial fraction expansion, as in the Jordan canonical form. The eigen values of the system are diagonal elements of the state matrix. An equally simple method is presented by Hemanshu in [1]. This technique is discussed in Appendix C and demonstrated on the short period mode transfer function. The original 2x2 state matrix of the short period dynamics becomes a 4x4 matrix. If the full longitudinal mode is considered, the resulting matrix is 8x8—an improvement from the direct realisation.

A rather simpler but equally efficient method is discussed in [50]. The plant transfer matrix and the weighting functions are individually converted to state space form as shown by Eq. 4.6 to Eq. 4.8.

$$G_p = \begin{bmatrix} A_p & B_p \\ C_p & D_p \end{bmatrix} \quad (4.6)$$

$$W_u = \begin{bmatrix} A_u & B_u \\ C_u & D_u \end{bmatrix} \quad (4.7)$$

$$W_e = \begin{bmatrix} A_e & B_e \\ C_e & D_e \end{bmatrix} \quad (4.8)$$

The state equations of the system depicted in Fig. 4.4, are written as shown by Eq. 4.9 to Eq. 4.14. Substituting for y_p in Eq. 4.11 and Eq. 4.14, the equations are then presented in the state space notation of Eq. 4.15 and Eq. 4.16. For the 4x4 state matrix of the longitudinal dynamics with 2 inputs (elevator & thrust) and 2 corresponding outputs, the state matrix of the resulting system after this realisation has 8 elements. Due to its relative simplicity this is the preferred method for this study. Equation 4.17 is the compact notation of this state space equation.

$$\dot{X}_p = A_p X_p + B_p(d+u) \quad (4.9)$$

$$\dot{X}_u = A_u X_u + B_u u \quad (4.10)$$

$$\dot{X}_e = A_e X_e + B_e y_p \quad (4.11)$$

$$y_p = C_p X_p \quad (4.12)$$

$$z_2 = C_u X_u + D_u \quad (4.13)$$

$$z_1 = C_e X_e + D_e y_p \quad (4.14)$$

$$\begin{bmatrix} \dot{X}_p \\ \dot{X}_u \\ \dot{X}_e \end{bmatrix} = \begin{bmatrix} A_p & 0 & 0 \\ 0 & A_u & 0 \\ B_e C_p & 0 & A_e \end{bmatrix} \begin{bmatrix} X_p \\ X_u \\ X_e \end{bmatrix} + \begin{bmatrix} B_p \\ 0 \\ 0 \end{bmatrix} w + \begin{bmatrix} B_p \\ B_u \\ 1 \end{bmatrix} u \quad (4.15)$$

$$Y = \begin{bmatrix} D_e C_p & 0 & C_e \\ 0 & C_u & 0 \\ \text{---} & \text{---} & \text{---} \\ C_p & 0 & 0 \end{bmatrix} \begin{bmatrix} X_p \\ X_u \\ X_e \end{bmatrix} + \begin{bmatrix} 0 \\ 0 \\ - \\ 0 \end{bmatrix} w + \begin{bmatrix} 0 \\ D_u \\ - \\ 0 \end{bmatrix} u \quad (4.16)$$

$$G_{ac} = \left[\begin{array}{c|cc} A & B_1 & B_2 \\ \hline C_1 & D_{11} & D_{12} \\ C_2 & D_{21} & D_{22} \end{array} \right] \quad (4.17)$$

4.2.2 Weighting functions selection

For the H_2 optimal controller synthesis techniques used in this study, it is essential to use the weighting function W_u . It is not possible to calculate a feasible solution if the controlled input in the output equation D_{12} is zero. From Eq. 4.16 it is evident that if $W_u = 1$ then D_{12} is a null matrix. The weights are typically selected to reflect the frequency response of the foregoing signal in accordance with required performance objectives. The weights can be adjusted to achieve a compromise between conflicting objectives, hence they are used as tuning parameters in optimisation techniques such as the H_∞ mixed sensitivity problem.

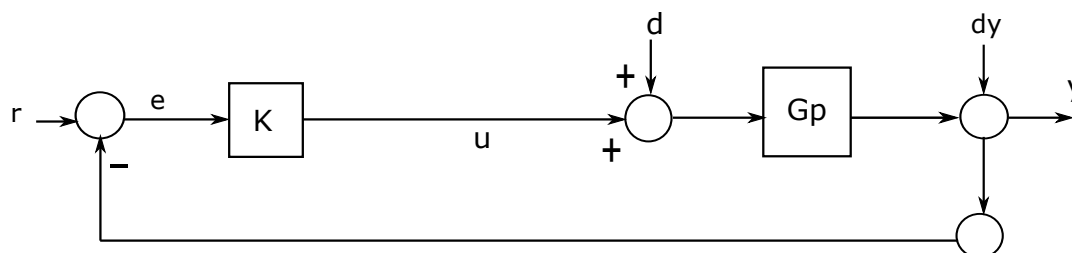


Figure 4.6: Feedback control system

The function W_e is selected to approximate the frequency response performance requirements of the output signal y . From Eq. 4.18 it can be seen that for good reference tracking behaviour the output y must be equal to r , hence the complementary sensitivity function T must be 1. This can be achieved by setting the gain to a high value. The effect of both input and output disturbances (d & dy respectively, Fig. 4.6) on y can be minimised with a high gain, such that the sensitivity function S is approximately zero. Whilst these objectives are achievable with a high gain, from Eq. 4.18 it may be observed that a high gain will increase the effect of high frequency sensor noise n on the output. Another disadvantage of high gain values is evident in Eq. 4.20. A large value of K results in high

actuator inputs which may cause saturation.

$$y = T(r-n) + S(Gp.dy) + S(d) \quad (4.18)$$

$$e = S(r-d) + T(Gp.n) - S(Gp.dy) \quad (4.19)$$

$$u = KS(r-n) + KS(d) + T(dy) \quad (4.20)$$

This is the typical trade-off between performance objectives of feedback systems. This problem is solved by shaping the frequency response, such that the gain is high at low frequencies where disturbance is dominant and tracking is required. At high frequencies the gain is set to a low value such that high frequency noise is attenuated. In H_∞ design techniques it is typical to shape the frequency response of the sensitivity function to achieve the ideal shape that meets the preceding objectives. This behaviour is shown in Fig. 4.7. The effect of the sensitivity function on the tracking error can be seen from equation Eq. 4.19. The error must be kept low in the frequency region of r,d and dy .

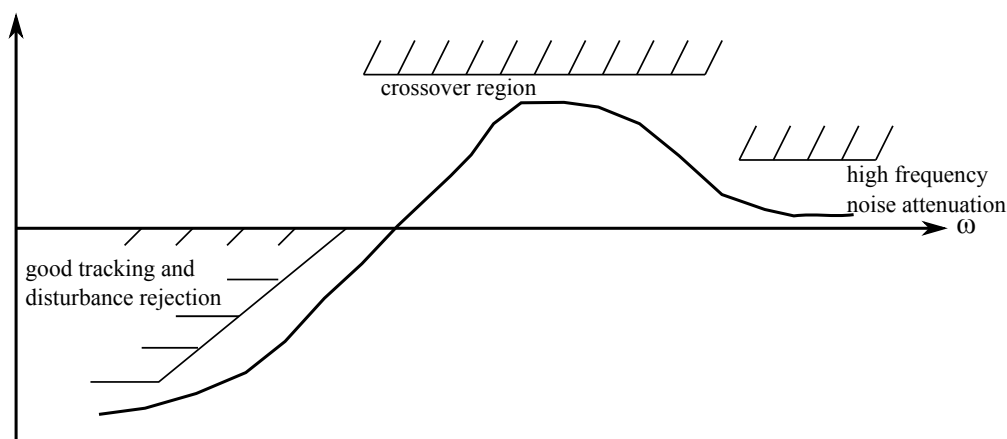


Figure 4.7: Typical sensitivity function

The maximum peak and bandwidth of the sensitivity function (shown as M_s and ω_b respectively in Fig. 4.8a) can be calculated from the time domain specifications (rise time, settling time, peak overshoot). Equation 4.21 is the first order approximation of the sensitivity function.

$$|S| = \frac{s}{\frac{s}{M_s} + \omega b} \quad (4.21)$$

The weight W_e is selected to normalise the sensitivity function such that $|W_e S| \approx 1$ as illustrated in Fig. 4.8. As such, W_e is thus the inverse of $|S|$. Since the controller synthesis

techniques used in this chapter cannot compute a solution for systems with unobservable poles on the imaginary axis, the integrator is converted to a pole at $\omega b\epsilon$.

$$W_e = \frac{\frac{s}{M_s} + \omega b}{s + \omega b\epsilon} \quad (4.22)$$

The high frequency poles of the B747 have value $\omega = 1.02$, a suitable ωb was selected

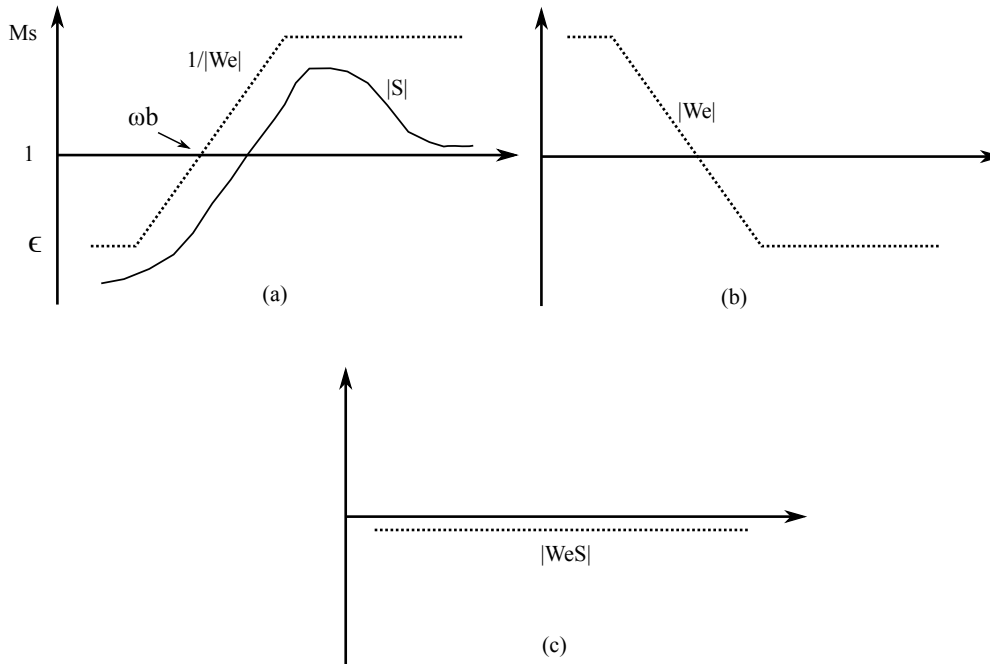


Figure 4.8: Sensitivity function normalisation

to be 1.2. $M_s = 1.3$ was chosen so as to attain a damping ratio of 0.6. The pole position $\omega b\epsilon$ may be any value less than 1; a value of 0.1 was chosen.

The selection of actuator weight function W_u is dependent on the operational parameters of the actuators. For example, the average bandwidth of the B747 elevators is $30^\circ/\text{s}$. Figure 4.9 shows the typical frequency response of actuators. Similarly to the selection of W_e , W_u is the inverse of the actuator function. Since the approximation of the actuator input is a simple high pass filter, a faraway pole is introduced in W_u to make it a proper function.

$$W_u = \frac{s + \frac{\omega_{bc}}{M_u}}{\epsilon_c s + \omega_{bc}} \quad (4.23)$$

The bandwidth of the approximating function was selected to be slightly above the average elevator bandwidth, $\omega_{bc} = 0.645$, the gain $M_u = 10$ and $\epsilon_c = 0.001$.

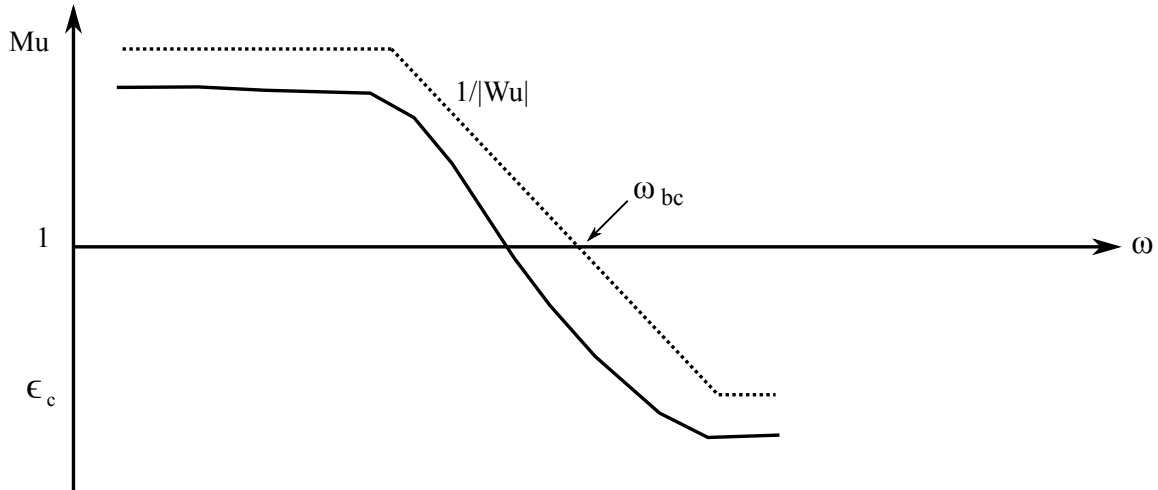


Figure 4.9: Weight function W_u

4.3 Formulation of the control problem

The H_2 control problem is to find a controller K that stabilises the system G_p and minimises the H_2 norm of the transfer matrix T_{zw} from w to z [50]. As previously discussed this is the function that describes the transmission of disturbances in the system. The control objective is thus to compute a gain that keeps a certain measure (the H_2 norm) of the disturbance function to a minimum. The norm of any system is the measure of its input–output gain at different frequencies.

4.3.1 The \mathcal{L}_2 and H_2 norm

For a continuous time scalar signal $x(t)$, the \mathcal{L}_2 norm is defined as the energy contained in the signal over a period of time, shown by Eq. 4.24. An example of the \mathcal{L}_2 norm is the energy across a resistor, if $R = 1$ then the norm is as depicted by Eq. 4.25.

$$\|x(t)\|_2 = \int_{t_1}^{t_2} x(t)^2 dt \quad (4.24)$$

$$\|E(t)\|_2 = \int_{t_1}^{t_2} I(t)^2 R dt \quad (4.25)$$

If $x(t)$ is a vector signal then the \mathcal{L}_2 norm is defined as shown by Eq. 4.26.

$$\|x(t)\|_2 = \left[\int_{t_1}^{t_2} x(t)^T x(t) dt \right]^{\frac{1}{2}} \quad (4.26)$$

The H_2 norm of a system is the energy contained in the system for different signals. In the frequency domain it is the average gain of the system for all frequencies as viewed

from the bode plot. For a strictly proper and stable transfer function T_{zw} it is defined as shown by Eq. 4.27, where T_{zw}^H is the complex conjugate transpose of T_{zw} .

$$\|T_{zw}\|_2 = \sqrt{\frac{1}{2\pi} \int_{-\infty}^{\infty} \text{trace}(T_{zw}^H(j\omega)T_{zw}(j\omega)) d\omega} \quad (4.27)$$

The H_2 of a system can therefore be defined as the square root of the integral of the Frobenius norm of the system T_{zw} between $-\infty$ and ∞ . For a square matrix A , the Frobenius norm is as shown by Eq. 4.28.

$$\|A\|_F = \text{trace}(A^H A) \quad (4.28)$$

The trace of a matrix B is defined as the sum of its diagonal values, as illustrated in Eq. 4.29.

$$B = \begin{bmatrix} a & b & c \\ d & e & f \\ g & h & i \end{bmatrix} \quad \text{trace}(B) = a + e + i \quad (4.29)$$

If the definition of Eq. 4.27 is considered in the s -domain, then from the definition of the Laplace transform, $\|T_{zw}\|_2$ is equal to the \mathcal{L}_2 norm of the output signal to an impulse input (Eq. 4.30). Hence, in the longitudinal control system of Fig. 4.4, for an impulse input w , the square of the \mathcal{L}_2 norm of the output is equal to the square of the H_2 norm of the transfer function from w to z . The H_2 control problem can thus be expressed as: *find K that stabilises Gp and minimises $\|z\|_2^2$.*

$$\|T_{zw}\|_2^2 = \|z\|_2^2 \quad (4.30)$$

In section 4.2 it is presented that the controller synthesis techniques employed in this study are based on state space systems. From Parseval's theorem (Appendix C) the energy contained in the time domain is the same as the energy contained in the frequency domain. The preceding definition of the H_2 norm can thus be applied in the state space representation of the system in Fig. 4.4.

4.3.2 Linear Quadratic Regulator (LQR) Problem

The H_2 optimal control problem is an extension of the LQR problem. As such, it is necessary to first discuss the basic concepts of this method in order to provide an un-

derstanding of H_2 optimisation. The LQR infinite time problem (as t goes to ∞ , $x(t)$ is driven to the origin), can be stated as:

For the dynamic system of Eq. 4.31 and Eq. 4.32, find a control law $u(t)$ such that the performance index on Eq. 4.33 is minimised.

$$\dot{x} = Ax + Bu \quad x_{t_0} = x_0 \quad (4.31)$$

$$y = Cx + Du \quad (4.32)$$

$$J(t) = \frac{1}{2} \int_0^{\infty} [x^T(t)Qx(t) + u^T(t)Ru(t)] dt \quad (4.33)$$

Assuming that the state $x(t)$ is controllable by input $u(t)$, the control objective of this problem is to compute a controller that can drive the state to a small neighbourhood of the origin within finite time. A suitable performance index thus consists only of the \mathcal{L}_2 norm of the state vector. The primary objective is to regulate the energy of the states, i.e. prevent an exponential increase by keeping the energy confined to a region close to the origin. Such a system would however result in large control inputs being used to achieve this criterion. Hence, there is a further requirement to minimise the \mathcal{L}_2 norm of the control input. Equation Eq. 4.33 is now a convex combination of the performance index of the \mathcal{L}_2 norm of $x(t)$ and $u(t)$ (the subject of convex functions is discussed in section 5.1.3). Q and R are positive semi-definite and positive definite matrices respectively, used as weighting functions to tune the system. These can be adjusted to tune the system to achieve a given set of performance requirements for conflicting objectives similar to the functions discussed in 4.2.2. The scalar $1/2$ is used in the performance index to simplify the mathematical computation of the minimum of the function and does not in any way alter the value of the solution.

In the H_2 control problem, the performance index to minimise is energy of the output from disturbance inputs $\|z\|_2^2$. For the system of section 4.2.1, the output z is shown in Eq. 4.34.

$$z = C_1x + D_{12}u \quad (4.34)$$

From the definition of the \mathcal{L}_2 norm of a vector signal in Eq. 4.26, the norm of the output z can be written as shown in Eq. 4.35.

$$\|z(t)\|_2^2 = \int_0^{\infty} (C_1x(t) + D_{12}u(t))^T (C_1x(t) + D_{12}u(t)) dt \quad (4.35)$$

If $D_{12}^T C_1 = 0$, then Eq. 4.35 can be written as shown in Eq. 4.36.

$$\|z(t)\|_2^2 = \int_0^\infty x(t)^T C_1^T C_1 x(t) + u(t)^T D_{12}^T D_{12} u(t) dt \quad (4.36)$$

A comparison of the H_2 performance index from Eq. 4.36 and LQR index from Eq. 4.33 shows that the two are similar. When $D_{12}^T C_1$ is not zero the problem is an extension of the LQR problem.

4.4 Solution of the optimal control problem: Calculus of variations approach

Several techniques may be used to solve dynamic optimisation problems, however, only the interior point method and calculus of variations approach will be considered in this study. The latter method is discussed in [54], [55], and [50]. A major disadvantage of the calculus of variations approach is that if the system has poles close to the imaginary axis, then a feasible solution does not exist. As discussed in Chapter 2 the B747's phugoid mode has imaginary poles, as such this method cannot synthesise a feasible solution. It is, however, discussed here to give insight into how the disturbance rejection problem is handled in H_2 optimisation and thus provides a basis for analysis of the solution in Chapter 6. The solution of the optimisation problem of this study, using the interior point method, is discussed in chapter 5.

The H_2 control problem can be formulated into a constrained optimisation problem:

Find the control input $u(t)$ such that the function $\|C_1 x + D_{12} u\|_2^2$ is minimised and the condition $\dot{x} = Ax + B_2 u$ is satisfied.

To solve a constrained dynamic optimisation problem, it must first be converted to an unconstrained problem. If the performance index and equality constraint have continuous partial derivatives then a (co-state) variable named a Lagrange multiplier, $\lambda(t)$, can be used to merge the two into one function as shown by Eq. 4.37. The subject on the use of Lagrange multipliers in optimisation problems is dealt with in section 5.3.2.

$$J(.) = \int_0^\infty (C_1 x(t) + D_{12} u(t))^T (C_1 x(t) + D_{12} u(t)) dt + \lambda^T(t)(Ax + B_2 u - \dot{x}(t)) \quad (4.37)$$

In this approach, it is assumed that the state $x(t)$ is controllable with inputs $u(t)$ and the objective is to find an optimal trajectory for which the function $J(.)$ is a minimum. This

is illustrated in Fig. 4.10. In the finite horizon optimisation problem the final time (TF) for the state to reach a specified value is given. The time domain specification of the solution can, therefore, be explicitly stated. The H_2 optimal control problem is however an infinite horizon problem, i.e. $x(t)$ goes to the origin as t goes to ∞ . The objective is to minimise disturbance rejection and no specification is given on performance. As such, the resulting controller may provide ideal disturbance rejection but unacceptable performance for the problem of this study. The solution is computed by considering the

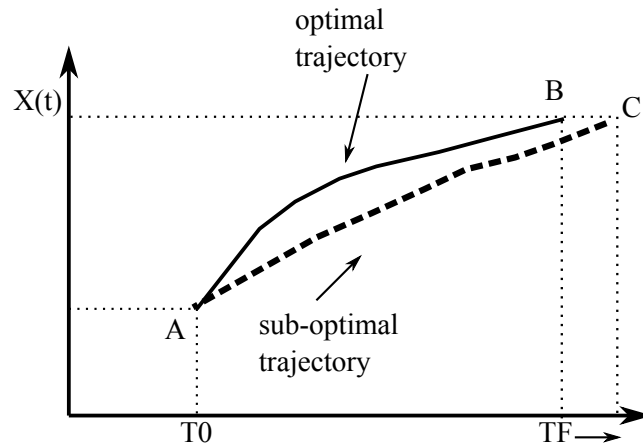


Figure 4.10: Optimal trajectory search

incremental of the function (suboptimal path minus optimal path, see Fig. 4.10) and using Taylor series expansion to estimate the optimal path. A necessary condition for the function to be an extremum (minimum/maximum) is that its first derivative is zero. A sufficient condition for it to be a maximum is that its 2nd derivative be positive definite (section 5.3.3). The Hamiltonian matrix in Eq. 4.38 is obtained by differentiating the first derivative of the incremental function with respect to $u(t)$, $x(t)$, and $\lambda(t)$.

$$\begin{bmatrix} \dot{x}(t) \\ \dot{\lambda}(t) \end{bmatrix} = \begin{bmatrix} A - B_2 R^{-1} D_{12}^T C_1 & B_2 R^{-1} B_2^T \\ -C_1^T C_1 + C_1^T D_{12} R^{-1} D_{12}^T C_1 & -(A - B_2 R^{-1} D_{12}^T C_1)^T \end{bmatrix} \begin{bmatrix} x(t) \\ \lambda(t) \end{bmatrix} \quad (4.38)$$

$$R = D_{12}^T D_{12}$$

The similarity transform from Eq. 4.39 is used on the Hamiltonian system and the resulting algebraic Riccati equation (ARE) is shown by Eq. 4.40. The Equation is solved to find the value of P . The relationship between P and the closed-loop gain K is as depicted by Eq. 4.41 [54]. If any complex conjugate eigenvalues of A in the Hamiltonian matrix

are close to the imaginary axis, then the ARE is not solvable and thus an alternative method is required to find a feasible solution.

$$\begin{bmatrix} \mathbf{I} & \mathbf{0} \\ \mathbf{P} & \mathbf{I} \end{bmatrix} \begin{bmatrix} \bar{\mathbf{x}}(t) \\ \bar{\lambda}(t) \end{bmatrix} = \begin{bmatrix} \mathbf{x}(t) \\ \lambda(t) \end{bmatrix} \quad (4.39)$$

$$\begin{aligned} \mathbf{A}_n^T \mathbf{P} + \mathbf{P} \mathbf{A}_n + \mathbf{P} \mathbf{B}_2 \mathbf{R}^{-1} \mathbf{B}_2^T \mathbf{P} - \mathbf{C}_1^T \mathbf{C}_1 + \mathbf{C}_1^T \mathbf{D}_{12} \mathbf{R}^{-1} \mathbf{D}_{12}^T \mathbf{C}_1 &= \mathbf{0} \\ \mathbf{A}_n &= \mathbf{A} - \mathbf{B}_2 \mathbf{R}^{-1} \mathbf{D}_{12}^T \mathbf{C}_1 \end{aligned} \quad (4.40)$$

$$\mathbf{K} = \mathbf{R}^{-1} (\mathbf{D}_{12}^T \mathbf{C}_1 + \mathbf{B}_2^T \mathbf{P}) \quad (4.41)$$

4.5 Conclusion

In this chapter, the horizontal tail damage problem was represented as a robust control problem. Relevant uncertainty model structures were discussed and the most suitable one selected. The uncertainty model is then interpreted into a MIMO state space model through a linear fractional transformation and a relatively simple state space realization method. H_2 control fundamentals are discussed, followed by the formulation of the aircraft problem as an H_2 control problem. LQR control and its similarity to H_2 control is discussed in order to provide an understanding of the optimal solution. Finally, the calculus of variations approach to solving optimization problems is presented. Although this method does not provide a feasible solution for the problem of this study, it is discussed in-order to give insight into the expected solution.

Chapter 5

Solution of FBW Control Problem through Convex Optimisation

This chapter focuses on the formulation of the H_2 optimal control problem, from chapter 4, as a convex optimisation problem through the use of linear matrix inequalities, and solving it using the interior point method. A brief overview of convex optimisation is presented as well as its main advantages and disadvantages. First, the use of linear matrix inequalities for solving control problems is discussed. Second, the disturbance rejection H_2 control problem of this study is formulated as an LMI. A discussion of the primal-dual interior point method, as a solver for optimisation problems, is presented.

5.1 Convex optimisation overview

The standard optimisation problem can be stated as:

Minimise $F_0(x)$

subject to $F_i(x) \leq b_i \quad i = 1, \dots, m$

In the case of convex optimisation, however, both the objective and constraint function must belong to a convex set.

5.1.1 Convex sets

A set is said to be convex if for any two points within the set, the straight line joining them is also within the set. This is illustrated in Fig. 5.1. For every variation of μ between

0 and 1 in Eq. 5.1, x must be within the set. When $\mu = 0$, $x = x_2$ and when $\mu = 1$ then $x = x_1$. From Fig. 5.1 it can be seen that for all values of μ between 0 and 1, x lies within the set in the pentagon (a); whilst when μ is 0.5, x is outside the set depicted in (b).

$$x = \mu x_1 + (1 - \mu)x_2 \quad 0 \leq \mu \leq 1 \quad (5.1)$$

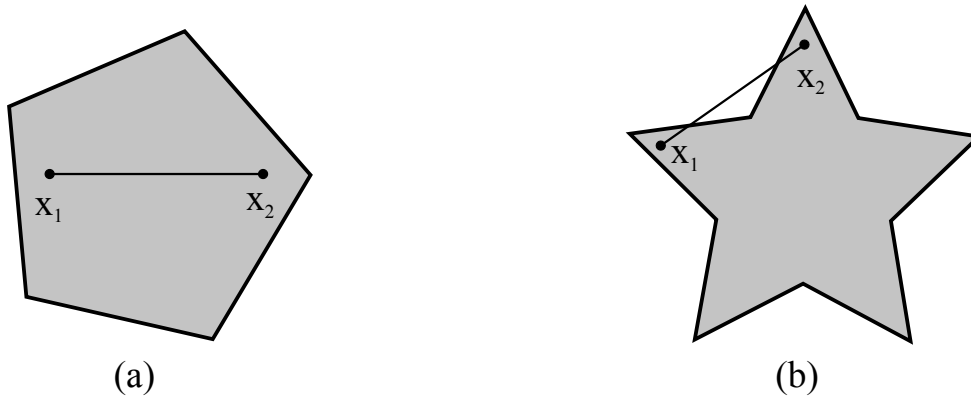


Figure 5.1: Example of convex and non-convex sets

Examples of convex sets that are of particular importance in this chapter, are the set of all positive semi-definite matrices and the set of all negative definite matrices. From appendix C, the definition of positive semi-definiteness is stated as:

A real and symmetric matrix A is positive semi-definite if $x^T A x \geq 0$ for all $x \neq 0$ (Appendix D).

Consider 2 positive semi-definite matrices A and B in the set and substituting for x_1 and x_2 in Eq. 5.1. Since μ is a positive scalar, it is evident that the sum of the first and second terms of Eq. 5.1 is positive semi-definite for all values of μ between 0 and 1.

$$C = x^T (\mu A + (1 - \mu)B)x \quad (5.2)$$

5.1.2 Convex and concave functions

A function (mapping between sets) is convex if for any two points, x_1 and x_2 within the set, Eq. 5.3 is satisfied. This is equivalent to the statement that for any line joining two points on the function, the function must be below the line. An illustration of this is shown in Fig. 5.2

$$f(\mu x_1 + (1 - \mu)x_2) \leq \mu f(x_1) + (1 - \mu)f(x_2) \quad 0 \leq \mu \leq 1 \quad (5.3)$$

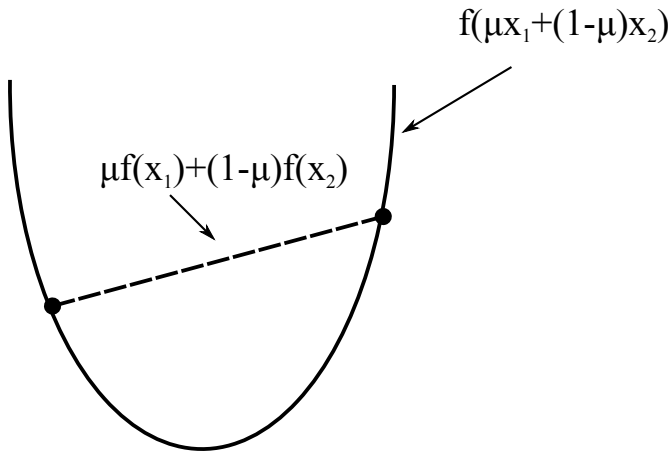


Figure 5.2: Convex function

A function is said to be concave in a convex set if $f(y) = -f(x)$ and $f(x)$ is a convex function.

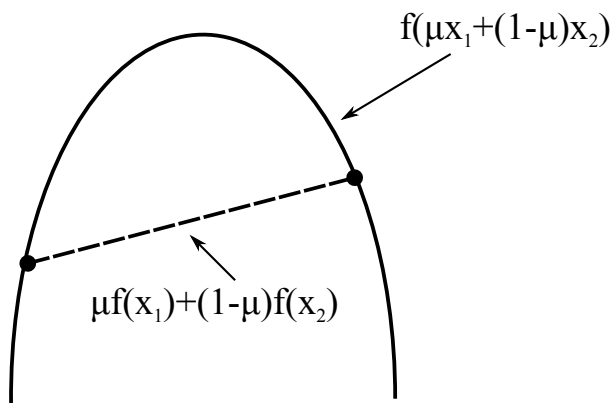


Figure 5.3: Concave function

5.1.3 Convex combinations

It is sometimes necessary to combine multiple convex sets to reformulate the optimisation problem into a form that is more suitable for a particular solver. Since the function must still be convex after such a manipulation, it is thus important to review operations that preserve convexity. This section will, however, focus on only the operations used in this study—the extensive details of convex combinations can be found in [56]. If S_1 and S_2 are convex sets, then:

The sum of two sets is convex

$$S_1 + S_2 = \{x_1 + x_2 \mid x_1 \in S_1, x_2 \in S_2\} \quad (5.4)$$

The Cartesian product of two sets is convex

$$S_1 * S_2 = \{x_1, x_2 \mid x_1 \in S_1, x_2 \in S_2\} \quad (5.5)$$

The image of a convex set S under an affine function $f(x)$ is convex

$$f(x) = AP + AP + Q \quad f(S) = \{f(x) \mid P \in S\} \quad (5.6)$$

5.1.4 Global and local optimality

A locally optimal point is one that minimises the objective function in the feasible space within its neighbourhood. As such it is not necessarily the lowest point in the whole feasible space. If both the objective and constraint functions are differentiable, local optimisation methods can be used. This approach is relatively simpler and requires less computational time for problems with a large number of variables. In global optimisation the local optimal point is a minimum in the whole feasible region. There is, therefore, no other point within the feasible space that is less than the optimal value obtained through a global optimisation technique. This method is evidently less efficient than local optimisation and computation of the solution requires more time, especially for large scale problems. Convex optimisation is a global optimisation method and as such the solution is a minimum in the whole feasible space.

5.2 Linear Matrix Inequalities

Many multivariable control problems can be formulated as a set of linear matrix inequalities and solved with modern convex programming solvers. A standard LMI is of the form depicted in Eq. 5.7 [57].

$$F(x) = F_0 + \sum_{i=1}^m x_i F_i > 0 \quad (5.7)$$

The inequality must satisfy the requirements:

- the matrices F_i must be real, positive definite, and symmetric.
- F_0 must be a positive real Hermitian (a matrix is Hermitian if it is equal to its complex

conjugate transpose).

- $F(x)$ must be an affine mapping of the decision variables x_i ,

Non-strict LMIs are positive semi-definite, as shown in Eq. 5.8

$$F(x) = F_0 + \sum_{i=1}^m x_i F_i \geq 0 \quad (5.8)$$

5.2.1 Formulation of the H_2 control problem as an LMI

The optimisation problem of this study is to minimise the H_2 norm of the longitudinal dynamics transfer function between the output and disturbance input, i.e. $\|T_{zw}\|_2$. From Eq. 4.17 in chapter 4, the transfer function can be written as depicted in Eq. 5.9.

$$\begin{aligned} z(s) &= C_1(sI - A)B_1 \\ z(t) &= C_1 \exp(At)B_1 \end{aligned} \quad (5.9)$$

From the definition in Eq. 4.27, the H_2 norm of the system $z(t)$ can be written as shown by Eq. 5.10, and rearranged to Eq. 5.11.

$$\|z\|_2^2 = \text{trace} \int_0^\infty B_1^T \exp(A^T t) C_1^T C_1 \exp(At) B_1 dt \quad (5.10)$$

$$\|z\|_2^2 = \text{trace} \int_0^\infty C_1 \exp(At) B_1 B_1^T \exp(A^T t) C_1^T dt \quad (5.11)$$

Let $P = \int_0^\infty \exp(At) B_1 B_1^T \exp(A^T t) dt$, then $\|z\|_2^2 = \text{trace}(C_1 P C_1^T)$.

Assuming the system of Eq. 5.9 is stable and the symmetric positive definite matrix P exists, then the Lyapunov function (Appendix D) in Eq. 5.12 is obtained.

$$AP + PA^T + B_1 B_1^T < 0 \quad (5.12)$$

Since $(A + A^T)$ and $B_1 B_1^T$ are symmetric it is evident that Eq. 5.12 is an LMI and P is the decision variable. $F_0 = -B_1 B_1^T$ and $F_i = -AP - P_i A^T$.

With state feedback $K = D_K$, the “new” A matrix is $(A + B_2 K)$, so that Eq. 5.12 becomes Eq. 5.13.

$$(A + B_2 K)P + P(A + B_2 K)^T + B_1 B_1^T < 0 \quad (5.13)$$

From a comparison of Eq. 5.13 to the properties of LMIs in section 5.2, it can be seen that the inequality is no longer an LMI due to the term $(B_2 K P)$. The two variables can

be combined into one decision variable $Y = KP$, then substituting in Eq. 5.13 to obtain the LMI in Eq. 5.14

$$AP + B_2Y + PA^T + B_2Y^T + B_1B_1^T < 0 \quad (5.14)$$

With state feedback the output matrix C_1 becomes $(C_1 + D_{12}D_K)$ and the H_2 norm can be calculated as shown in Eq. 5.15. This can be simplified into the two inequalities in Eq. 5.16 and Eq. 5.17.

$$\text{trace}[(C_1 + D_{12}D_K)P(C_1 + D_{12}D_K)^T] < z \quad (5.15)$$

$$(C_1 + D_{12}D_K)P(C_1 + D_{12}D_K)^T < z, \quad (5.16)$$

$$\text{trace}(z) < 1 \quad (5.17)$$

Equation 5.16 can be formulated into an LMI by applying Schur's lemma (Appendix C). The resulting inequality is shown in Eq. 5.17.

$$\begin{bmatrix} P & (C_1P + D_{12}Y)^T \\ (C_1P + D_{12}Y) & z \end{bmatrix} > 0 \quad (5.18)$$

The optimal solution to the H_2 problem is obtained by solving Eq. 5.14, Eq. 5.17, and Eq. 5.18. The feedback gain is $K = YP^{-1}$.

5.3 Solution of LMIs: Interior point method

Freely available software, such as SeDuMi and SDPT3, are widely used to solve matrix inequalities. SDPT3, through the YALMIP interface, was selected as the solver in this study. It is relatively simple to use, runs on Matlab, and has acceptable convergence time for the LMI problem of this research. The software executes the primal-dual interior point method to find a solution to a semi-definite programming (SDP) minimisation problem. The interior point method is based on Newton's optimisation method and combines multiple techniques such as the use of Lagrange multipliers, the log barrier function, and the duality theorem. These techniques are discussed in the following sections and an algorithm of the primal-dual interior point method is presented.

5.3.1 Newton's method

Assuming that for a given function $f(x)$ its second derivative can be computed, the objective is to find x for which the function is at its minimum. Newton's method provides an iterative search algorithm to find the value of x at the stationary point where the function is not decreasing any further. Approximate $f(x)$ in the neighbourhood $x = x^k$ using a Taylor series expansion.

$$m = f(x^k + \Delta x) \approx f(x^k) + \nabla f^T(x^k)\Delta x + \frac{1}{2}\Delta x^T \nabla^2 f(x^k)\Delta x \quad (5.19)$$

The function is a minimum when its rate of change is zero, i.e. $\frac{\partial m(x)}{\partial x} = 0$

$$\frac{\partial m(x)}{\partial x} = \nabla f(x^k) + \nabla^2 f(x^k)\Delta x = 0 \quad (5.20)$$

Since $\Delta x = x - x^k$, then by substituting for Δx in equation Eq. 5.20 and rearranging, Eq. 5.21 is obtained.

$$x = x^k - [\nabla^2 f(x^k)]^{-1} \nabla f(x^k) \quad (5.21)$$

If x is the current value and x^k is the previous iteration, then

$D_k = -[\nabla^2 f(x^k)]^{-1} \nabla f(x^k)$ is called the search direction for which the function is decreasing. The minimisation algorithm can be summarised as:

step 0 Given an initial value of x^0 set k to 0.

step 1 $D_k = -[\nabla^2 f(x^k)]^{-1} \nabla f(x^k)$ if $D_k = 0$ stop iteration.

step 2 Set step size $\alpha^k = 1$.

step 3 set $x = x^k + \alpha^k D_k$, for $k = k + 1$ and go to step 1

This process is repeated until the search direction D_k is zero, i.e. the function is stationary and not decreasing any further. The value of x at this iteration is the point where the function is a local minimum and a solution to the minimisation problem. A more detailed discussion of this method can be found in [55].

5.3.2 Constrained problems: Lagrange multipliers

A constrained optimisation problem is of the form:

Minimise $f(x)$

Subject to: $g(x) = 0$

$h(x) \leq 0$

The objective is to find the value of the decision variable x , for which the function is a minimum. The solution must satisfy both the equality constraint $g(x)$ and the inequality constraint $h(x)$. The Lagrange multiplier approach is commonly used in optimisation problems to truncate the objective function with the equality constraint. The inequality constraint can be converted to an equality constraint by adding a variable such that the function is equal to the specified value ($h(x) + S^2 = 0$). The variable is squared to impose a sign restriction on it.

The concept of Lagrange multipliers can be explained by considering the example in Fig. 5.4. The constraint $g(x)$ is imposed on the contour lines of the objective function $f(x)$. Assuming that both functions are differentiable, when the gradient of $f(x)$ is evaluated

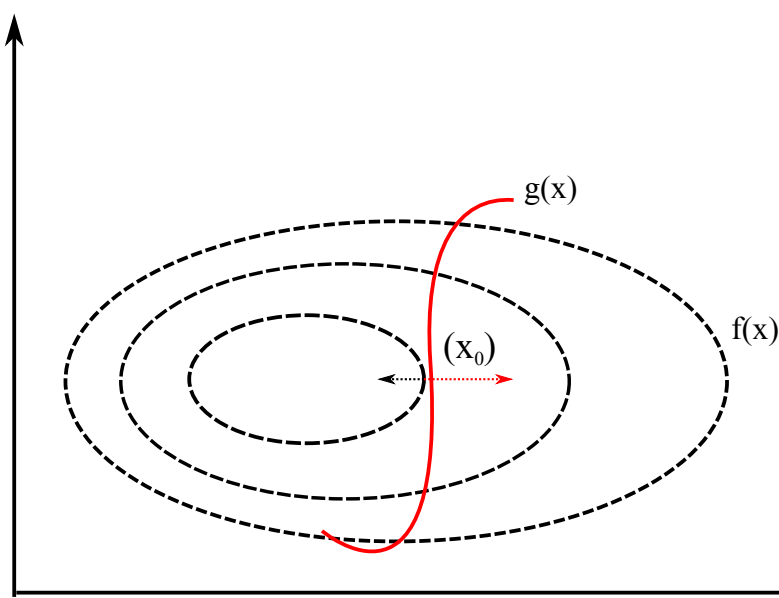


Figure 5.4: Contours of objective function against constraint function illustrating tangential point

at the point (x_0) , the result is a vector perpendicular to the contour line passing through the point. At this point, the two functions $f(x)$ and $g(x)$ are tangents—their gradient vectors are, therefore, along the same direction. One gradient is a multiple of the other and the scale factor between the two is λ_0 . This is shown in Eq. 5.22.

$$\nabla f(x_0) = \lambda_0 \nabla g(x_0) \quad (5.22)$$

The Lagrangian function (named after Joseph Louis Lagrange) of the optimisation problem is an expression of the objective function and equality constraints.

$$L(x, \lambda, \mu, S) = f(x) + \lambda(g(x)) + \mu(h(x) + S^2) \quad (5.23)$$

5.3.3 Karush-Kuhn Tucker (KKT) conditions

Let (x^*) be a regular point on the feasible set. If it is a local minimum for the function $f(x)$ subject to $g(x) = 0$ and $h(x) \leq 0$, then the following conditions are true.

For the Lagrangian function $L(x, \lambda, \mu, S) = f(x) + \lambda(g(x)) + \mu(h(x) + S^2)$:

$$\frac{\partial L(.)}{\partial x} = \frac{\partial f(x)}{\partial x} + \lambda \frac{\partial g(x)}{\partial x} + \mu \frac{\partial (h(x) + S^2)}{\partial x} = 0 \quad (5.24)$$

$$\frac{\partial L(.)}{\partial \lambda} = g(x) = 0 \quad (5.25)$$

$$\frac{\partial L(.)}{\partial \mu} = h(x) + S^2 = 0 \quad (5.26)$$

$$\frac{\partial L(.)}{\partial S} = 2\mu S = 0 \quad (5.27)$$

$$S^2 \geq 0 \text{ if } h(x) \leq 0 \quad (5.28)$$

$$\mu \geq 0 \quad (5.29)$$

These equations are collectively called the KKT necessary conditions. They characterise the function at the point where it is a minimum within the feasible region [55]. The solution of these equations, therefore, solves the minimisation problem. If the function $f(x)$ is convex then $\frac{\partial f(x)}{\partial x} = \nabla f(x)$.

5.3.4 Primal-Dual Problems

Primal Problem:

$$\text{Maximise: } C^T x$$

$$\text{Subject to: } Ax \leq b$$

The dual of the primal problem can be stated as

$$\text{Minimise: } b^T y$$

$$\text{Subject to: } Ay \geq c$$

Example:

Primal Problem:

$$\text{Maximise } 9x_1 + 2x_2$$

$$\text{Subject to: } 2x_1 + 5x_2 \leq 10$$

$$4x_1 + 3x_2 \leq 12$$

Dual Problem:

$$\text{Minimise: } 10y_1 + 12y_2$$

$$\text{Subject to: } 2y_1 + 4y_2 \geq 9$$

$$5y_1 + 3y_2 \geq 2$$

Theorem: *if x is a feasible solution to the primal problem and y is a solution to the dual problem, then $y^T b \geq x^T C$.*

Proof: Since x is a feasible solution it satisfies the constraints $Ax \leq b$ and $x \geq 0$. Similarly, if y is a feasible solution of the dual problem, it satisfies $A^T y \geq c$ and $y \leq 0$.

Multiplying both sides of the duality constraint by x : $x^T A^T y \geq x^T c$ which can be rearranged as $y^T Ax \geq C^T x$ and substituting b for Ax then $y^T b \geq C^T x$

Theorem: *suppose \bar{x} and \bar{y} are feasible solutions to the primal and dual problems respectively, if $C^T \bar{x} = b^T \bar{y}$ then \bar{x} and \bar{y} are the optimal solutions to their respective problems*

Proof: Let y be an arbitrary solution to the dual problem. If \bar{x} is the solution to the

primal problem then $\mathbf{b}^T \mathbf{y} \geq \mathbf{C}^T \bar{\mathbf{x}}$. Therefore, if $\mathbf{b}^T \bar{\mathbf{y}} = \mathbf{C}^T \bar{\mathbf{x}}$ then $\mathbf{b}^T \bar{\mathbf{y}} = \mathbf{C}^T \bar{\mathbf{x}} < \mathbf{b}^T \mathbf{y}$

Duality gap

The duality gap can be defined as $\mathbf{b}^T \mathbf{y} - \mathbf{C}^T \mathbf{x}$. This is the difference between the primal function at point \mathbf{x} and the dual function at point \mathbf{y} . Since at the optimal point the two functions have the same value, the dual gap is thus used to determine the iteration stopping criteria when searching for the function minimum/maximum. For example, in the Newton method described in section 5.3.1, the iteration of the primal and dual problem can be done simultaneously and when $\mathbf{b}^T \mathbf{y} - \mathbf{C}^T \mathbf{x} < \epsilon$ then stop the iteration.

5.3.5 Log Barrier function

In section 5.3.2 and 5.3.3 the inequality constraint is converted to an equality by introducing a variable, such that the solution still satisfies the inequality. The log barrier method is an alternative approach to handling inequalities in optimisation. For the problem:

Minimise $f(\mathbf{x})$

Subject to $h_i(\mathbf{x}) \leq 0 \quad i = 1, \dots, m$

$$\mathbf{Ax} = \mathbf{b}$$

If h_i is twice differentiable and convex for all $i = 1, \dots, m$ then the log barrier function can be defined as shown in Eq. 5.30.

$$\phi(\mathbf{x}) = - \sum_{i=1}^m \log(-h_i(\mathbf{x})) \quad (5.30)$$

Since $h_i(\mathbf{x})$ is always less than or equal to zero, the function is multiplied by -1 to enable computation of its log function. The function $\phi(\mathbf{x})$ is less than zero for all values of $h_i(\mathbf{x})$ and approaches infinity as $h_i(\mathbf{x})$ goes toward zero. As such, the log barrier function is in the domain of all strictly feasible points for the inequality. If I is defined as the indicator function $\log(-h_i(\mathbf{x}))$ (and ignoring the equality constraint), then the optimisation problem can be written as shown by Eq. 5.31.

$$f(\mathbf{x}) + \sum_{i=1}^m I\{-h_i(\mathbf{x}) \leq 0\}(\mathbf{x}) \quad (5.31)$$

If the indicator function is multiplied by $\frac{1}{t}$, the behaviour of the function for different values of t is illustrated by Fig. 5.5. The larger the value of t is, the closer the approxi-

mation to the indicator function. The optimisation problem can, therefore, be stated as

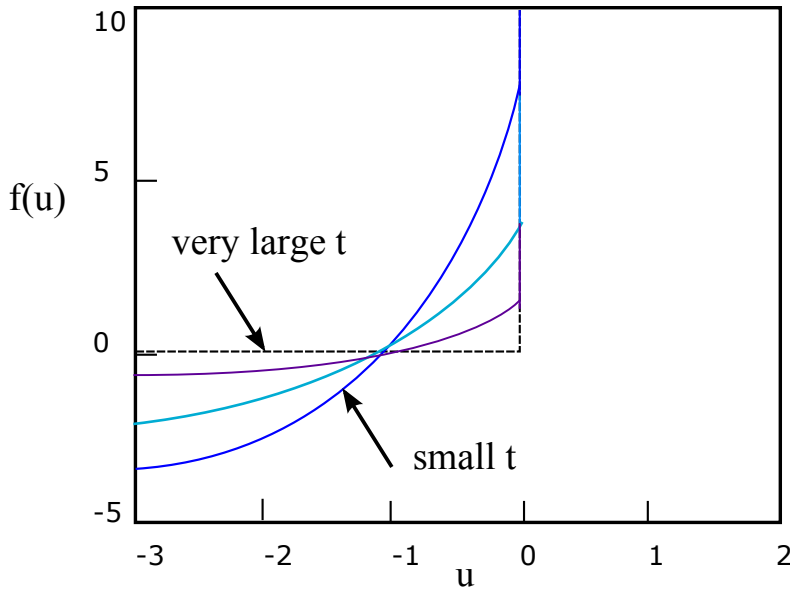


Figure 5.5: Indicator function $\frac{1}{t} \log(-u)$ for different values of t

minimise:

$$f(x) - \frac{1}{t} \sum_{i=1}^m \log(-h_i(x)) \quad (5.32)$$

The larger the value of t , the more accurate the function's approximation.

5.3.6 Central path

By replacing the inequality constraint, the minimisation problem of section 5.3.5 can be defined as:

$$\text{Minimise } tf(x) + \phi(x)$$

$$\text{Subject to } Ax = b$$

If the equality constraint is truncated to the objective function with a Lagrange multiplier, as discussed in section 5.3.2, then the KKT conditions for optimality of the Lagrangian function are as shown by Eq. 5.33 to Eq. 5.35.

$$t \nabla f(x^*(t)) - \sum_{i=1}^m \frac{1}{h_i(x^*(t))} \nabla h_i(x^*(t)) + A^T w = 0 \quad (5.33)$$

$$h_i(x^*(t)) \leq 0 \quad (5.34)$$

$$Ax^*(t) = b \quad (5.35)$$

These equations can be solved iteratively (e.g. using the Newton method in section 5.3.1) by computing x at every iteration until a stopping criteria is reached. The central path is defined as the solution $x(t)$ as a function of t . As previously discussed, the estimation accuracy of the function in Eq. 5.32 improves as t is increased. Thus, by traversing the feasibility region by increasing t at every iteration, the solution $x(t)$ of the estimated function becomes the solution of the actual function. Figure 5.6 shows the central path from the interior point of the feasible region to the optimal point x^* .

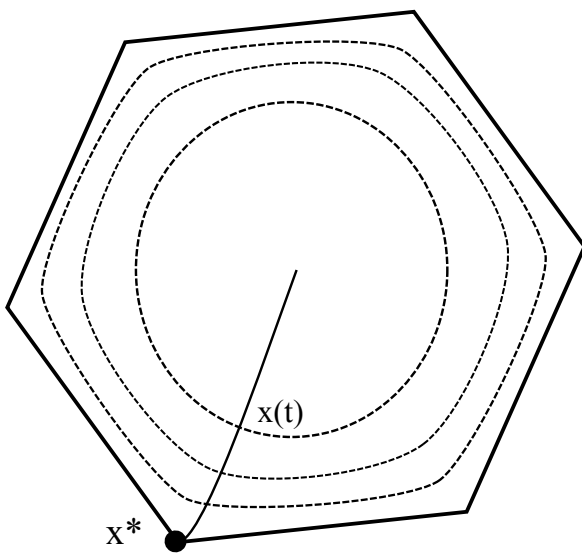


Figure 5.6: Central path illustrating contours of log barrier function as t varies

5.3.7 Dual points from central path

A dual of the original problem (defined in section 5.3.5) can be created from the central path. This enables the computation of a duality gap which is used in an iteration as a measure of how far the current value of the function is from optimality. If $u^*(t)$ and $v^*(t)$ are as defined by Eq. 5.36 and Eq. 5.37, then the dual path can be defined as the set of points (u,v) as t varies in the function depicted by Eq. 5.38.

$$u^*(t) = -\frac{1}{t h_i(x^*(t))} \quad (5.36)$$

$$\mathbf{v}^*(t) = \frac{\mathbf{w}}{t} \quad (5.37)$$

$$\nabla f(\mathbf{x}^*(t)) + \sum_{i=1}^m u^*(t) \nabla h_i(\mathbf{x}^*(t)) + A^T \mathbf{v}^*(t) = 0 \quad (5.38)$$

It is evident from their definition that $\mathbf{u}^*(t)$ and $\mathbf{v}^*(t)$ are feasible for the original problem, since they meet the condition for suitable Lagrange multipliers. Since $h_i(\mathbf{x}^*(t)) \leq 0$ then $u^*(t)$ is positive and $\mathbf{v}^*(t)$ has no sign restriction.

5.3.8 Primal-dual interior point method

The minimisation problem is restated here for convenience:

Minimise $f(\mathbf{x})$

subject to $h_i(\mathbf{x}) \leq 0 \quad i = 1, \dots, m$

$$A\mathbf{x} = \mathbf{b}$$

In this method the approach is to first convert the inequality constraint using the log-barrier function, as detailed in section 5.3.5. The central path is then created and from KKT conditions the set of equations to solve are identified. From Eq. 5.38, whilst $\mathbf{x}^*(t)$ is a solution for the central path, $(\mathbf{u}^*(t), \mathbf{v}^*(t))$ is the solution for the corresponding dual. A system $\mathbf{r}(\mathbf{x}, \mathbf{u}, \mathbf{v}) = 0$ is constructed from the perturbed KKT conditions of the problem and defined as shown in Eq. 5.39.

$$\mathbf{r}(\mathbf{x}, \mathbf{u}, \mathbf{v}) = \begin{bmatrix} \nabla f(\mathbf{x}) + D\mathbf{h}(\mathbf{x})^T \mathbf{u} + A^T \mathbf{v} \\ - \text{diag}(\mathbf{u})\mathbf{h}(\mathbf{x}) - \frac{1}{t} \\ A\mathbf{x} - \mathbf{b} \end{bmatrix} \quad (5.39)$$

$$\mathbf{h}(\mathbf{x}) = \begin{bmatrix} h_1(\mathbf{x}) \\ \vdots \\ h_m(\mathbf{x}) \end{bmatrix} \quad D\mathbf{h}(\mathbf{x}) = \begin{bmatrix} \nabla h_1^T(\mathbf{x}) \\ \vdots \\ \nabla h_m^T(\mathbf{x}) \end{bmatrix}$$

Since this function consists of a nonlinear set of equations, if it is linearised using Newton's method for solving nonlinear equations then the problem is similar to approximating the

function in a small neighbourhood of x, u, v such that $r(x + \Delta x, u + \Delta u, v + \Delta v) = 0$. The search direction to make the function zero can be determined similarly to the Newton's optimisation technique, discussed in section 5.3.1. By using a first order Taylor series expansion the function can be approximated as shown by Eq. 5.40. The resulting search direction is shown by Eq. 5.40.

$$r(x, u, v) + Dr(x, u, v) \begin{bmatrix} \Delta x \\ \Delta u \\ \Delta v \end{bmatrix} = 0 \quad (5.40)$$

$$\begin{bmatrix} \Delta x \\ \Delta u \\ \Delta v \end{bmatrix} = r(x, u, v) \begin{bmatrix} \nabla^2 f(x) + \sum_{i=1}^m u_i \nabla^2 h_i(x) & Dh(x)^T & A^T \\ - \text{diag}(u) Dh(x) & - \text{diag}(h(x)) & 0 \\ A & 0 & 0 \end{bmatrix}^{-1} \quad (5.41)$$

Considering the KKT conditions of the dual path in section 5.3.7, the dual function can be defined as shown by Eq. 5.42. The duality gap can be obtained by evaluating the primal objective function $f(x)$ and the dual $G(u, v)$. The difference between these two is, generally what is referred to as, the duality gap and is used to determine the stopping criteria for iteration. In this method, however, the difference is called the surrogate duality gap because the dual points obtained along the dual path are not necessarily feasible. Equation 5.43 shows the difference between primal and dual functions. The last term is zero since $Ax - b = 0$. In addition to the surrogate duality gap the primal and dual conditions ($Ax - b = 0$ and $\nabla f(x) + Dh(x)^T u + A^T v = 0$ respectively) are checked to determine how far from feasibility the solution is.

$$G(u^*(t), v^*(t)) = f(x^*(t)) + \sum_{i=1}^m u_i^*(t) h_i(x^*(t)) + v^{*T}(t) (Ax^*(t) - b) \quad (5.42)$$

$$f(x^*(t)) - G(u^*(t), v^*(t)) = - \sum_{i=1}^m u_i^*(t) h_i(x^*(t)) \quad (5.43)$$

The primal-dual interior point method can be outlined as follows:

Step 0: select strictly feasible initial values of x^0, u^0, v^0 , define the surrogate duality gap $\eta^0 = -h(x^0)^T u^0$ and $\mu > 1$.

Step 1: define $t = \mu\eta^{k-1}/m$

Step 2: compute update direction Δy ($\Delta y = \Delta x, \Delta u, \Delta v$ in Eq. 5.41)

Step 3: determine step size s

Step 4: update $y^k = y^{k-1} + s\Delta y$

Step 5: compute $\eta^k = -h(x^k)^T u^k$

Step 6: stop if $\eta^k \leq \epsilon$ and $(\|\nabla f(x) + Dh(x)^T u + A^T v\| + \|Ax - b\|)^{1/2} \leq \epsilon$

The variables x, u, v are initialised to be strictly feasible, the step size ('s' in step 3 of the iteration) must be selected such that the solution does not depart from the feasible set, i.e. $h \leq 0$ and $u \geq 0$. The interior point method uses backtracking line search to determine a suitable step size at each iteration.

Consider the update direction Δu , if $(u + \Delta u)$ is the full update in the iteration then s in $(u + s\Delta u)$ is the smallest value for which the constraint $u \leq 0$ is satisfied.

5.3.9 SDPT3

SDPT3 is publicly available software designed to solve primal and dual semi-definite, quadratic and linear programming problems. It was originally developed to provide efficient and robust algorithms for simple semi-definite programming problems with matrix dimensions of the order of a hundred. It is primarily coded in MATLAB, with some subroutines in C incorporated through Mex files [58]. SDPT3 implements the infeasible primal-dual predictor-corrector path-following method and is employed in this study to solve the LMI H_2 optimisation problem.

5.3.10 YALMIP

SDP solvers typically use compact formats which may be difficult and time-consuming for the user. YALMIP (Yet Another LMI Parser) was designed to make development of control-oriented SDP problems simpler by interfacing between the user on the MATLAB platform and the solver. It is a free toolbox and allows the user to define the programming problem in basic MATLAB commands. The latest version, YALMIP 3, supports linear programming, quadratic programming, second order cone programming, semi-definite programming with LMIs, and bilinear matrix inequalities (BMI) [59].

5.4 Conclusion

A convex approach to solving optimisation problems was presented. Basic principles of convex optimisation such as convex and concave functions, convex sets and convex combinations as well as local and global optimality were discussed. An overview of linear matrix inequalities was presented followed by a discussion of the formulation of the aircraft control problem as a set of linear matrix inequalities. An SDPT3 solver executing the interior point method was used to solve the inequalities. A detailed discussion of the interior point method was therefore presented.

Chapter 6

Development of a Robust System

In chapter 4, the B747 longitudinal dynamics control problem was formulated into an H_2 optimisation problem. Chapter 5 discussed a method of synthesising a solution through convex optimisation. This chapter is focused on the analysis of the solution and development of a more robust FBW system based on the results of the analysis. First, tuning of the control system to obtain the required closed-loop behaviour is discussed. An analysis of the gain matrix is then presented and compared to a different class of aircraft to derive conclusions about disturbance rejection capabilities of the B747 class of aircraft. The generic FBW system of chapter 3 is developed, based on this discussion and the advantages and disadvantages of the new system are presented.

6.1 H_2 optimal control solution

In chapter 4 a suitable uncertainty model that represents the damaged aircraft problem of this study was discussed. For convenience it is presented in Fig. 6.1. The longitudinal

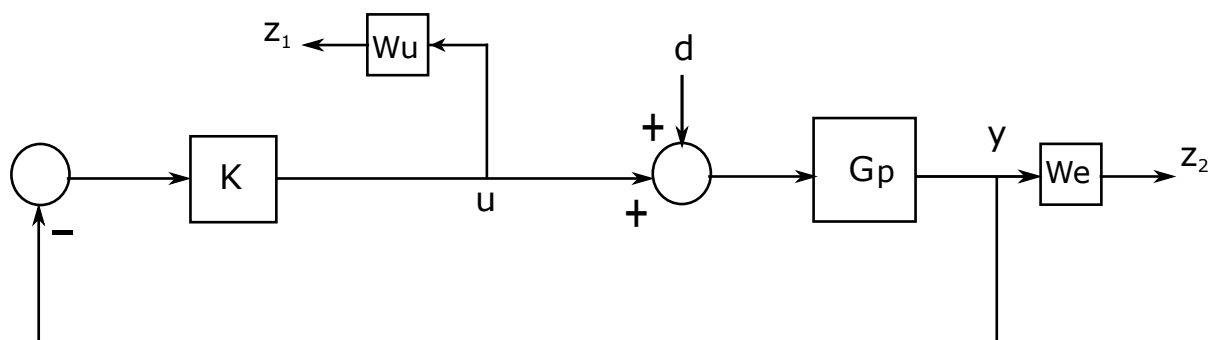


Figure 6.1: Longitudinal control system with pitch input disturbance

control problem is written as a state space model; this is described in section 4.2.1. It is then formulated into an LMI and solved as presented in section 5.3. The optimal solution is greatly dependent on the weighting matrices W_u and W_e . Tuning of these to achieve the required closed-loop behaviour, is discussed in section 4.2.2. It is presented in section 4.2 that the ideal system must provide disturbance rejection without significantly moving the poles from their open-loop position, i.e. the feedback gains must be small. In the design of an FBW system in chapter 3, the gains used are in the region of $K < 1$. It is, therefore, desirable to keep the gains within this range.

The full state feedback longitudinal system of the B747 consists of two inputs (elevator and throttle) and an output vector of 4 states $[V \ \alpha \ q \ \theta]$, which are airspeed, angle of attack, pitch rate, and pitch angle respectively. The state feedback control diagram is shown in Fig. 6.2. For a state vector X , the actuator input U is defined as $U = KX$. If the weighting functions are selected according to the guidelines provided in chapter 4, then the gain matrix is as shown in Eq. 6.1.

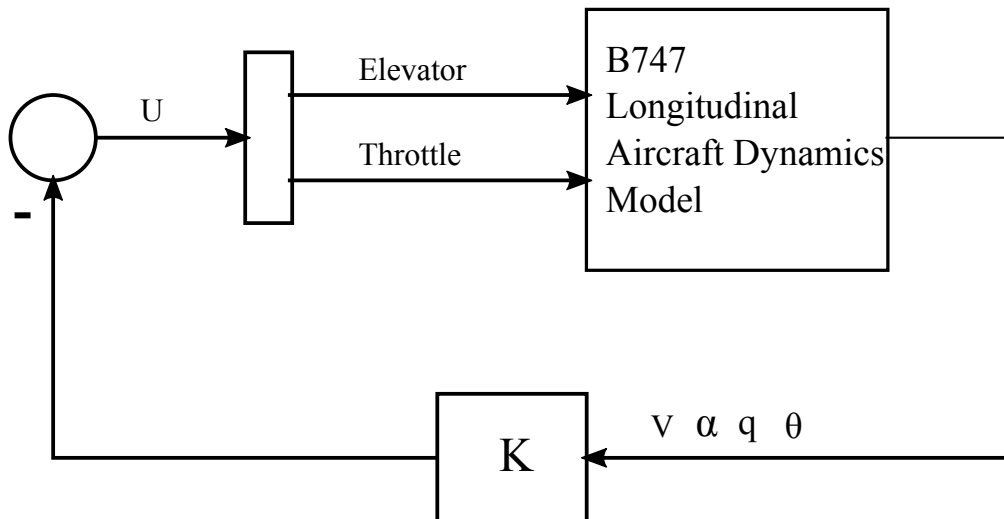


Figure 6.2: H_2 full state feedback optimal control system

$$K = \begin{bmatrix} 1.5781 & 2.5429 & -1.2241 & -6.5193 \\ 0.0034 & 0.0036 & -0.0032 & -0.0097 \end{bmatrix} \quad (6.1)$$

It is evident that this selection of weights results in large gain values and thus tuning is necessary. If the parameters of W_u are kept at original values and $W_e = 1$, then the gains

are as shown in Eq. 6.2. This matrix is considered to be within the acceptable range.

$$\mathbf{K} = \begin{bmatrix} 0.0001 & 0.0093 & -0.0049 & -0.0115 \\ 0.0000 & 0.0000 & 0.0000 & 0.0000 \end{bmatrix} \quad (6.2)$$

An observation of the gain matrix (Eq. 6.2) shows that elevator is the primary control actuator for robustness of the longitudinal system. From a comparison of the two gain matrices obtained from different weights, it is evident that an adjustment of weighting functions results in change of gains—however, in both cases pitch angle gain is larger than pitch rate gain for elevator input. This may be verified by observing the gains for a different combination of weighting functions in Appendix E.

6.2 H_2 optimal controller analysis

Pitch rate feedback is typically used for stability augmentation of longitudinal dynamics. From a root locus plot it may be shown that pitch angle stabilises the phugoid mode, however, it is often not used since it "pulls" short period poles towards the instability region. The optimal solution shows that for elevator control input, θ is larger than q . The effect of these two states on longitudinal robustness was investigated by comparing their root loci. Figure 6.3 shows that to move short period poles with q feedback from $\omega = 1.02$ (open-loop frequency) to $\omega = 1.2$, a gain of $K = 0.8$ is required. A comparison with θ feedback on Fig. 6.4 shows that nearly half the gain is required to move the poles to the same frequency with θ . The open-loop phugoid poles have the frequency $\omega = 0.0806$. Theta feedback with $K = 0.45$ increases the frequency by 14%, whilst q feedback with $K = 0.8$ changes ω by the same percentage. A larger gain value is required to move both short period and phugoid poles with q feedback than it is with θ feedback.

In chapter 4, section 4.2.2, it is discussed that to minimise the effect of input disturbance on the output of a system, the sensitivity function must be approximately zero. This can be achieved by setting the feedback gain K to a sufficiently high value. The consequence of increasing K is the increase in system bandwidth ω_n , which results in amplification of high frequency noise. The optimisation problem can be stated as: *finding a gain K for which the system has maximum possible input and output disturbance rejection for a small value of K .*

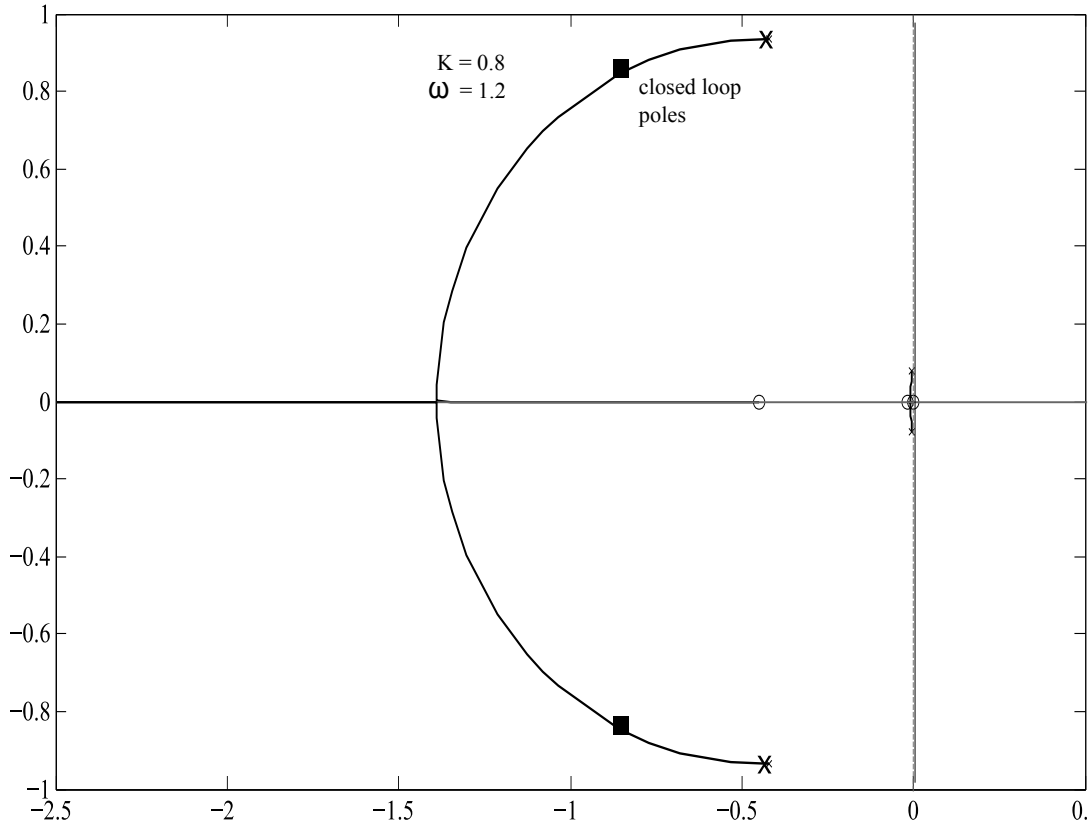


Figure 6.3: B747 pitch rate feedback root locus

From section 4.3.2 in the discussion of the formulation of the H_2 problem, the comparison of LQR control and H_2 shows that the objective in both methods consists of minimising the states using minimal actuation. For convenience the cost function for the assumption $D_{12}^T C_1 = 0$, is restated below:

$$\|z(t)\|_2^2 = \int_0^\infty x(t)^T C_1^T C_1 x(t) + u(t)^T D_{12}^T D_{12} u(t) dt \quad (6.3)$$

From this definition it is evident that the optimisation problem can be reduced to finding a small value of K to control the states and maintain their values within a small region close to the origin. It is therefore as expected, that pitch angle is the more dominant controller than pitch rate in the optimal solution; since the root loci comparison of these two states shows that θ moves the poles more for minimal gain.

To verify this assertion about H_2 optimisation, the controller was applied to a different aircraft class, a small lightweight UAV called the Phoenix (Appendix E, Fig. E.2) used in the study of wing damage in [16]. It is a lightweight, radio-controlled aircraft fitted with an electric motor and avionics pack. Its total mass is 7.770kg. Its operational bandwidth

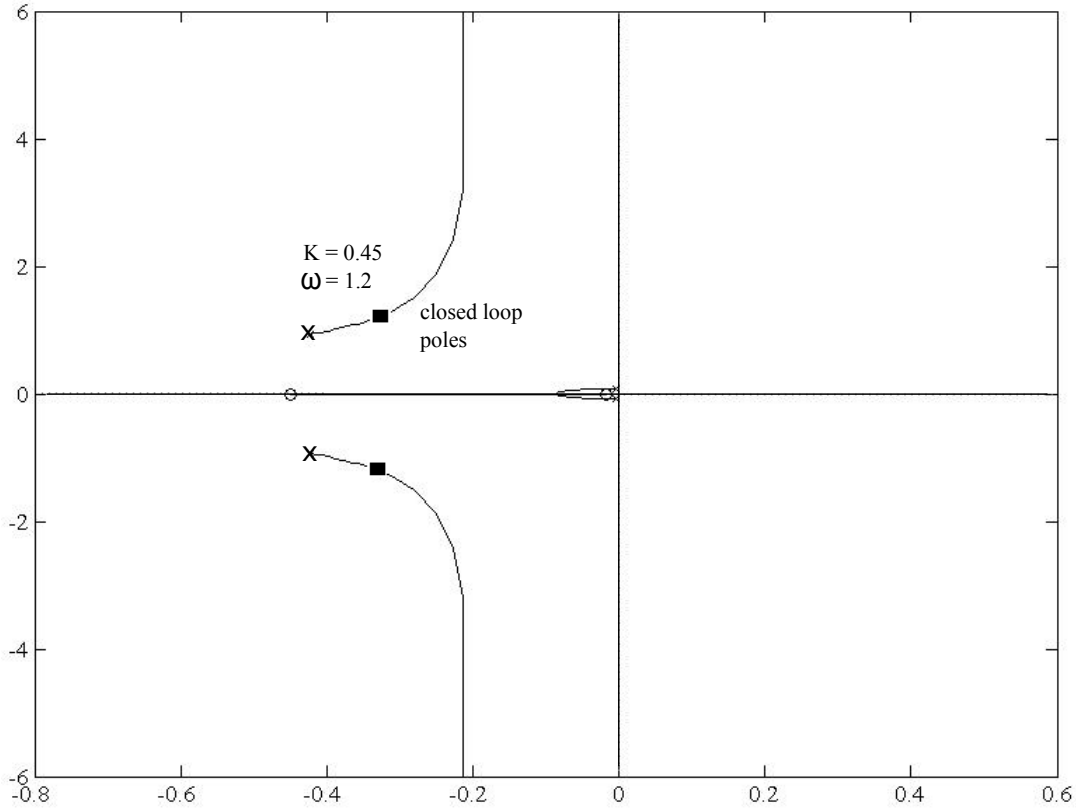


Figure 6.4: B747 pitch angle feedback root locus

is approximately 10 times higher than the B747 (short period frequency is 10.2 for this UAV, whilst it is 1.02 for the B747). The tuning weighting matrices W_u and W_e were selected as discussed in chapter 4. The bandwidth of output weight W_e is set to be just above the short period frequency at $\omega = 10.5$, M_s was set to 1.3 for a damping ratio of 0.6, and $\omega b \epsilon = 0.1$. The controller bandwidth was selected as 0.5rad/s, $M_u = 10$ and $\epsilon_c = 0.001$.

$$K_{UAV} = \begin{bmatrix} -7.8000 & -0.2170 & -10.2889 & 0.7763 \\ 0.1489 & 0.1279 & 0.9099 & 0.5246 \end{bmatrix} \quad (6.4)$$

The controller gain K_{UAV} from Eq. 6.4 shows that q is much larger than θ . From a comparison of the root locus plot of the two states, it is observed that both short period and phugoid mode are more sensitive to q than θ . Figure 6.5 shows that to move short period poles from $\omega = 10.2$ to $\omega = 11$ with θ feedback, a gain of $K = 0.328$ is required whilst only $K = 0.0298$ is needed to move the poles to the same position with q feedback (Fig. 6.6). The phugoid poles have $\omega = 0.572$ with θ feedback. A gain of $K = 0.27$ increases the frequency by 34% ($\omega = 0.762$), whilst with q feedback $K = 0.24$ decreases

the frequency by 34%.

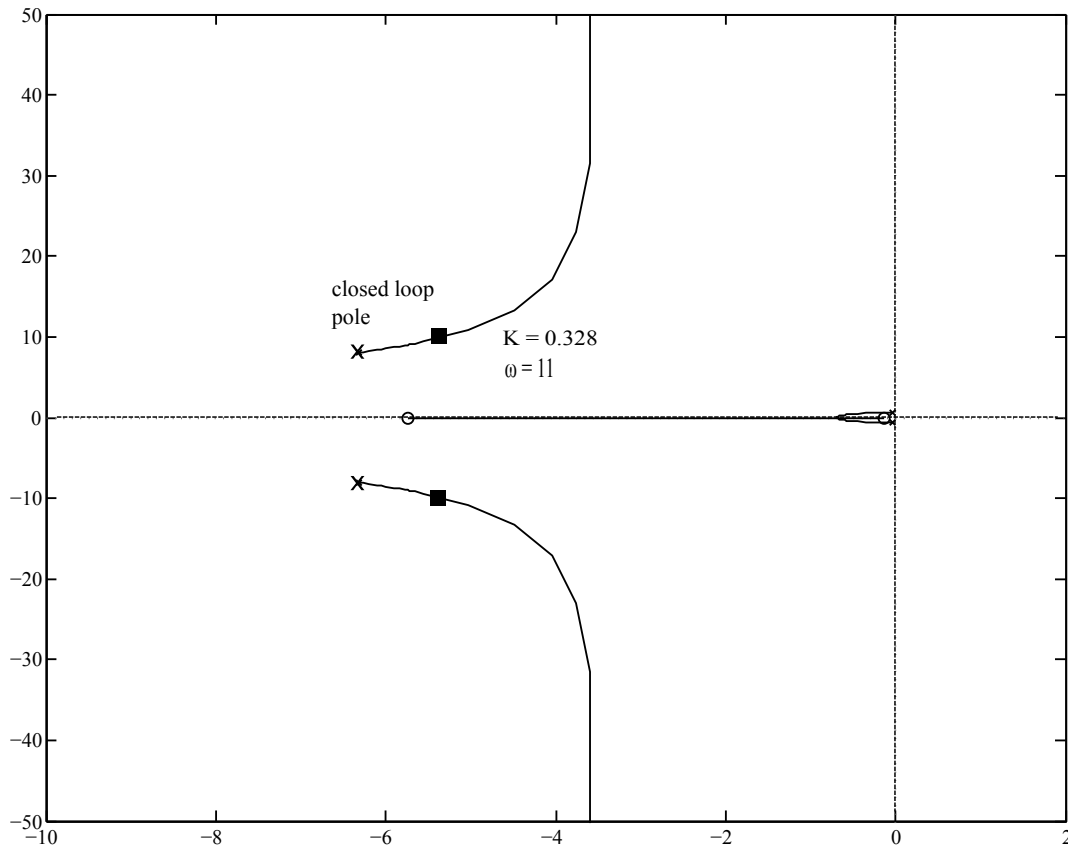


Figure 6.5: Phoenix θ -feedback root locus

It is evident that H_2 optimal control prioritises controllability with minimum actuation, whilst no consideration is made for performance of the closed-loop system—i.e. controllability of the aircraft modes with elevator input through θ feedback on the B747 takes precedence over the resulting loss of performance. In chapter 4 it was demonstrated through the use of calculus of variations how an infinite horizon problem such as H_2 optimisation does not specify any requirements on the closed-loop system performance. The objective is to minimise transmission of disturbances and attain closed-loop stability, this loss of performance is thus typically expected from this method.

6.3 Frequency Domain Analysis: q and θ

Aircraft data for both the UAV and B747 are provided in Appendix E. The moment of inertia about the pitching axis I_{yy} is 44 877 574.145 kgm^2 for the Boeing aircraft and 0.534706983 kgm^2 for the UAV. From a comparison of the 2 values it can be said that

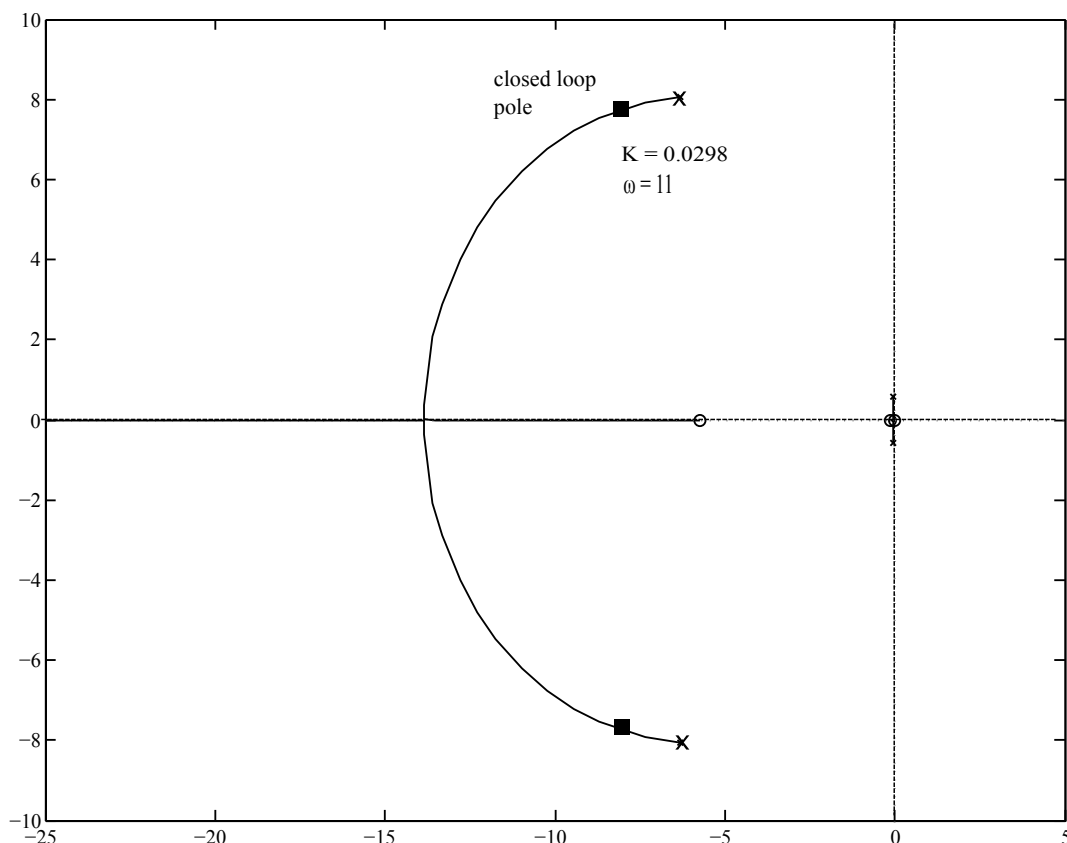


Figure 6.6: Phoenix q-feedback root locus

the large B747 is more resistant to rotation, thus much more effort is required to rotate about the pitching axis than for the small UAV. This may be verified by observing the frequency response (Bode plot) for pitch rate of the 2 aircraft. Figures 6.7 and 6.8 show the plots for the B747 and UAV respectively. For the B747 it can be seen that the gain is within a region close to 0db for the operational frequencies of the aircraft. The UAV plot shows a much larger gain (in a region close to 20db) in the operating frequencies. Suppose it was required to instantly increase the pitch rate from 0 to an arbitrary value, in a manoeuvre, since the system gain as observed from the bode plot is small for the B747, large elevator input would be used whilst minimal actuation is required for the small UAV.

A large system gain within the operational bandwidth is desirable for ideal actuator utilization and robustness (i.e attenuation of disturbance signals). Figure 6.9 shows the sensitivity functions for q and θ feedback for the B747. With θ feedback the aircraft has low sensitivity to disturbances within its operating frequencies (gain is below 0db in the frequency range of short period and phugoid mode). For q feedback the sensitivity

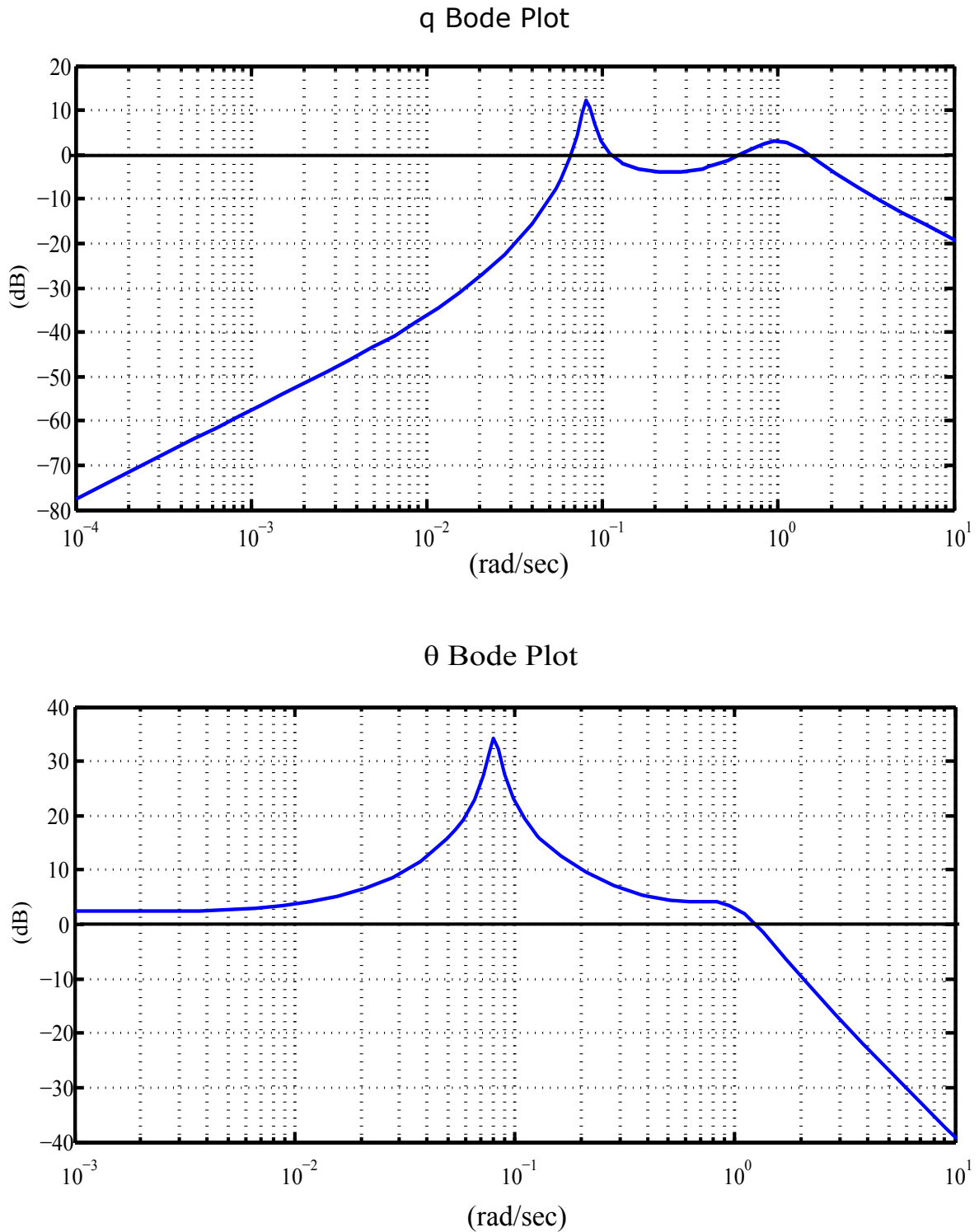


Figure 6.7: B747 q and θ bode plot

function is low at the phugoid frequency then instantly increases above this frequency. It can thus be concluded that θ feedback provides better robustness than q feedback for the aircraft class of the B747 for a range of frequencies within its operational bandwidth. At very low frequencies (≤ 0.01 rad/s), it can be observed from fig. 6.9 that for θ feedback, the

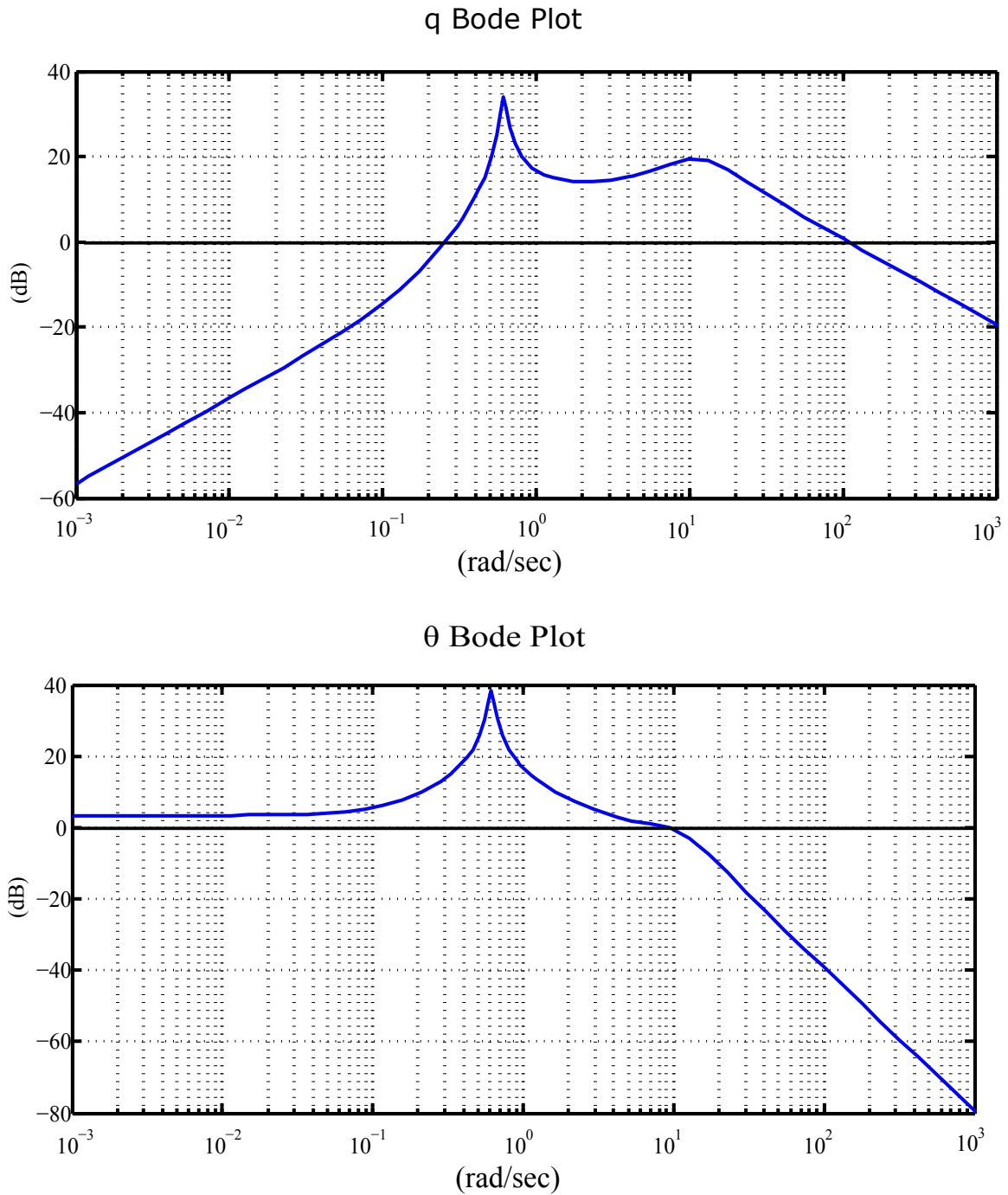


Figure 6.8: Phoenix q and θ bode plot

system has relatively high sensitivity to disturbance signals. This is another disadvantage of θ feedback.

It can be observed from the B747 plot in Fig. 6.7 that for θ control the system has a higher loop gain below $\omega = 1$ and a steeper descent slope above this frequency. The difference between the 2 plots, q and θ , can be explained as illustrated by Fig. 6.10. Pitch angle is the product of q and an integrator $\frac{1}{s}$. Since the frequency response of an

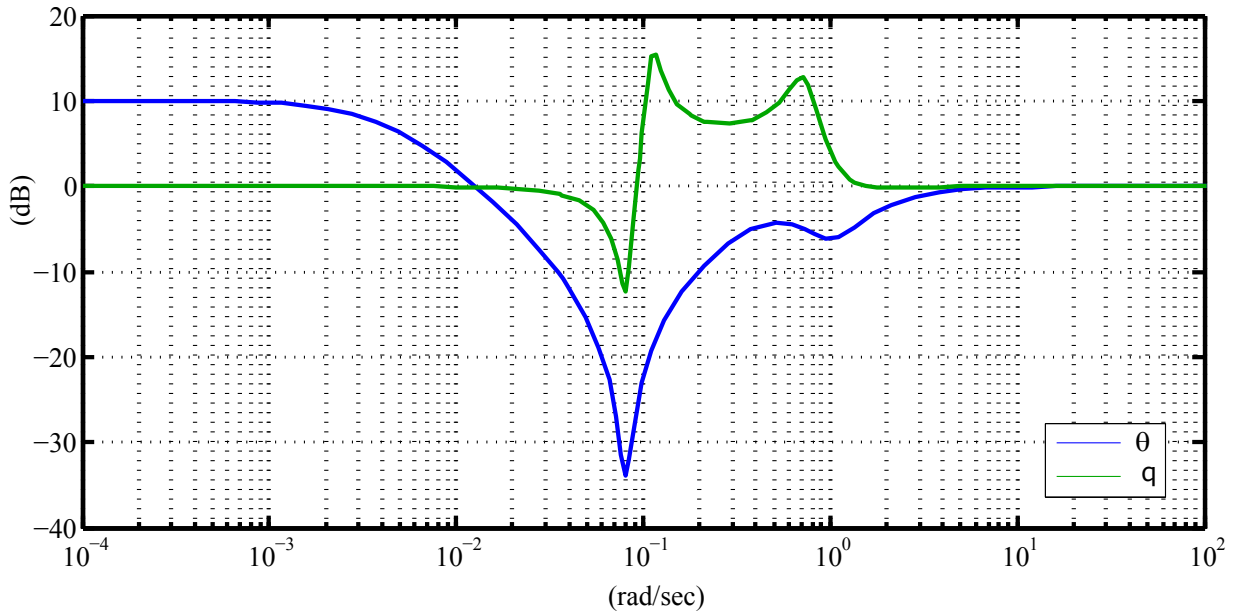


Figure 6.9: B747 Sensitivity Function $S = \frac{1}{1+G}$

integrator consists of a -20db slope with a crossover frequency $\omega = 1$, the log sum of these 2 functions yields the behaviour seen on the θ plot. Whilst this integration is an advantage to the robustness and elevator efficiency of the B747; for the UAV at frequencies above $\omega = 1$ the loop gain descends steeply thus greatly reducing its controllability for elevator input. It can therefore be concluded that integration improves elevator effectiveness and robustness for aircraft with slow closed-loop poles (with frequencies up to $\omega = 1$), whilst for aircraft with fast closed-loop poles integration reduces elevator effectiveness.

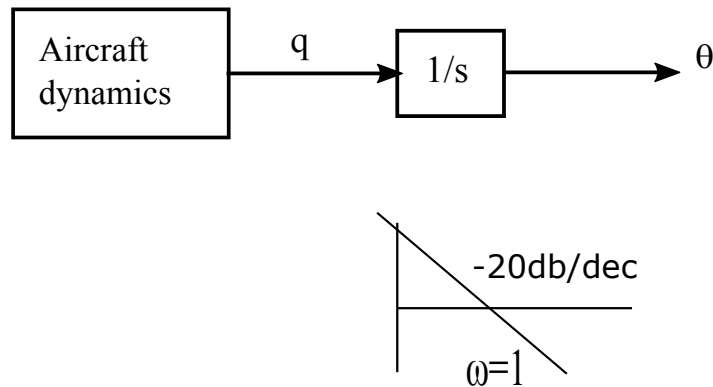


Figure 6.10: Integration illustrating difference between q and θ feedback

6.4 Robust Fly-by-Wire

Table 6.1 shows the 3 aerodynamic coefficients most affected by tail damage. For an aircraft in trim configuration, if it suddenly loses part of its horizontal tail, the pitching moment will change, resulting in longitudinal trim perturbation. Pitch moment due to angle of attack ($C_{m\alpha}$) is the most significant contributor to the change in pitching moment. From the relationship of θ and α , a perturbation in angle of attack is equal to a perturbation in pitch angle. It can thus be said that for tail loss, C_m is most affected by θ disturbances followed by the change in elevator effectiveness and q disturbance. Hypothetically, if change in these two parameters ($C_{m\theta}$ and C_{mq}) could be minimised by rejecting disturbances in θ and q through feedback of both—using minimal elevator (since its effectiveness is decreased by 52% after damage) ideal robustness would be achieved.

Coefficients	Conventional Aircraft	40% tail Removed	Change(%)
$C_{m\alpha}$	-1.15	-0.15	86.95
$C_{m\delta e}$	-1.43	-0.686	51.99
C_{mq}	-20.7	-10.095	51.23

Table 6.1: Most affected aerodynamic coefficients

The study presented in chapter 3 showed that the FBW aircraft with 50% tail loss had level 3 short term longitudinal handling qualities—phugoid poles are real and one becomes unstable. It was thus deemed necessary to improve the robustness of FBW to horizontal tail damage by minimising short period poles movement, such that they are contained within level 2 handling qualities with half the stabiliser removed, and ideally keep phugoid poles away from the imaginary axis. With reference to Fig. 3.9 in section 3.5, suppose the closed-loop short period poles of the C^* aircraft are to be moved far into level 1, such that with 50% tail loss they are within level 2. If the frequency of these poles is increased with a blend of q and θ feedback then the FBW system of Fig. 3.2 can be augmented as depicted in Fig. 6.11.

The pole placement procedure is maintained to the description of C^* design in chapter 3, i.e. the ratio of pitch rate to normal load factor must be 12.4. The root locus design pole placement for each successive loop is shown in Fig. 6.12. It is evident from the nz

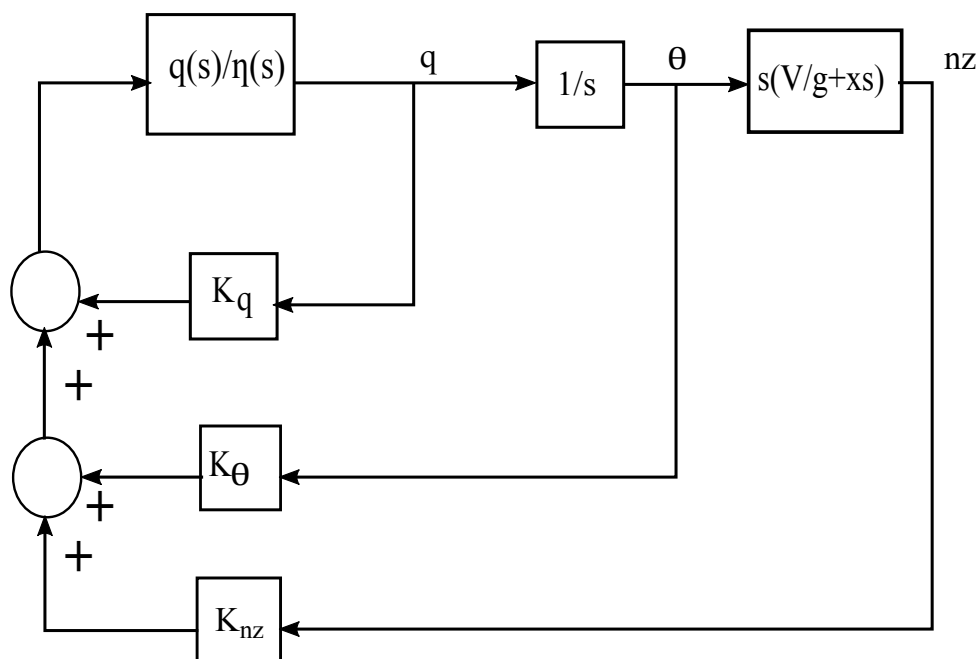


Figure 6.11: C^* with θ feedback

loop closure that the closed-loop system has an increased frequency as desired, but also an undesirable reduction in damping. As expected this is introduced by the addition of θ into the C^* . The original system in chapter 3, section 3.3.2, had a damping ratio of 0.6 whilst this system has a damping ratio of 0.54. The closed-loop poles and zeros of the aircraft are shown in Fig. 6.13—the phugoid mode is well damped with a ratio of 0.7.

To investigate the advantages and disadvantages of using θ to increase short period ω instead of q , the augmented FBW was compared to the original C^* design through which the gain was increased by q feedback only. In the $C^*\theta$ design in Fig. 6.12, the closed-loop frequency is 1.36. To attain this with the pure C^* a gain of $K_q = 1.4$ and $K_{nz} = 0.11$ is required. Figure 6.14 shows the bode plots of the 2 systems. At low frequencies below $\omega = 1$ the loop gain for the 2 systems is approximately equal. A much larger value of the feedback gain K_θ is required to raise the gain such that it is above the C^* gain. This gain increase is, however, limited by θ 's destabilising effect on the short period mode. The phase plot of $C^*\theta$ has a steeper descent in the region of crossover frequency. From the approximation of ζ for a second order system without zeros (Eq. 6.5), it can be seen that the damping ratio of the short period mode is reduced by the θ feedback. The phase plot shows a reduction in phase margin for the system with θ control.

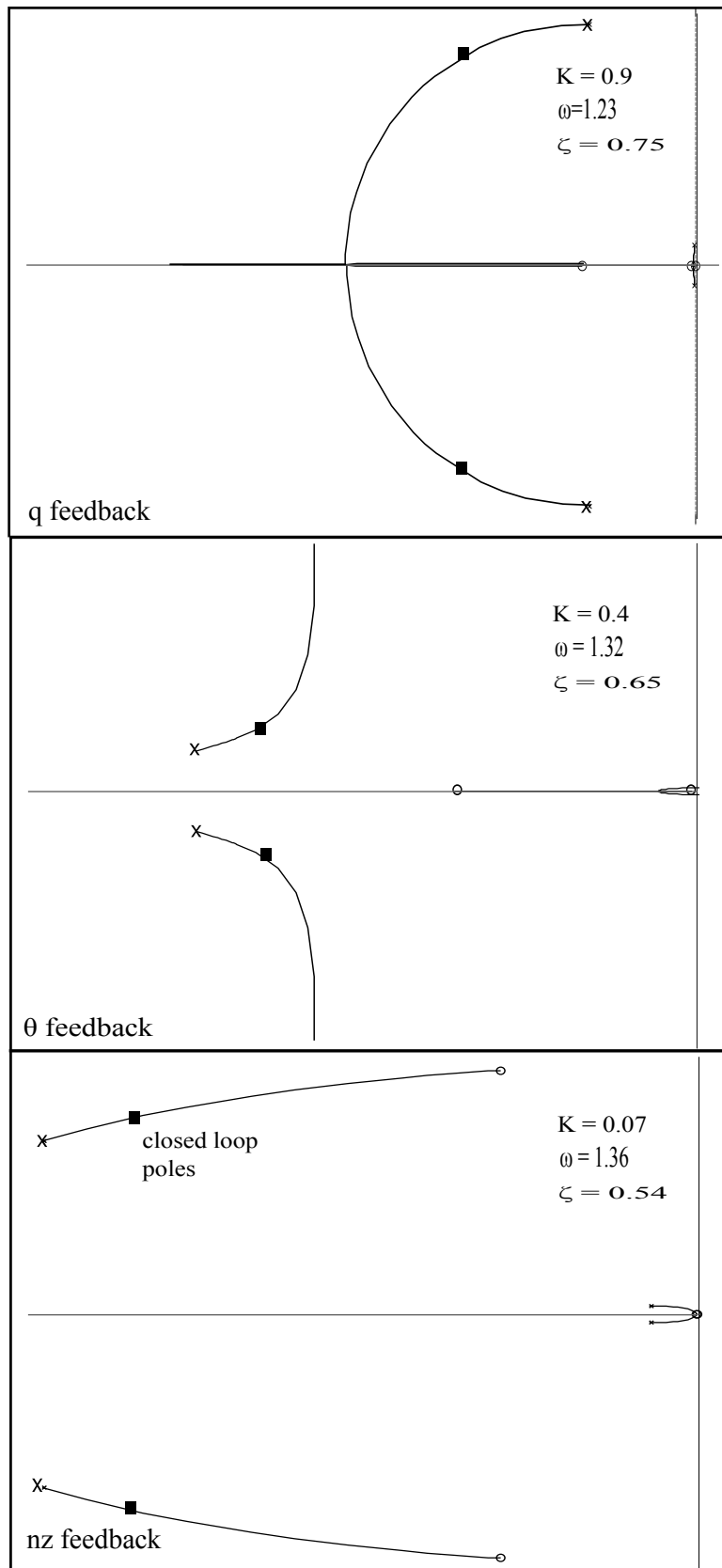


Figure 6.12: Pole placement for C^* with θ feedback system

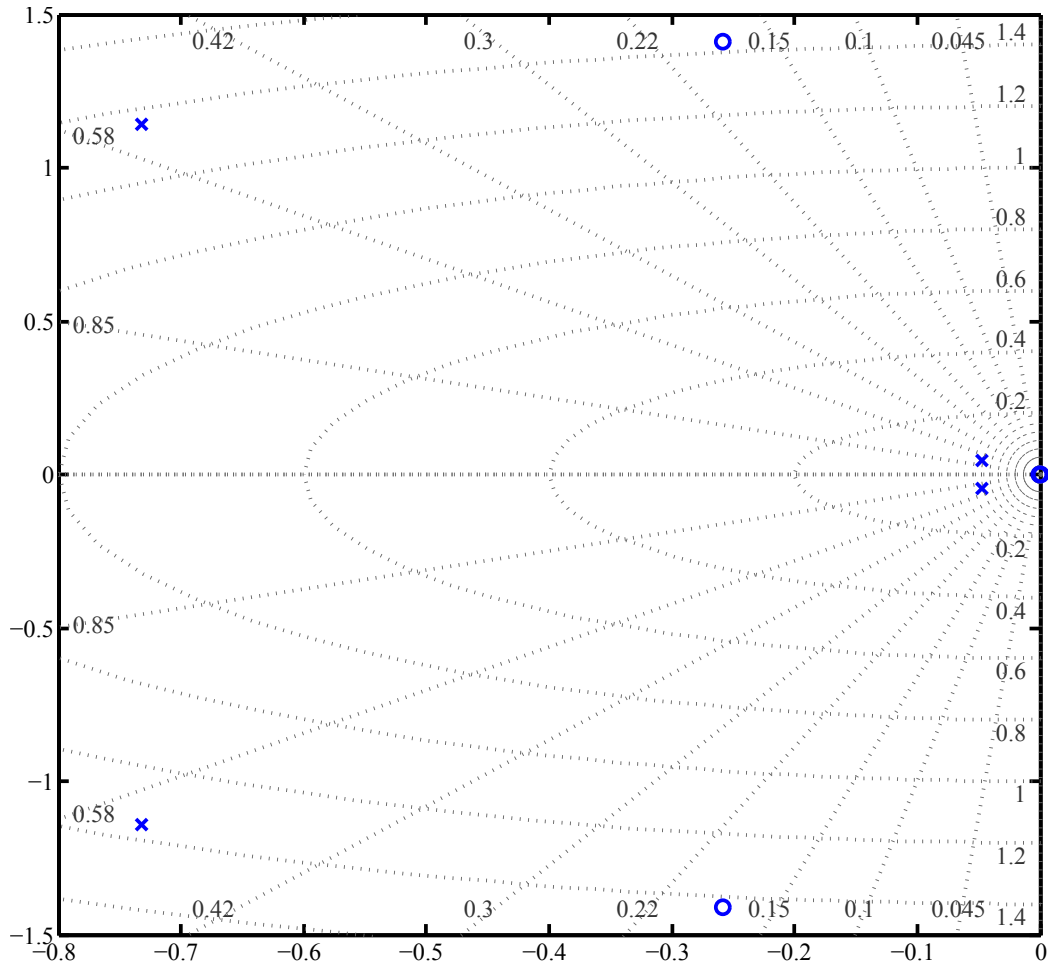


Figure 6.13: Closed-loop poles and zeros for C^* with θ feedback system

$$\zeta = \frac{PM}{100} \quad (6.5)$$

The short period frequency for both closed-loop systems has been increased from 1.02 to 1.36. From the discussion in section 6.3 at high frequencies above 1, θ feedback reduces robustness and elevator effectiveness. This can be seen from the plot in Fig. 6.14. The C^* system has a higher loop gain than the $C^*\theta$ system. In order to quantify the loss in robustness of the short period poles due to introducing θ , the $C^*\theta$ and C^* closed-loop aircraft are both subjected to damage and the resulting change in poles position is shown in Fig. 6.15 and Fig. 6.16 respectively.

In chapter 3, the comparison for robustness between FBW and open-loop aircraft was carried out by comparing the change in frequency ω . If a similar approach is adopted in this analysis then Fig. 6.15 shows that the $C^*\theta$ aircraft is more robust than the open-

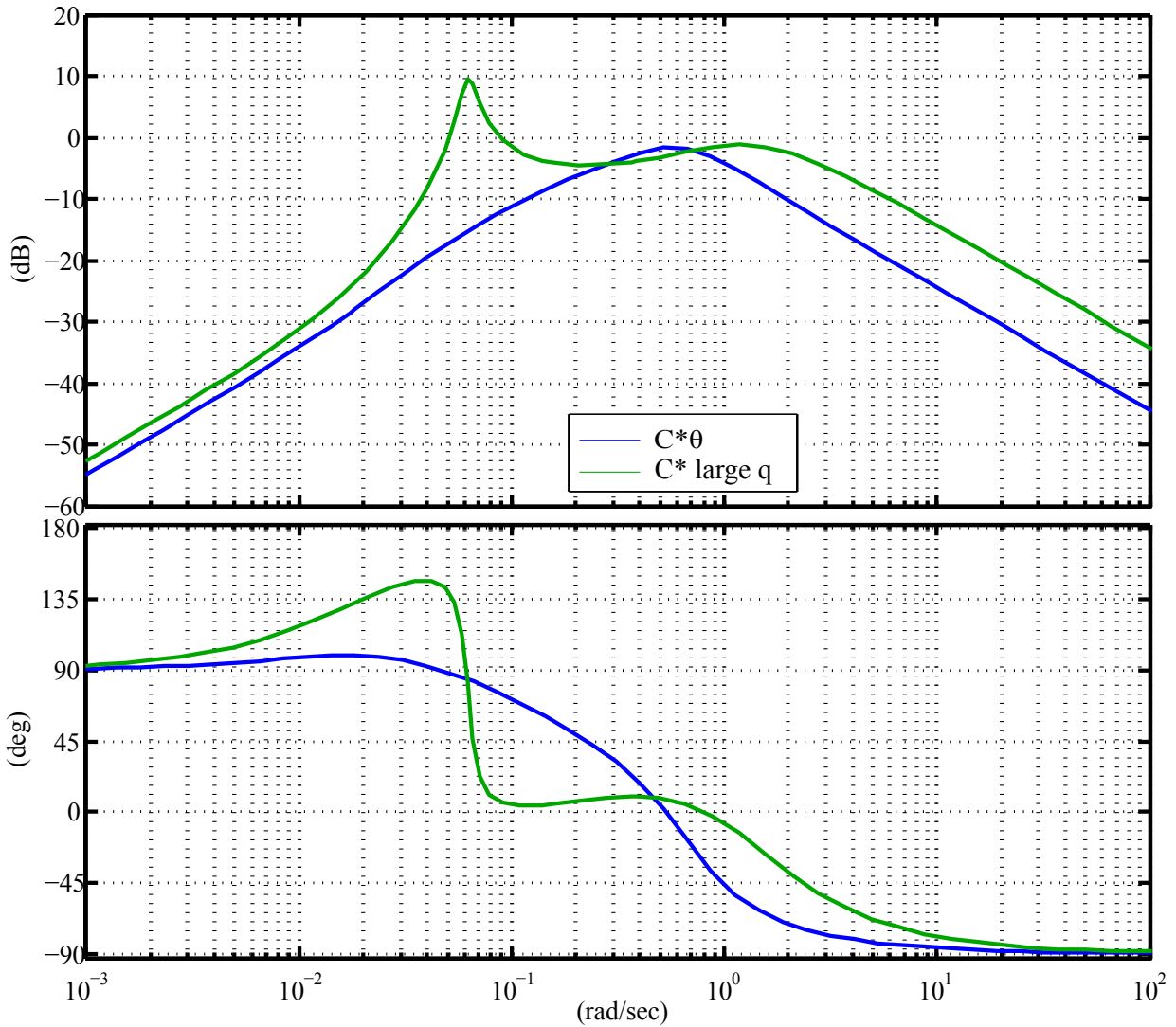


Figure 6.14: C^* with θ feedback vs C^* with large q feedback

loop aircraft. This can be seen more clearly from the comparison in Table 6.2. Figure

Controller	0% Damage	40% Damage	% change
open-loop	1.02	0.447	56
$C^*\theta$	1.36	0.80	41

Table 6.2: Comparison of % change in ω of short period poles after 40% damage, for $C^*\theta$ and open-loop aircraft

6.16 shows damaged closed-loop poles for the original C^* system with large gains. The comparison of change in ω can be seen more clearly from Table 6.3. With an ω robustness of 37.5% it is evident that q feedback provides more short period robustness than θ feedback, however the difference is only 3.5%.

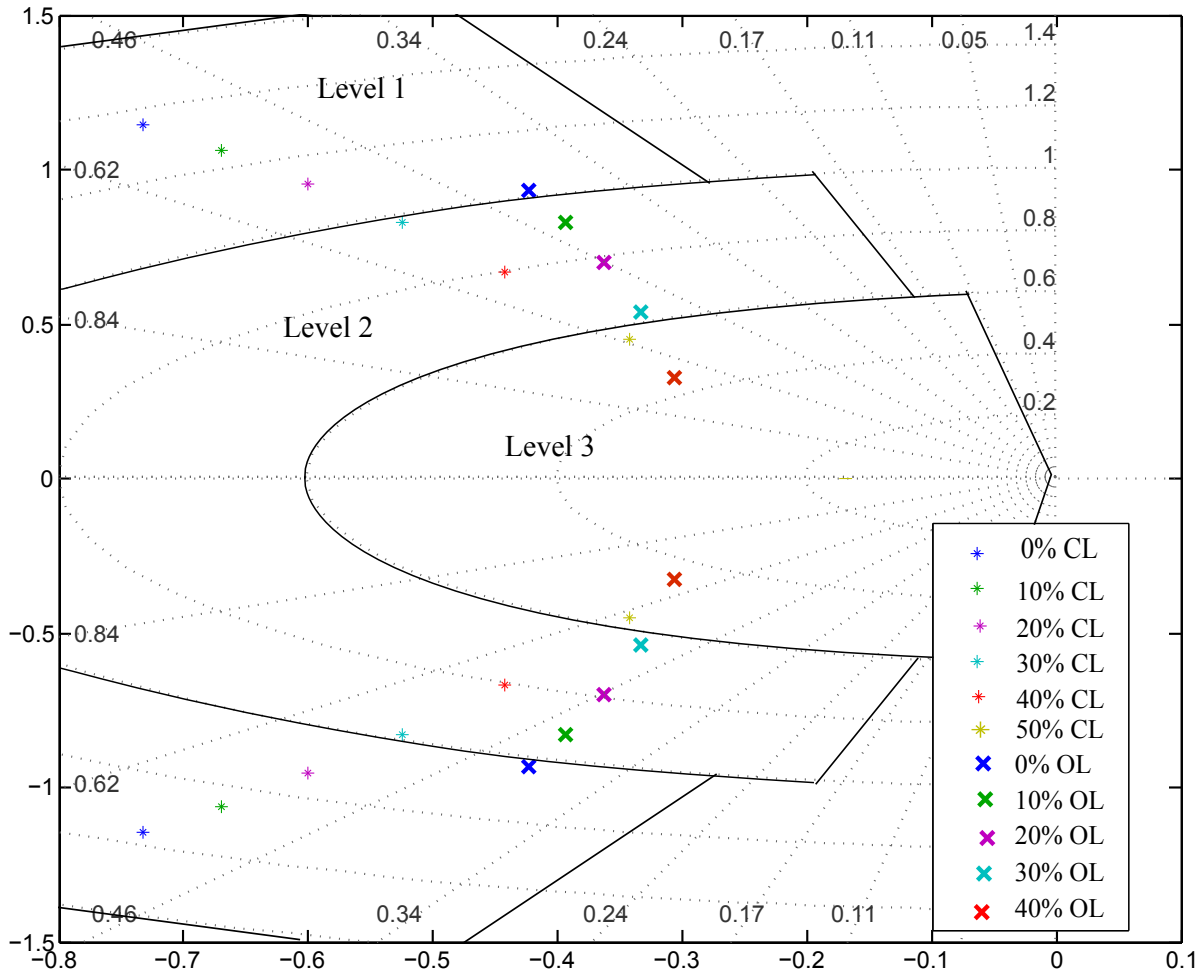


Figure 6.15: Damaged short period open-loop poles vs c^* with θ feedback

Controller	0% Damage	40% Damage	% change
open-loop	1.02	0.447	56
C^*	1.36	0.85	37.5

Table 6.3: Comparison of % change in ω of short period poles after 40% damage, for C^* with large q feedback and open-loop aircraft

6.4.1 Steady State and Transient Response

The outer loop of the Airbus FBW system, discussed in chapter 3, consists of integration to improve steady state error and a zero to cancel the transient effects of the integrator pole. If this loop is designed as discussed in section 3.6, the closed-loop short period frequency is increased from 1.36 to 1.38, whilst the damping ratio remains unchanged. Phugoid pole damping reduces from 0.7 to 0.5.—while this is a significant change, it is nonetheless still an improvement from the original system which had unstable poles. As presented in chapter 3, this additional loop does not modify the robustness of the system.

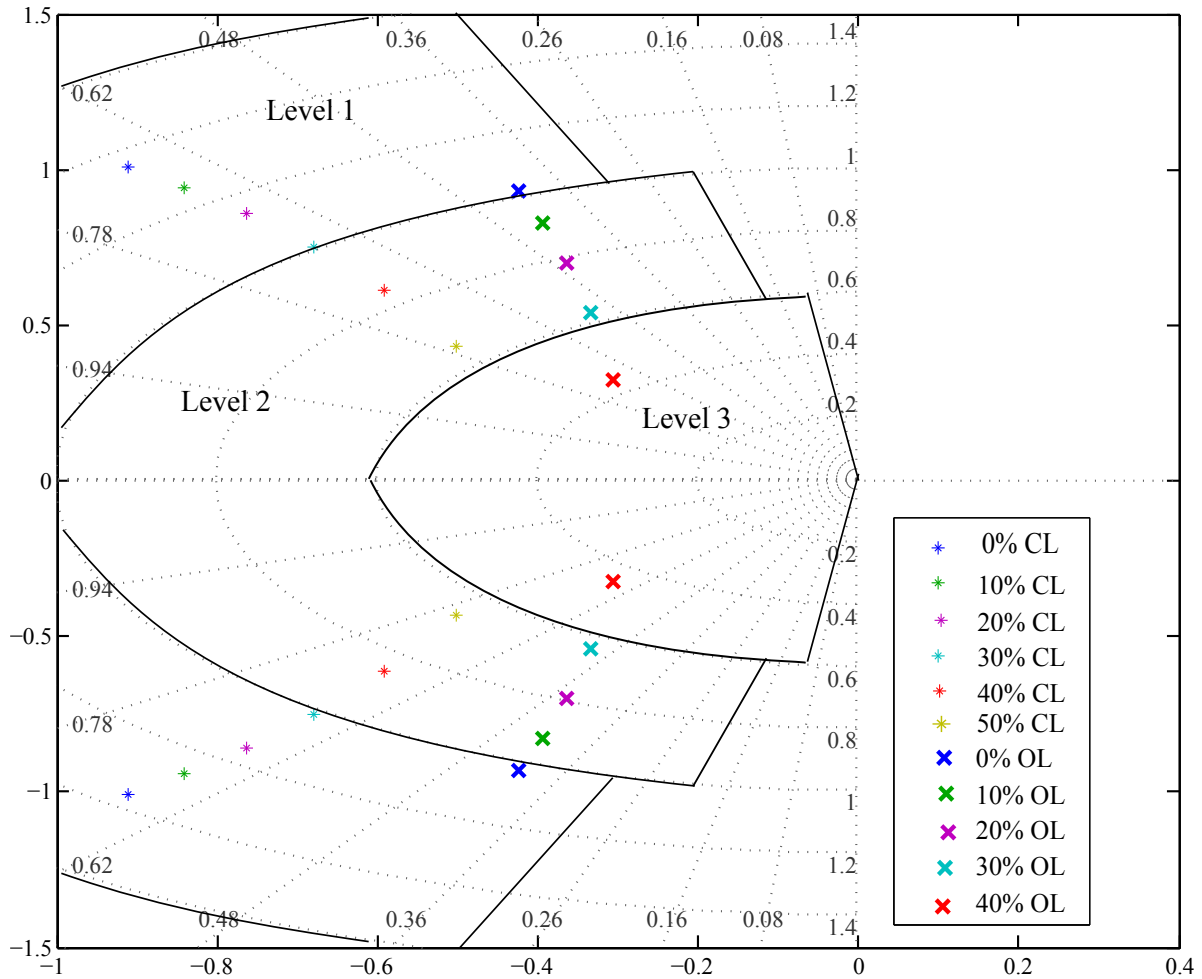


Figure 6.16: Damaged short period open-loop poles vs C^* with large q feedback

The damaged aircraft poles for the case of 50% stabiliser loss is shown in Fig. 6.17 against undamaged poles. With 50% damage the short period poles are within level 2 handling qualities, phugoid poles are real but stable.

It can therefore be concluded that introducing θ into the C^* FBW system provides the following advantages:

1. Stable and well-damped phugoid poles that retain stability after 50% tail loss.
2. Increases the short period poles sufficiently, such that they are within level 2 handling qualities after damage.

The disadvantages are a slight reduction in short period damping (from 0.6 to 0.54) and an insignificant reduction in robustness to tail damage.

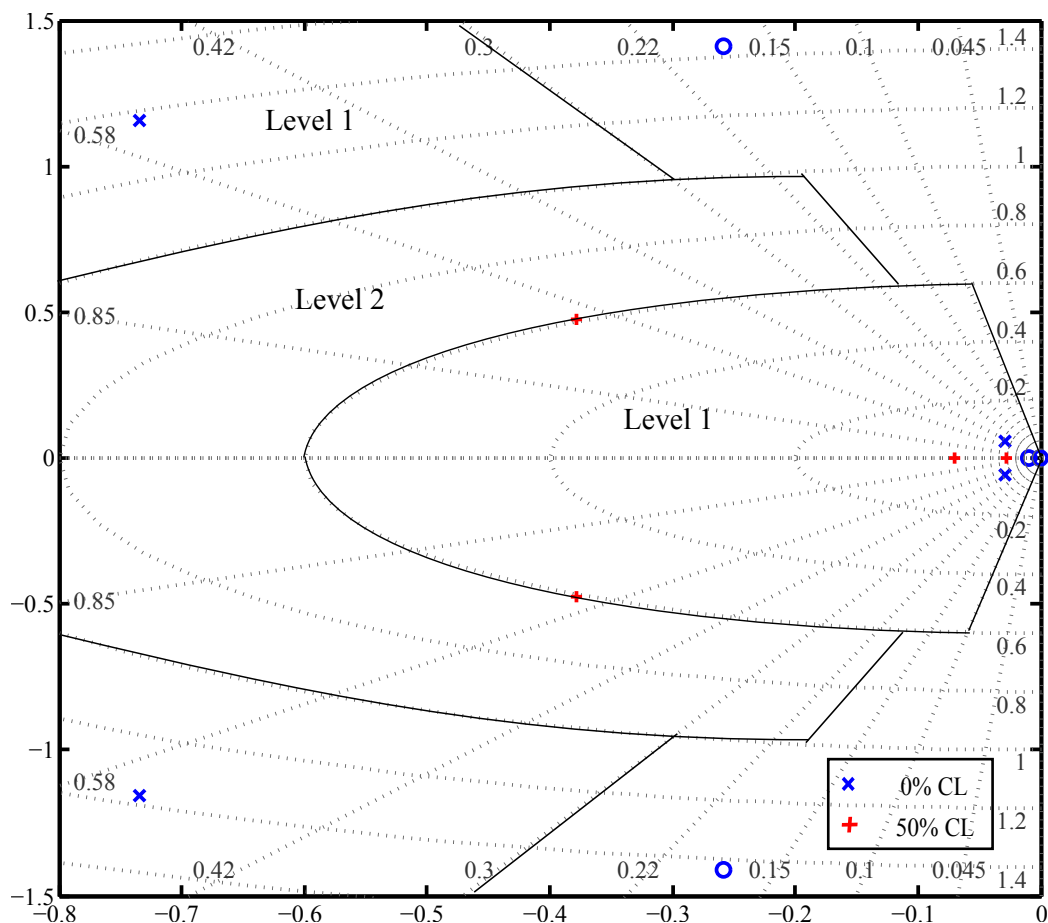


Figure 6.17: The pole plot of the closed-loop C^* system with θ feedback, illustrating change in poles after 50% tail damage

6.4.2 The Ideal Robust System

In SISO control design by loop-shaping, the objective is to attain a high loop gain in the bandwidth of the system for good tracking and low sensitivity to disturbances [60]. At the crossover frequency the loop must have a steep slope for high frequency disturbance attenuation, this behaviour is shown by Fig. 6.18. At frequencies above crossover it is desirable that the loop remains at low gain values to minimise the effect of uncertainties, since these are more dominant at high frequencies.

Suppose the original C^* FBW system in chapter 3 were to be modified according to Fig. 6.19, where an outer loop is added to shape the loop such that it meets these ideal robustness objectives. The integrator gain K_3 must be high enough to raise the gain to above 0dB. As presented in section 6.3, the integrator will raise the gain below $\omega = 1$ but further reduce it above this frequency, thus making the short period poles less robust. This can be countered by placing the zero close to the short period poles to raise the gain

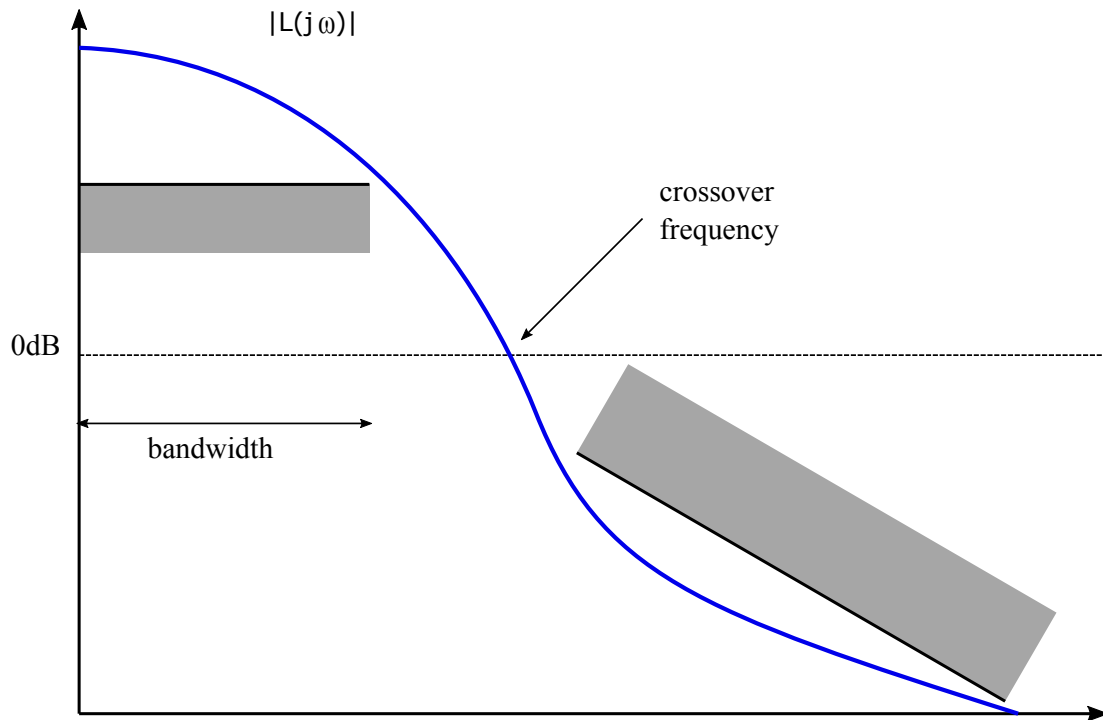


Figure 6.18: SISO loop for a robust system

to counteract the pole effect. Figure 6.20 shows the bode plot for the case of $K_3 = 0.1$ and the zero at $(s+1)$.

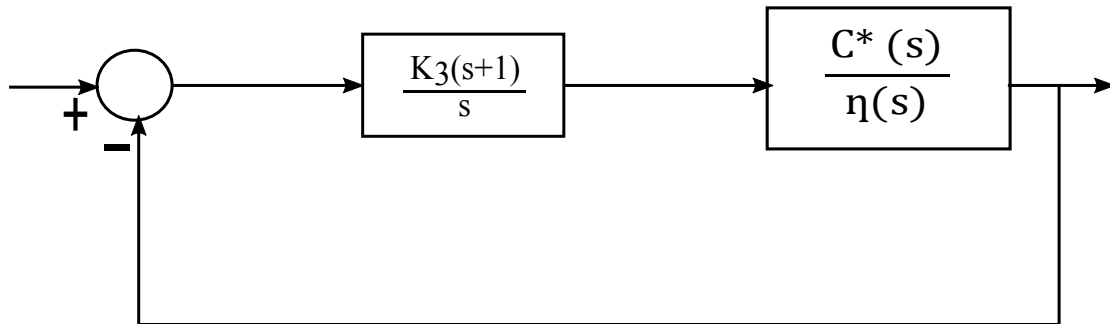


Figure 6.19: C^* with outer loop

From the bode plot it can be seen that this loop results in the required behaviour for frequencies below the phugoid poles and also improves short period mode robustness. The system is however unstable. This can be seen more clearly in Fig. 6.21, where the C^* poles without the outer loop are plotted against the poles of C^* with the outer loop designed for robustness. It can thus be seen that robustness of the system for both short period and phugoid mode is unattainable through loop-shaping since the phugoid poles become unstable.

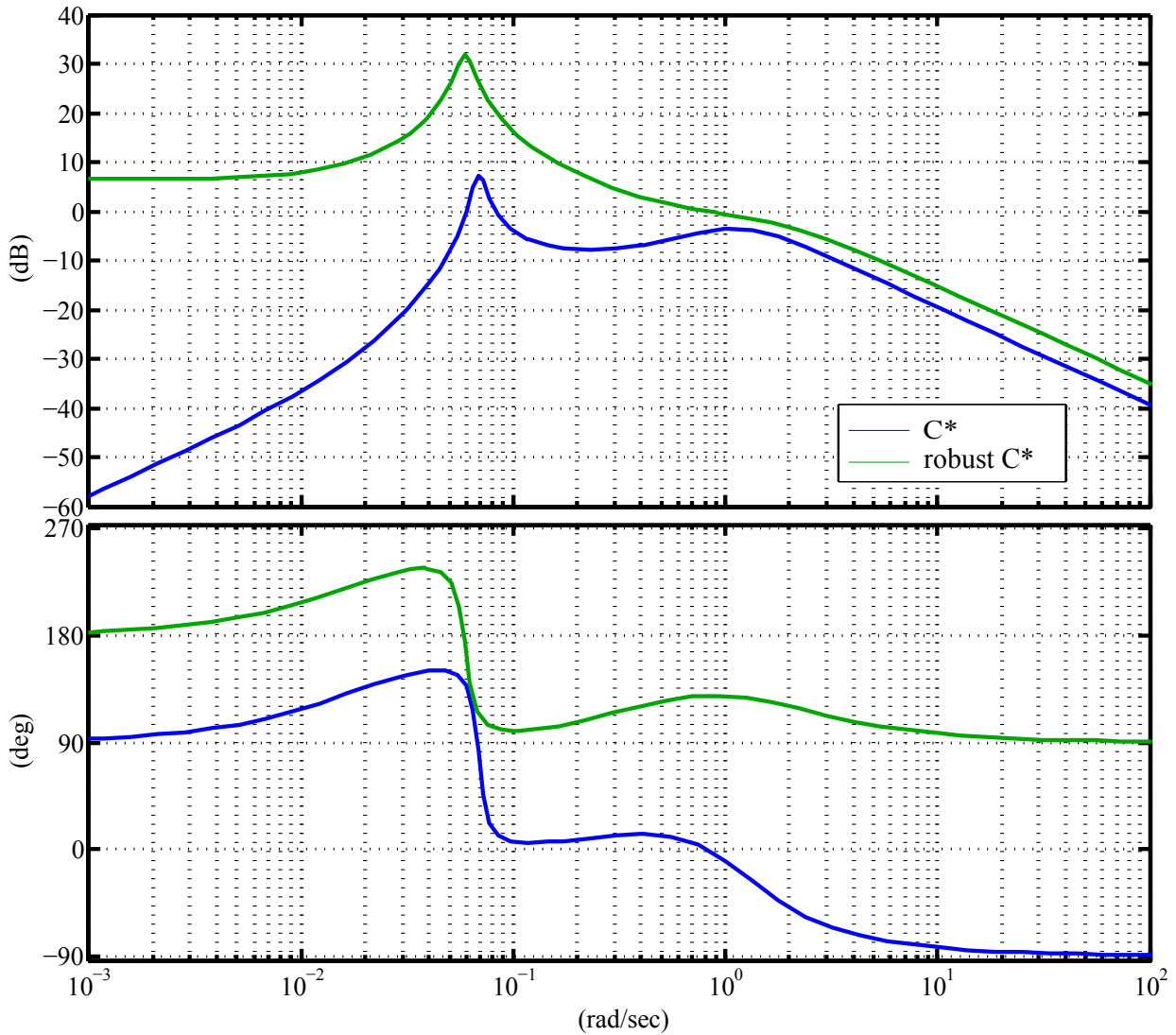


Figure 6.20: C^* vs. C^* augmented for robustness

6.5 Conclusion

Analysis of an H_2 optimal controller implemented on the B747 shows that θ feedback provides better robustness than the conventionally used q feedback for this class of aircraft. By comparison to a different class it is established that θ feedback is only beneficial for aircraft that have a short period mode with frequencies up to 1rad/s. Pitch angle feedback is introduced to the generic C^* FBW. While this is shown to be beneficial to the phugoid mode, it is detrimental to the short period mode since the poles are moved to a higher frequency above the 'beneficial region'. A reduction in short period damping and insignificant loss of robustness results. The difficulty in improving robustness of the short period mode is demonstrated by loop-shaping design to meet robustness objectives. It is shown that the phugoid poles of the aircraft are too close to the instability region, there-

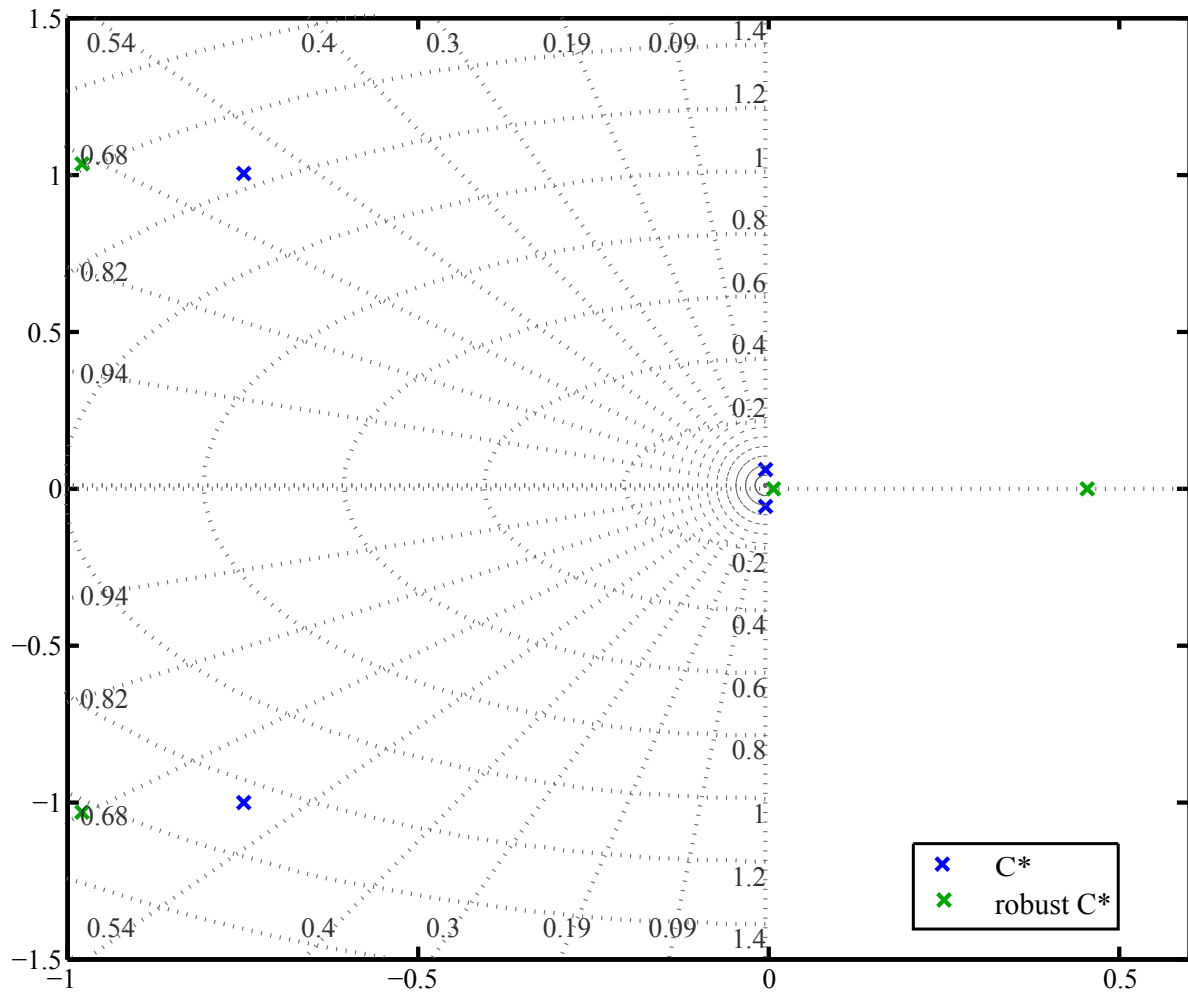


Figure 6.21: Poles of robust system illustrating unstable phugoid poles

fore, for an attempt to increase the loop gain to attain robustness, the system quickly becomes unstable.

Chapter 7

Conclusion

This chapter concludes the thesis. It consists of a summary of the work that was carried out to analyse the effect of horizontal tail damage; an investigation to FBW robustness; and an optimisation approach to improving it. A highlight of the key concepts from the analysis is presented in a list of original contributions. Further research work related to this study is discussed in the final section.

7.1 Summary

The effects of asymmetric horizontal tail damage on a large transport aircraft were investigated by using AVL to model the aerodynamic change of a Boeing 747 and observing how the eigenvalues of the dynamic equations change as a result of damage. A static stability analysis of the damaged aircraft was carried out by viewing the change in static margin at each interval of tail loss. The results showed that the aircraft is statically stable for damage up to 40% spanwise stabiliser loss. Short period poles are most affected and gradually move towards the instability region with increasing damage. The Dutch roll mode frequency is reduced due to roll coupling as a result of the loss in symmetry. The phugoid mode is not significantly changed, however, when the aircraft becomes statically unstable the poles move to a new equilibrium.

A generic C* FBW system was designed and robustness of the closed-loop aircraft against tail damage was investigated by comparing the change in eigenvalues with those of the open-loop aircraft. It was concluded that the FBW system improves robustness such

that with 50% stabiliser loss the aircraft is stable—instability only occurs above 50%. A study of change in handling qualities showed that although stable, the aircraft with 50% tail loss had level 3 handling qualities and was therefore deemed unsafe to fly. It was therefore considered necessary to improve the C* FBW system such that the closed-loop poles are within an acceptable level of handling qualities.

H_2 optimisation was implemented on the B747 to investigate an alternative strategy to improving the FBW system. Formulation of the optimal control problem was discussed and controller synthesis through the use of calculus of variations presented. This method was, however, considered unsuitable since the aircraft has poles on the imaginary axis. The H_2 control problem was then formulated into a linear matrix inequality and an SDP solver based on the primal-dual interior point method was used to solve it.

An analysis of the optimal solution showed that for the large transport class of aircraft, pitch angle feedback provides better robustness than pitch rate feedback. Since the difference between θ and q feedback is an integrator, it was concluded that the -10dB/dec slope of the integrator increases the system gain at low frequencies below 1rad/s. Hence, the higher loop gain of θ feedback. From classical control it is known that a high loop gain results in low sensitivity to disturbance signals, thus, θ feedback was considered to provide the desirable loop behaviour. The disadvantage of this approach is that for frequencies above 1rad/s the loop gain descends steeper, consequently degrading the robustness of modes above this frequency. Feedback of both θ and q increases the frequency above 1rad/s, the loss in system robustness was however considered insignificant for a suitable value of K_θ for the system of this study. Whilst a large feedback gain is necessary to raise the low frequency gain sufficiently for robustness, the disadvantage of a large θ gain is the reduction of short period damping. This gain was, therefore, selected to be only high enough to shift the phugoid poles away from the imaginary axis and move the short period poles far into level 1, such that with 50% damage they remain in level 2 of the handling qualities standard.

The final section of this analysis presents a discussion on the design of an ideal C* system that meets the required robustness objectives, i.e. short period and phugoid modes must be within the low sensitivity region. It is shown that due to the marginally stable phugoid poles of this airframe structure, improvement of short period robustness is not attainable

through the loop-shaping approach.

7.2 Contributions to the field

Original contributions to the field from this study are:

1. The change in flight dynamics due to tail damage was presented and a clear analysis provided for the resulting behaviour. Whilst similar past studies show the change in aerodynamic coefficients and stability margins, this research presents a detailed analysis of the change in static and dynamic behaviour as well as trim qualities of the damaged aircraft.
2. An evaluation of the robustness of a generic FBW system against tail damage of a large transport aircraft. Results of the robustness analysis are published in the *Aeronautical Journal* [34].
3. A presentation of degradation in the aircraft's handling qualities due to tail damage. This provides a more informative idea concerning the pilot's capability to successfully complete their mission task.
4. The use of linear matrix inequalities and optimisation techniques to analyse disturbance rejection qualities of an aircraft with available actuators, through feedback of a more suitable combination of states.
5. Framing the complexities of multi-mode FBW design as a robust control optimisation problem under horizontal stabiliser damage. A suitable uncertainty modelling structure was used to represent the tail damage problem, and weighting functions employed to tune the system to meet FBW design requirements.
6. A novel fly-by-wire control law that ensures stability of longitudinal poles and acceptable handling qualities after 50% stabiliser loss.
7. Insight to how the marginal phugoid poles of the open-loop aircraft are a limiting factor to robustness improvement for the class of large transport aircraft.

7.3 Further Research

The following ideas are suggestions for future research topics related to this study:

- In chapter 4 it is presented that H_2 control is an infinite horizon optimisation technique. This method minimises disturbance rejection without consideration for closed-loop system performance. A finite horizon optimization approach may be investigated, as a possible solution to analyse disturbance rejection qualities of an aircraft.
- The optimal controller in chapter 6 shows that pitch angle and angle of attack feedback gains have much larger values than pitch rate and airspeed. This study was focused on comparing pitch angle to the traditionally employed pitch rate feedback system. Further research may consist of investigating angle of attack as a feedback state for improving robustness on the longitudinal system.
- The convex optimisation method employed in this study on longitudinal dynamics can be implemented on a lateral dynamics model, to investigate if a different combination of state feedback may result in a more robust design strategy.
- The damaged aircraft control problem may be formulated into an H_∞ sensitivity problem. The resulting controller can be compared to H_2 controller of this study to establish if one method provides a more robust solution than the other.
- The problem of tail damage was investigated for a trimmed aircraft in cruise configuration. It was shown that with 40% damage, the FBW aircraft has level 2 (acceptable) handling qualities. When the aircraft is in the landing phase, its aerodynamic behaviour is different from when it is in cruise, as such the handling qualities requirements are more stringent. Research may be carried out to investigate the change in handling qualities in the landing phase.

Appendices

Appendix A

Aircraft Equations of Motion

A.1 Euler Angles

The angles of rotation about the 3 principal axes of a right-handed axis system are called Euler angles. Consider the two axes systems in Fig. A.1, (x_0, y_0, z_0) and (x_3, y_3, z_3) . If the objective is to translate components from one to the other (for example transforming the gravity vector from inertial to body axis), then the transformation can be computed as outlined:

Rotate about x_3 through the angle ϕ

$$\begin{bmatrix} x_3 \\ y_3 \\ z_3 \end{bmatrix} = \begin{bmatrix} 1 & 0 & 0 \\ 0 & \cos \phi & \sin \phi \\ 0 & -\sin \phi & \cos \phi \end{bmatrix} \begin{bmatrix} x_2 \\ y_2 \\ z_2 \end{bmatrix} \quad (\text{A.1})$$

Rotate about y_2 through the angle θ

$$\begin{bmatrix} x_2 \\ y_2 \\ z_2 \end{bmatrix} = \begin{bmatrix} \cos \theta & 0 & -\sin \theta \\ 0 & 1 & 0 \\ -\sin \theta & 0 & \cos \theta \end{bmatrix} \begin{bmatrix} x_1 \\ y_1 \\ z_1 \end{bmatrix} \quad (\text{A.2})$$

Rotate about z_1 through the angle ψ

$$\begin{bmatrix} x_1 \\ y_1 \\ z_1 \end{bmatrix} = \begin{bmatrix} \cos \psi & \sin \psi & 0 \\ -\sin \psi & \cos \psi & 0 \\ 0 & 0 & 1 \end{bmatrix} \begin{bmatrix} x_0 \\ y_0 \\ z_0 \end{bmatrix} \quad (\text{A.3})$$

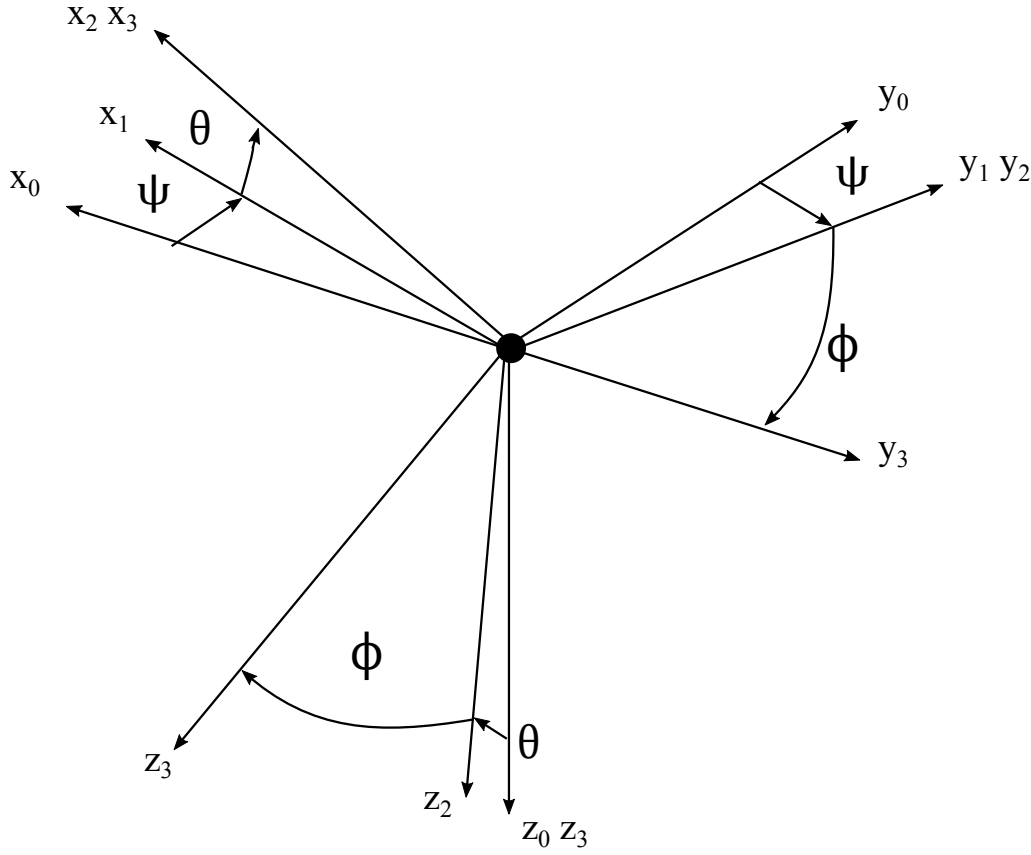


Figure A.1: Euler Angles

$$\begin{bmatrix} x_3 \\ y_3 \\ z_3 \end{bmatrix} = \begin{bmatrix} 1 & 0 & 0 \\ 0 & \cos \phi & \sin \phi \\ 0 & -\sin \phi & \cos \phi \end{bmatrix} \begin{bmatrix} \cos \theta & 0 & -\sin \theta \\ 0 & 1 & 0 \\ -\sin \theta & 0 & \cos \theta \end{bmatrix} \begin{bmatrix} \cos \psi & \sin \psi & 0 \\ -\sin \psi & \cos \psi & 0 \\ 0 & 0 & 1 \end{bmatrix} \begin{bmatrix} x_0 \\ y_0 \\ z_0 \end{bmatrix} \quad (\text{A.4})$$

The transformation matrix is the product of the 3 rotations as computed in Eq. A.4. This is the Direct Cosine Matrix (DCM) associating (x_0, y_0, z_0) and (x_3, y_3, z_3) . The transformation from (x_3, y_3, z_3) to (x_0, y_0, z_0) can be obtained by inverting the DCM.

$$\text{DCM} = \begin{bmatrix} \cos \theta \cos \psi & \cos \theta \sin \psi & -\sin \theta \\ \sin \phi \sin \theta \cos \psi - \cos \phi \sin \psi & \sin \phi \sin \theta \sin \psi - \cos \phi \cos \psi & \sin \phi \cos \theta \\ \cos \phi \sin \theta \cos \psi + \sin \phi \sin \psi & \cos \phi \sin \theta \sin \psi - \sin \phi \cos \psi & \cos \phi \cos \theta \end{bmatrix} \quad (\text{A.5})$$

Acceptable limits for Euler angles:

$$\left\{ \begin{array}{l} -180^\circ \leq \psi \leq +180^\circ \\ -90^\circ \leq \theta \leq +90^\circ \\ -180^\circ \leq \phi \leq +180^\circ \end{array} \right\} \quad (\text{A.6})$$

Angular Velocities Transformation: This matrix is obtained by imposing the velocities on the axes diagram of Fig. A.1 and computing the association of the two systems as previously described. This method is discussed in detail in [35].

$$\begin{bmatrix} p \\ q \\ r \end{bmatrix} = \begin{bmatrix} 1 & 0 & -\sin \theta \\ 0 & \cos \phi & \sin \phi \cos \theta \\ 0 & -\sin \phi & \cos \phi \cos \theta \end{bmatrix} \begin{bmatrix} \dot{\phi} \\ \dot{\theta} \\ \dot{\psi} \end{bmatrix} \quad (\text{A.7})$$

A.2 Time derivative of a vector

Consider a 3-dimensional vector \mathbf{R} in the reference frame A. If it is written as a product of its vector magnitude and unit vector direction $\mathbf{R}i$, then its differential can be written as shown by Eq. A.8 by applying the product rule. The derivative of a unit vector direction is a product of the vector and its angular velocity of rotation from one reference frame to the next—this is depicted by Eq. A.9. By substituting Eq. A.9 into Eq. A.8 the time derivative of a vector in Eq. A.10 can be obtained.

$$\frac{\partial \mathbf{R}}{\partial t} \Big|_A = \dot{\bar{\mathbf{R}}}(t) i^B(t) + \bar{\mathbf{R}}(t) \frac{\partial i^B(t)}{\partial t} \Big|_A \quad (\text{A.8})$$

$$\frac{\partial i^B(t)}{\partial t} \Big|_A = \omega^{BA} \times i^B(t) \quad (\text{A.9})$$

$$\frac{\partial \mathbf{R}}{\partial t} \Big|_A = \dot{\bar{\mathbf{R}}}(t) i^B(t) + \omega^{BA} \times \mathbf{R}(t) \quad (\text{A.10})$$

A.3 Moments and Products of Inertia

Moment of inertia is defined as resistance to rotation. It is a function of mass and distance from the centre of rotation. An illustration is shown in Fig. A.2.

$$\begin{aligned} I_{xx} &= \int_v \rho (y^2 + z^2) \partial v \\ I_{yy} &= \int_v \rho (x^2 + z^2) \partial v \\ I_{zz} &= \int_v \rho (x^2 + y^2) \partial v \end{aligned} \quad (\text{A.11})$$

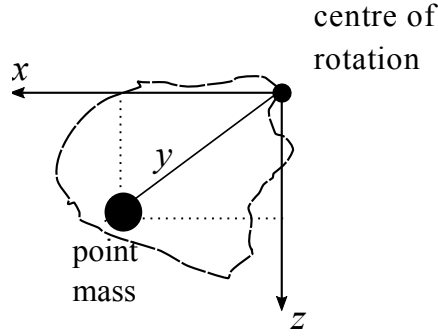


Figure A.2: Moment of Inertia ($I_{yy} = \int_v \rho (x^2 + z^2) \partial v$)

Product of inertia is a measure of symmetry of mass distribution around the principal axis of inertia. If an object is symmetrical about an xz plane then the product of inertia

$I_{xz} = \int_v \rho xz \partial v$ is zero.

$$\begin{aligned} I_{xy} &= I_{yx} = \int_v \rho xy \partial v \\ I_{yz} &= I_{zy} = \int_v \rho yz \partial v \\ I_{zx} &= I_{xz} = \int_v \rho xz \partial v \end{aligned} \quad (\text{A.12})$$

A.4 Induced Incidence Angles

For an airfoil moving in a free-stream at velocity V and generating an angle of attack α , the resulting lift force is as shown by Eq A.13.

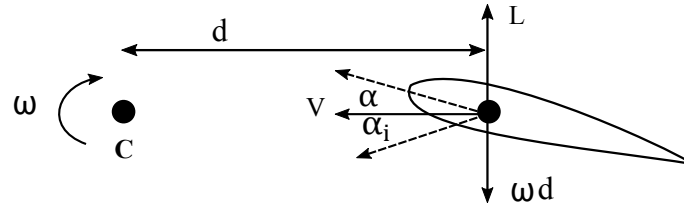


Figure A.3: Airfoil illustrating induced angle of incident

$$L = \frac{1}{2} \rho V^2 S C_{L\alpha} \alpha \quad (\text{A.13})$$

If the airfoil is rotated at the point C in Fig. A.3, its actual translational velocity is the vector sum of V and ωd ; and the angle of attack is a sum of α and α_i . The lift force is therefore as depicted by Eq A.14 and the estimation of the incidence angle is shown by

Eq A.15.

$$L = \frac{1}{2}\rho V^2 S C_{L\alpha}(\alpha + \alpha_i) \quad (\text{A.14})$$

$$\alpha_i = \tan^{-1} \frac{\omega d}{V} \quad (\text{A.15})$$

A linearisation of α_i is made using small angle approximation and from substituting the result into Eq A.14 the lift force can be approximated as seen by Eq A.17.

$$L = \frac{1}{2}\rho V^2 S C_{L\alpha}(\alpha + \frac{\omega d}{V}) \quad (\text{A.16})$$

$$L = qS(C_{L\alpha}\alpha + \frac{d}{2V}C_{L\alpha}\omega) \quad (\text{A.17})$$

Appendix B

Longitudinal Fly-by-Wire Control System

B.1 FBW transfer function derivation from block diagram

Figure B.1 shows the C* FBW used on an Airbus aircraft. Each loop must be formulated into a transfer function in order to integrate the control system into the B747 aircraft model. This section details how each loop is reduced to a transfer function in a multiple loop closure design.

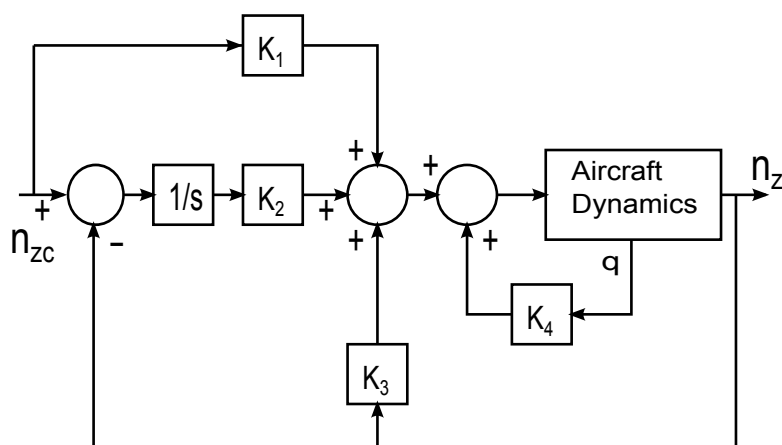


Figure B.1: Longitudinal control system in C* alternate law

The innermost loop consist of pitch rate (q) feedback to elevator input, the open-loop transfer function is shown by Eq. B.2.

$$G(s) = \frac{q(s)}{\eta(s)} \quad (\text{B.1})$$

Equation B.2 is the closed-loop function as depicted by Fig. B.2.

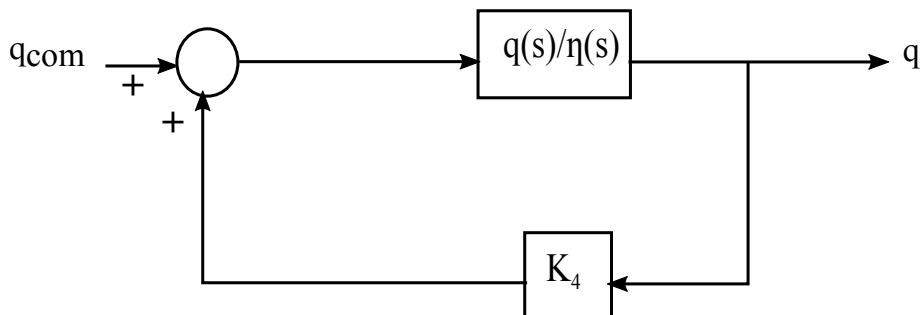


Figure B.2: q-feedback inner loop

$$G_4(s) = \frac{G(s)}{1 + G(s)K_4} \quad (\text{B.2})$$

The closed-loop pitch rate feedback transfer function becomes the open-loop function in the forward path of the next loop (nz-feedback). If this loop is closed with a gain K_3 in the feedback path as illustrated by Fig. B.3, then Eq. B.3 becomes the new closed-loop transfer function.

$$G_3(s) = \frac{G_4(s)}{1 + G_4(s)K_3} \quad (\text{B.3})$$

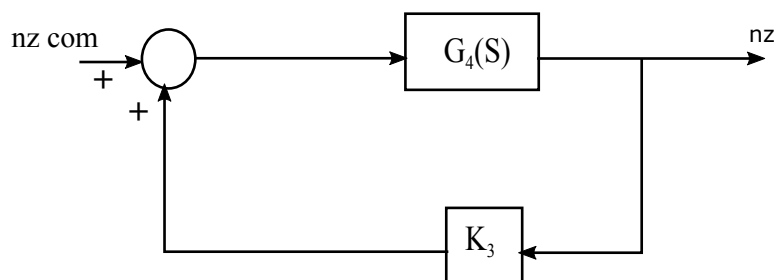


Figure B.3: nz-feedback loop

The outer loop of the control system consist of two loops: integration to improve steady state error and another to add a zero close to the origin in order to cancel out the

undesirable transient effects of the integrator pole. Consider the actuator input to G_3 , (a) in Fig. B.4. Eq. B.4 is the expression for a in terms of the system input $R(s)$ and output $Y(s)$. Derivation of the system transfer function from $R(s)$ to $Y(s)$ is outlined in Eq. B.4 to Eq. B.9.

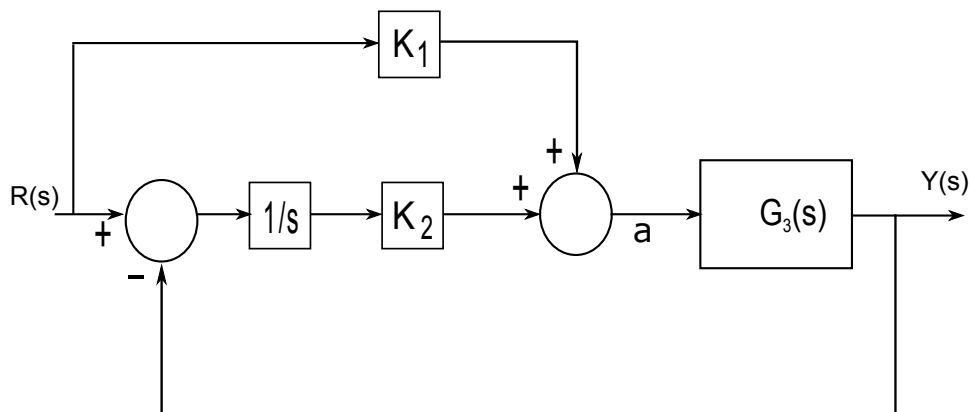


Figure B.4: Outer loop

$$a = K_1 R(s) + [R(s) - Y(s)] \frac{K_2}{s} \quad (\text{B.4})$$

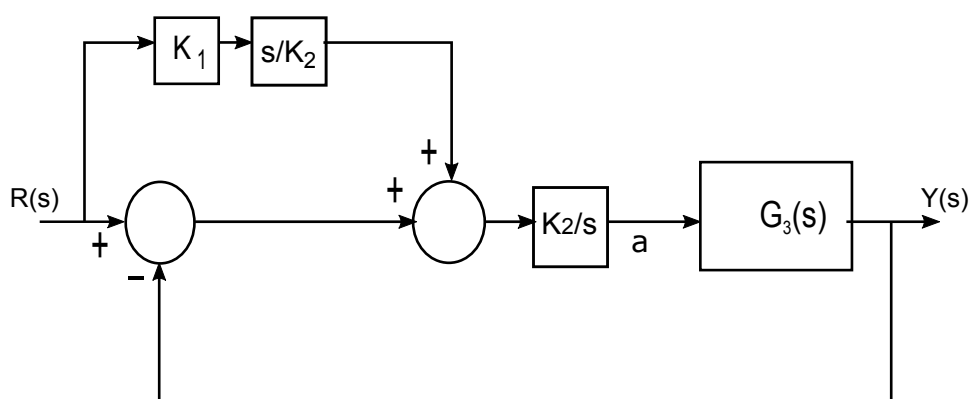


Figure B.5: Step 1: outer loop simplification showing "a" in Eq. B.5

$$a = [K_1 \frac{s}{K_2} R(s) + R(s) - Y(s)] \frac{K_2}{s} \quad (\text{B.5})$$

$$a = [R(s) + K_1 \frac{s}{K_2} R(s) - Y(s)] \frac{K_2}{s} \quad (\text{B.6})$$

$$r(s) = [1 + \frac{K_1}{K_2} s] R(s) \quad (\text{B.7})$$

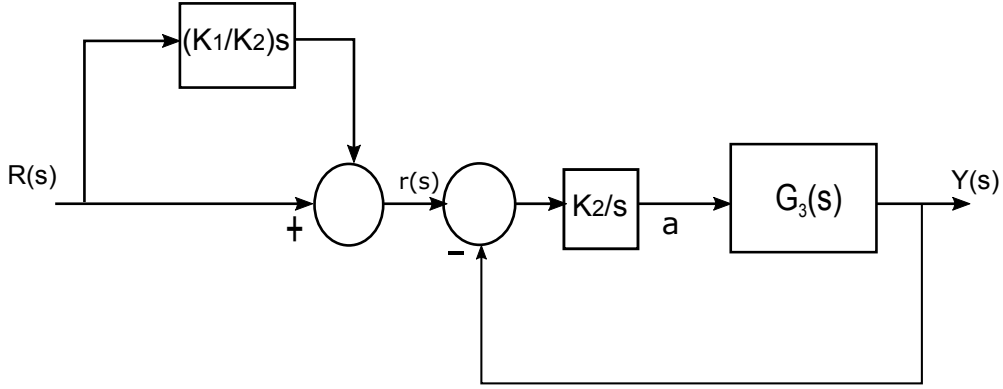


Figure B.6: Step 2: outer loop simplification showing "a" in Eq. B.6 and $r(s)$ in Eq. B.7

$$G_2 = \frac{Y(s)}{r(s)} = \frac{G_3 \frac{K_2}{s}}{1 + G_3 \frac{K_2}{s}} \quad (\text{B.8})$$

$$G_1 = \frac{Y(s)}{R(s)} = \frac{[s + \frac{K_2}{K_1}] G_3 \frac{K_2}{s}}{1 + G_3 \frac{K_2}{s}} \quad (\text{B.9})$$

B.2 Steady state error

Consider the closed-loop system of Fig. B.6, without integration and an additional pole it can be redrawn as illustrated in Fig. B.7.

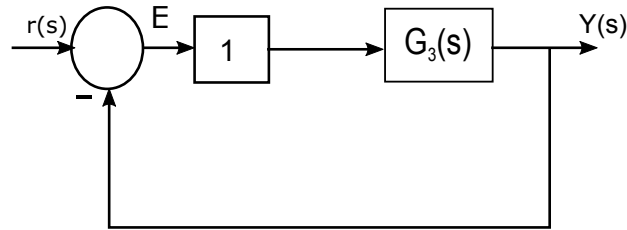


Figure B.7: C* FBW illustrating steady state error without an integral controller

The error may be expressed as:

$$E(s) = \frac{1}{1 + G_3} R(s) \quad (\text{B.10})$$

$$G_3 = \frac{C^*(s)}{\eta(s)} = \frac{K_{c^*} s (s + \frac{1}{T_{\theta 3}}) (s + \frac{1}{T_{\theta 4}})}{(s^2 + 2\zeta_p \omega_p s + \omega_p^2) (s^2 + 2\zeta_{sp} \omega_{sp} s + \omega_{sp}^2)} \quad (\text{B.11})$$

The steady state error is defined as: $E_{ss} = \lim_{s \rightarrow 0} sE(s)$. If Eq. B.11 is substituted into Eq. B.10, then for a step input $R(s)$, the steady state error can be written as:

$$E_{ss} = \lim_{s \rightarrow 0} s \frac{1}{1 + \frac{K_{c^*} s (s + \frac{1}{T_{\theta 3}})(s + \frac{1}{T_{\theta 4}})}{(s^2 + 2\zeta_p \omega_p s + \omega_p^2)(s^2 + 2\zeta_{sp} \omega_{sp} s + \omega_{sp}^2)}} \frac{1}{s} \quad (\text{B.12})$$

$$E_{ss} = 1 \quad (\text{B.13})$$

Ideally the steady state must be 0. If G_3 is multiplied by an integrator term $\frac{K_2}{s}$ then Eq. B.12 can be written as:

$$E_{ss} = \lim_{s \rightarrow 0} s \frac{1}{1 + \frac{K_{c^*} s (s + \frac{1}{T_{\theta 3}})(s + \frac{1}{T_{\theta 4}})}{(s^2 + 2\zeta_p \omega_p s + \omega_p^2)(s^2 + 2\zeta_{sp} \omega_{sp} s + \omega_{sp}^2)}} \frac{1}{s} \quad (\text{B.14})$$

$$E_{ss} = \frac{1}{1 + \frac{K_2 K_{c^*} (\frac{1}{T_{\theta 3}} \frac{1}{T_{\theta 4}})}{\omega_p^2 \omega_{sp}^2}} \quad (\text{B.15})$$

For the C* closed-loop B747 transfer function:

$$G_3 = \frac{C^*(s)}{\eta(s)} = \frac{-17.7176s(s + 0.0009877)(s + 0.01819)}{(s^2 + 0.0111s + 0.003581)(s^2 + 2.716s + 1.904)} \quad (\text{B.16})$$

$$E_{ss} = \frac{1}{1 + 0.0466K_2} \quad (\text{B.17})$$

Appendix C

H2 Optimal Control

C.1 MIMO Systems - transfer function to state-space

[1]: An example for B747 short period dynamics

Equation C.1 and Eq. C.2 is the system transfer matrix describing the open loop mapping between the outputs z,y and the inputs w,u . from Fig. 4.4 in chapter 4.

$$G(s) = \begin{bmatrix} 0 & 1 \\ G_p & G_p \end{bmatrix} \quad (C.1)$$

$$\begin{bmatrix} z \\ y \end{bmatrix} = \begin{bmatrix} 0 & 1 \\ \frac{-1.099s-0.4996}{s^2+1.942s+1.55} & \frac{-1.099s-0.4996}{s^2+1.942s+1.55} \end{bmatrix} \begin{bmatrix} w \\ u \end{bmatrix} \quad (C.2)$$

By considering one input at a time: starting with w (first column of $G(s)$), an intermediate output z_{11} is written as:

$$z_{11}(s) = \frac{w(s)}{s^2 + 1.942s + 1.55} \quad (C.3)$$

and rearranging to:

$$z_{11}(s)(s^2 + 1.942s + 1.55) = w(s) \quad (C.4)$$

then defining the variables x_1 and x_2 as $x_1 = \dot{z}_{11}$, $x_2 = z_{11}$, $\dot{x}_2 = x_1$ and by substituting for these into Eq. C.4 to obtain:

$$\dot{x}_1 = -1.942x_1 - 1.55x_2 + w(s) \quad (C.5)$$

Repeating the steps for the second column:

$$z_{12}(s) = \frac{u(s)}{s^2 + 1.942s + 1.55} \quad (\text{C.6})$$

$$z_{12}(s)(s^2 + 1.942s + 1.55) = u(s) \quad (\text{C.7})$$

$$x_3 = \dot{z}_{12}, \quad x_4 = z_{12}, \quad \dot{x}_4 = x_3$$

$$\dot{x}_3 = -1.942x_3 - 1.55x_4 + u(s) \quad (\text{C.8})$$

And substituting for z and y in the original equations Eq. C.2:

$$z = 0 + z_{12}(s^2 + 1.942s + 1.55) \quad (\text{C.9})$$

$$z = 0 - 1.942x_3 - 1.55x_4 + u(s) + 1.942x_3 + 1.55x_4 \quad (\text{C.10})$$

$$z = u \quad (\text{C.11})$$

$$y = z_{11}(-1.099s - 0.4996) + z_{12}(-1.099s - 0.4996) \quad (\text{C.12})$$

$$y = -1.099x_1 - 0.4996x_2 + -1.099x_3 - 0.4996x_4 \quad (\text{C.13})$$

Then the state-space representation can be formulated as:

$$\begin{bmatrix} \dot{x}_1 \\ \dot{x}_2 \\ \dot{x}_3 \\ \dot{x}_4 \end{bmatrix} = \begin{bmatrix} -1.942 & -1.55 & 0 & 0 \\ 1 & 0 & 0 & 0 \\ 0 & 0 & -1.942 & -1.55 \\ 0 & 0 & 1 & 0 \end{bmatrix} \begin{bmatrix} x_1 \\ x_2 \\ x_3 \\ x_4 \end{bmatrix} + \begin{bmatrix} 1 \\ 0 \\ 0 \\ 0 \end{bmatrix} w + \begin{bmatrix} 0 \\ 0 \\ 1 \\ 0 \end{bmatrix} u \quad (\text{C.14})$$

$$Y = \begin{bmatrix} 0 & 0 & 0 & 0 \\ -1.099 & -0.4996 & -1.099 & -0.4996 \end{bmatrix} \begin{bmatrix} x_1 \\ x_2 \\ x_3 \\ x_4 \end{bmatrix} + \begin{bmatrix} 0 \\ 0 \end{bmatrix} w + \begin{bmatrix} 1 \\ 0 \end{bmatrix} u \quad (\text{C.15})$$

C.2 Parseval's Theorem

Consider 2 signals, $x(t)$ and $y(t)$, for which the Laplace transform of both exists. If the objective is to integrate the product of these 2 between an interval of $-\infty$ and ∞ then the problem can be expressed as:

$$I = \int_{-\infty}^{\infty} x(t) \cdot y(t) dt \quad (\text{C.16})$$

The inverse Laplace of $y(t)$ is shown below.

$$y(t) = \frac{1}{2\pi j} \int_{-j\infty}^{j\infty} y(s) e^{st} dt \quad (\text{C.17})$$

If the expression of $y(t)$ in Eq. C.17 is substituted into Eq. C.16, then the signal's product becomes:

$$I = \frac{1}{2\pi j} \int_{-\infty}^{\infty} x(t) \int_{-j\infty}^{j\infty} y(s) e^{st} dt \quad (\text{C.18})$$

By rearranging Eq. C.18 to obtain Eq. C.19 and considering the Laplace transform of $x(t)$, Eq. C.20 is obtained.

$$I = \frac{1}{2\pi j} \int_{-j\infty}^{j\infty} y(s) \int_{\infty}^{\infty} x(t) e^{st} dt \quad (\text{C.19})$$

$$I = \frac{1}{2\pi j} \int_{-j\infty}^{j\infty} y(s) \cdot x(-s) \quad (\text{C.20})$$

If $y(t)=x(t)$ then from Eq. C.16 and Eq. C.20:

$$I = \int_{-\infty}^{\infty} x^2(t) dt = \frac{1}{2\pi j} \int_{-j\infty}^{j\infty} x(s) \cdot x(-s) ds \quad (\text{C.21})$$

and considering the signal in the frequency domain, then:

$$\int_{-\infty}^{\infty} x^2(t) dt = \frac{1}{2\pi j} \int_{-j\infty}^{j\infty} x(jw) \cdot x(-jw) dw \quad (\text{C.22})$$

From the definition of the H_2 norm of a signal, Parseval's theorem proves that energy contained in the time domain is the same as energy contained in the frequency domain.

Appendix D

Convex Optimisation

D.1 Positive and Negative Definite Matrix

Consider a matrix P ,

1. if $x^T Px > 0$ for any $x \neq 0$ then the matrix is positive definite.
2. if $x^T Px \geq 0$ for any $x \neq 0$ then the matrix semi-positive definite
3. if $x^T Px < 0$ for any $x \neq 0$ then the matrix is negative definite
4. if $x^T Px \leq 0$ for any $x \neq 0$ then the matrix is semi-negative definite

P is said to be indefinite if $x^T Px > 0$ for some values of $x \neq 0$ and $x^T Px < 0$ for some values of $x \neq 0$.

D.1.1 Test for Positive and Negative Definiteness

Sylvester's criterion may be used to check if a symmetric matrix P is positive or negative definite. If P is not symmetric then the transform Eq. D.1 can be used to convert it to a symmetric matrix.

$$\frac{P + P^T}{2} \tag{D.1}$$

The criterion for a positive definite matrix is:

1. All diagonal elements of P must be positive and non-zero.

2. All leading principal minors P must be positive and non-zero.

For a negative definite matrix:

1. All diagonal elements of $-P$ must be negative and non-zero.
2. All leading principal minors of $-P$ of even order must be positive and non-zero.
3. All leading principal minors of $-P$ of odd order must be negative and non-zero.

An alternative method to check if a matrix is positive or negative definite is to compute its eigenvalues, if they are all positive then the matrix is positive definite and if they are all negative then it is negative definite.

D.2 Lyapunov Functions

$$\dot{X} = AX \quad (\text{D.2})$$

For the system D.2, if there exist a symmetric matrix P such that Eq. D.3, a continuously differentiable function is positive definite and $\dot{V}(X) = XPX$ is negative semi-definite, then the system (D.2) is stable and Eq. D.3 is said to be the Lyapunov function for the system [26].

$$V(X) = XPX \quad (\text{D.3})$$

If the function Eq. D.3 is differentiated, then Eq. D.4 is obtained whereby $\dot{V}(X) = -X^T QX$.

$$-X^T QX = \dot{X}^T P X + X^T P \dot{X} \quad (\text{D.4})$$

By substituting for Eq. D.2 in Eq. D.4, Eq. D.5 is obtained.

$$\begin{aligned} -X^T QX &= A^T X P X + X^T P A X \\ -Q &= A^T P + P A \end{aligned} \quad (\text{D.5})$$

Let $P = \int_0^\infty \exp(A^T t) B_1 B_1^T \exp(At) dt$ and $-Q = -B_1 B_1^T = \int_0^\infty d \exp(A^T t) B_1 B_1^T \exp(At)$, then by using product rule to differentiating $-Q$ (Eq. D.6) and substituting for P the

Lyapunov equation Eq. D.6 is obtained.

$$-Q = \int_{t=0}^{\infty} [A^T (\exp(A^T t) B_1 B_1^T \exp(At)) + (\exp(A^T t) B_1 B_1^T \exp(At)) A] dt \quad (\text{D.6})$$

$$-B_1 B_1^T = A^T P + P A \quad (\text{D.7})$$

Appendix E

Robust Fly-By-Wire System

E.1 Weighting functions and corresponding gain for B747 optimal controller

$$W_u = \frac{50(s + 100)}{s + 1000} \quad (\text{E.1})$$

$$W_e = \frac{1}{s + 0.001} \quad (\text{E.2})$$

$$K = \begin{bmatrix} 0.0453 & 0.1472 & -0.0594 & -0.3699 \\ 0.0000 & 0.0000 & -0.0000 & -0.0000 \end{bmatrix} \quad (\text{E.3})$$

E.2 B747 Aircraft Data for trim configurations 158m/s at an altitude of 6096m

Inertia:

$$m = 288756.9027 \text{ kg}$$

$$I_{xx} = 24675886.69 \text{ kgm}^2$$

$$I_{yy} = 44877574.145 \text{ kgm}^2$$

$$I_{zz} = 67384152.11 \text{ kgm}^2$$

Geometry:

$$\bar{c} = 8.193 \text{ m}$$

$$b = 59.643 \text{ m}$$



Figure E.1: Boeing 747 Aircraft

$$S = 510.97\text{m}^2$$

$$A = 6.9$$

Aerodynamics:

$$C_{D0} = 0.025$$

$$C_{L0} = 0.12579 \quad C_{L\alpha} = 4.67 \quad C_{Lq} = 5.13 \quad C_{L\delta E} = 0.320362143$$

$$C_{m0} = 0 \quad C_{m\alpha} = -1.15 \quad C_{mq} = -20.7 \quad C_{m\delta E} = -1.43$$

$$C_{y\beta} = -0.826183 \quad C_{yp} = 0.136709 \quad C_{yr} = 0.088041 \quad C_{y\delta R} = 0.1448 \quad C_{y\delta A} = 0$$

$$C_{l\beta} = -0.185332 \quad C_{lp} = -0.321364 \quad C_{lr} = 0.198369 \quad C_{l\delta R} = 0.0039 \quad C_{l\delta A} = 0.0129$$

$$C_{n\beta} = 0.132267 \quad C_{np} = -0.064426 \quad C_{nr} = -0.247319 \quad C_{n\delta R} = -0.1081 \quad C_{n\delta A} = 0.0015$$

E.3 Phoenix Aircraft Data for trim configurations

20m/s at an altitude of 30m

Inertia:

$$m = 7.770 \text{ kg}$$

$$I_{xx} = 0.553863416\text{kgm}^2$$

$$I_{yy} = 0.534706983\text{kgm}^2$$

$$I_{zz} = 0.972027056\text{kgm}^2$$

Geometry:

$$\bar{c} = 0.38\text{m}$$



Figure E.2: Phoenix UAV

$$b = 1.9\text{m}$$

$$S = 0.697500\text{m}^2$$

$$A = 5$$

Aerodynamics:

$$C_{D0} = 0.02830$$

$$C_{L0} = 0 \quad C_{L\alpha} = 4.229354 \quad C_{Lq} = 7.204948 \quad C_{L\delta E} = 0.418443$$

$$C_{m0} = 0 \quad C_{m\alpha} = -0.864255 \quad C_{mq} = -7.387185 \quad C_{m\delta E} = -0.928991$$

$$C_{y\beta} = -0.216357 \quad C_{yp} = 0.118043 \quad C_{yr} = 0.152937 \quad C_{y\delta R} = 0.115706 \quad C_{y\delta A} = 0.000136$$

$$C_{l\beta} = -0.060435 \quad C_{lp} = -0.414460 \quad C_{lr} = 0.136337 \quad C_{l\delta R} = 0.000736 \quad C_{l\delta A} = -0.257158$$

$$C_{n\beta} = 0.040747 \quad C_{np} = -0.034068 \quad C_{nr} = -0.070245 \quad C_{n\delta R} = -0.0503 \quad C_{n\delta A} = 0.0072$$

Bibliography

- [1] Pota, H.R.: MIMO systems - transfer function to state-space. *IEEE Transactions on Education*, vol. 39, pp. 97–99, 1996.
- [2] Sutherland, J.: Fly-by-wire flight control systems. In: *Joint Meeting of Flight Mechanics and Guidance and Control Panel of AGARD*. Oslo, Norway, 1968.
- [3] Niedermeier, D. and Lambregts, A.: Fly-by-wire augmented manual control - basic design considerations. In: *28th International Congress of the Aeronautical Sciences*. Brisbane, Australia, 2012.
- [4] Bartley, G.: Boeing B777: Fly-by-wire flight controls. *The Avionics Handbook*, 2001.
- [5] Perez, R., Liu, H. and Behdinan, K.: Relaxed static stability aircraft design via longitudinal control-configured MDO methodology. In: *Conference on Aerospace Technology and Innovation, Aircraft Design & Development Symposium*. Toronto, Canada, 2005.
- [6] JAL: Jal crash inquiry team examining damage in aft pressure bulk-head. *Aviation Week and Space Technology*, 1985. Vol. 123, no.8, pp. 28–30.
- [7] NTSB: In-flight separation of vertical stabilizer/American Airlines Flight 587/Airbus Industrie/A300-605R/N14053 Belle harbor, New York, November 12, 2001. National Transportation Safety Board Aircraft Accident Report, 2004.
Available at: www.nts.gov/investigations/AccidentReports/Reports/AAR0404.pdf
- [8] AAIPC: Final report A-00X/CENIPA/2008. Aeronautical Accident Investigation and Prevention Centre, 2008.
Available at: <http://www.skybrary.aero/bookshelf/books/546.pdf>
- [9] Learmount, D.: Crashed grob spn jet 'lost elevators and stabiliser'. *Flightglobal*. 19 December, 2006.

- [10] Liao, F., Wang, J.L. and Yang, G.-H.: Reliable robust flight tracking control: An lmi approach. *IEEE Transactions on Control Systems Technology*, vol. 10, pp. 76–89, 2002.
- [11] Willem Hermanus, P.: *System Identification for Fault Tolerant Control of Unmanned Aerial Vehicles*. Master's thesis, Stellenbosch University, South Africa, 2010.
- [12] Jean-Paul, A.: *Online System Identification for Fault Tolerant Control of Unmanned Aerial Vehicles*. Master's thesis, Stellenbosch University, South Africa, 2013.
- [13] Lionel, B.: *Control Allocation as Part of a Fault-Tolerant Control Architecture for UAVs*. Master's thesis, Stellenbosch University, South Africa, 2013.
- [14] Hendrik Mostert, O.: *An Analysis and Comparison of Two Methods for UAV Actuator Fault Detection and Isolation*. Master's thesis, Stellenbosch University, South Africa, 2013.
- [15] Willem Albertus, B.: *Fault Tolerant Adaptive Control of an Unmanned Aerial Vehicle*. Master's thesis, Stellenbosch University, South Africa, 2011.
- [16] Wiaan, B.: *Fault Tolerant Flight Control of a UAV with Asymmetric Damage to its Primary Lifting Surface*. Master's thesis, Stellenbosch University, South Africa, 2013.
- [17] Shah, G.: Aerodynamic effects and modelling of damage to transport aircraft. In: *AIAA Atmospheric Flight Mechanics Conference and Exhibition*. Honolulu, Hawaii, 2008.
- [18] Zhoa, J., Jiang, B. and Kaneshige, J.: Flight dynamics and hybrid adaptive control of damaged aircraft. *Journal of Guidance, Control, AND Dynamics*, vol. 31, pp. 293–302, 2008.
- [19] Tang, Y. and Paton, R.: Fault-tolerant flight control for nonlinear-uav. In: *20th Mediterranean Conference on Control & Automation (MED)*. Barcelona, Spain, 2012.
- [20] Li, X. and Liu, H.: A passive fault tolerant flight control for maximum allowable vertical tail damaged aircraft. *Journal of Dynamic Systems, Measurement AND Control*, vol. 134, pp. 293–302, 2012.
- [21] Bramesfeld, G., Maughmer, M. and Willits, S.: Piloting strategies for controlling a transport aircraft after vertical-tail loss. *Journal of Aircraft*, vol. 43, pp. 216–225, 2006.
- [22] DOD: MIL-STD-1797A flying qualities for piloted airplanes. Department of Defense Handbook. 19 December 1997.

- [23] Favre, C.: Fly-by-wire for commercial aircraft: The airbus experience. *International Journal of Control of Aircraft*, vol. 59, pp. 139–157, 1994.
- [24] Traverse, P., Lacaze, I. and Souyris, J.: Airbus fly-by-wire: A process towards total dependability. In: *25th International Congress of the Aeronautical Sciences*. Hamburg, Germany, 2006.
- [25] Syed, S., Khan, Z., Salman, M., Usman, A. and Aziz, A.: Adaptive flight control of an aircraft with actuator faults. In: *International Conference on Robotics and Emerging Allied Technologies in Engineering (iCREATE)*. Islamabad, Pakistan, 2014.
- [26] Slotine, J. and Weiping, L.: *Applied Nonlinear Control*. 1st edn. Prentice Hall, Inc, 1991. ISBN 0-13-040049-1.
- [27] Maybeck, S.P.: Multiple model adaptive algorithm for detecting and compensating sensor and actuator/surface failures in aircraft flight control systems. *International Journal of Robust and Nonlinear Control*, vol. 9, pp. 1051–1070, 1999.
- [28] Ye, D. and Yang, G.-H.: Adaptive fault-tolerant tracking control against actuator faults with application to flight control. *IEEE Transactions on Control Systems Technology*, vol. 14, pp. 1088–1096, 2006.
- [29] Nguyen, N., Krishnakumar, K. and Kaneshige, J.: Flight dynamics and hybrid adaptive control of damaged aircraft. *Journal of Guidance, Control and Dynamics*, vol. 31, pp. 751–764, 2008.
- [30] Sieberling, S., Chu, Q. and Mulder, J.: Robust flight control using incremental nonlinear dynamic inversion and angular acceleration prediction. *Journal of Guidance, Control and Dynamics*, vol. 33, pp. 1732–1742, 2010.
- [31] Wichai, S., Snell, S. and Hess, R.A.: Robust flight control design with handling qualities constraints using scheduled linear dynamic inversion and loop-shaping. *IEEE Transactions on Control Systems Technology*, vol. 8, pp. 483–494, 2000.
- [32] Chen, H. and Zhang, S.: Robust dynamic inversion flight control law design. In: *2nd International Symposium on Systems and Control in Aerospace and Astronautics*. Shenzhen, China, 2008.

- [33] Nabil, A., Benoit, B. and Ruxandra, B.: h_2 and h_∞ -optimal gust load alleviation for a flexible aircraft. In: *Proceedings of the American Control Conference*. Chicago, Illinois, 2000.
- [34] Dlamini, Z. and Jones, T.: Fly-by-wire robustness to flight dynamics change under horizontal stabiliser damage. *The Aeronautical Journal*, vol. 120, pp. 1005–1023, 2016.
- [35] Cook, M.: *Flight Dynamics Principles*. 2nd edn. Butterworth-Heinemann, 2007. ISBN 978-0-7506-6927-6.
- [36] Bacon, B. and Gregory, I.: General equations of motion for a damaged asymmetric aircraft. In: *AIAA Atmospheric Flight Mechanics Conference and Exhibition*. Hilton Head, South Carolina, 2007.
- [37] Etkin, B. and Reid, D.: *Dynamics of Flight Stability and Control*. 3rd edn. Butterworth-Heinemann, 2007. ISBN 0-471-03418-5.
- [38] DTIC: Equations of motion. USAF Test Pilot School, 1988.
Available at: www.dtic.mil/cgi-bin/GetTRDoc?AD=ADA319975
- [39] Talay, A.T.: Introduction to the aerodynamics of flight. NASA Langley Research Centre, 1975.
Available at: <http://history.nasa.gov/SP-367/contents.htm>
- [40] Karamcheti, K.: *Principles of Ideal Fluid Aerodynamics*. 1st edn. John Wiley and Sons, 1966. ISBN 978-0898741131.
- [41] Hanke, R. and Nordwall, D.: The simulation of a jumbo jet transport aircraft, volume II: Modelling data. Tech. Rep., The Boeing Company, Wichita, Kansas, US, 9 1970.
- [42] Blakelock, J.: *Automatic Control of Aircraft and Missiles*. 2nd edn. John Wiley and Sons, Inc, 1991. ISBN 0-471-50651-6.
- [43] Briere, D. and P., T.: AIRBUS A320/A330/A340 electrical flight controls - a family of fault-tolerant systems. In: *The Twenty-Third International Symposium on Fault-Tolerant Computing*. Dayton (OH), USA, 1993.
- [44] Field, E.: The application of a C*flight control law to large civil transport aircraft. Tech. Rep., Cranfield University, 3 1993.

- [45] Tobie, H., Elliott, E. and Malcolm, L.: A new longitudinal handling qualities criterion. In: *Proceedings of the Annual National Aerospace Electronics Conference*. Toulouse, France, 1966.
- [46] Zhou, K., Lixinb, W. and Xiangsheng, T.: Flying qualities reduction of fly-by-wire commercial aircraft with reconfiguration flight control laws. In: *The 2nd International Symposium on Aircraft Airworthiness (ISAA 2011)*. Beijing, China, 2011.
- [47] Stefani, R., Savant, C., Shahian, B. and Hostetter, G.: *Design of Feedback Control Systems*. 3rd edn. Saunders College Publishing, 1994. ISBN 0-03-098084-4.
- [48] Engelbrecht, J.: Control systems 314, 2013. Stellenbosch University, South Africa.
- [49] Gu, D.-W., Petkov, P. and Konstantinov, M.: *Robust Control Design with MATLAB*. 1st edn. Springer, 2007. ISBN 978-1-84628-091-7.
- [50] Zhou, K. and Doyle, C.: *Essentials of Robust Control*. 1st edn. Prentice Hall, 1998. ISBN 0-13-525833-3.
- [51] Gopal, M.: *Control Systems Principles and Design*. 2nd edn. McGraw-Hill, 2003. ISBN 0-07-123127-7.
- [52] Schutter, B.D.: Minimal state-space realization in linear system theory: An overview. *Journal of Computational and Applied Mathematics, Special Issue on Numerical Analysis in the 20th Century-Vol. I: Approximation Theory*, vol. 121, pp. 331–354, 2000.
- [53] Gilbert, E.G.: Controllability and observability in multi-variable control systems. *SIAM Journal on Control*, vol. 1, pp. 128–151, 1963.
- [54] Naidu, D.: *Optimal control systems*. 1st edn. CRC Press LLC, 2003. ISBN 0-8493-0892-5.
- [55] Jasbir, A.S.: *Introduction to optimum design*. 3rd edn. Elsevier, 2012. ISBN 978-0-12-381375-6.
- [56] Boyd, S. and Vandenberghe, L.: *Convex Optimization*. 1st edn. Cambridge University Press, 2004. ISBN 0-521-83378-7.
- [57] Boyd, S., El Ghaoui, L., Feron, E. and Balakrishnan, V.: *Linear Matrix Inequalities in System and Control Theory*. 1st edn. Society for Industrial and Applied Mathematics, 1994. ISBN 0-89871-334-X.

- [58] Toh, K.-C., Todd, M.J. and Tütüncü, R.H.: On the implementation and usage of SDPT3 - a MATLAB software package for semidefinite-quadratic-linear programming, version 4.0. 16 June 2010.
- [59] Löfberg, J.: Yalmip: A toolbox for modeling and optimization in matlab. In: *IEEE International Symposium on Computer Aided Control Systems Design*. Taipei, Taiwan, 2004.
- [60] Skogestad, S. and Postlethwaite, I.: *Multivariable Feedback Control: Analysis and Design*. 1st edn. John Wiley and Sons, 1996. ISBN 0-471-94330-4.